Synergistic Modeling of Advanced Manufacturing Processes with Functional Variables

Hongyue Sun

Dissertation Submitted to the Faculty of the Virginia Polytechnic Institute and State University in Partial Fulfillment of the Requirements for the Degree

of

Doctor of Philosophy
in
Industrial and Systems Engineering

Ran Jin, Chair
Jaime A. Camelio
Xinwei Deng
Zhenyu (James) Kong
William H. Woodall

April 7, 2017
Blacksburg, VA

Keywords: Advanced Manufacturing Processes Quality Modeling, Functional Data Analysis, *In situ* Process Variables, Synergistic Modeling

Synergistic Modeling of Advanced Manufacturing Processes with Functional Variables

Hongyue Sun

ABSTRACT

Modern manufacturing needs to optimize the entire product lifecycle to satisfy the customer needs. The advancement of sensing technologies has brought a data rich environment for manufacturing and provide a great opportunity for real-time, proactive quality assurance. However, due to the lack of methods for analyzing heterogeneous types of data, the transformation of data to information and knowledge for effective decision making in manufacturing is still a challenging problem. In particular, functional variables can represent the *in situ* process conditions and rich product performance information, and are widely encountered in various manufacturing processes. In this dissertation, I will focus on modeling of manufacturing processes with *in situ* process (functional) variables, and integrating these functional variables and other measured variables for the manufacturing modeling.

The modeling is explored by extracting informative features through the integration of multiple functional variables, functional variables and offline setting variables, and quantitative and qualitative quality variables. After an introduction in Chapter 1, three research tasks are investigated. First, a functional variable selection problem is studied in Chapter 2 to identify the significant functional variables as well as their features in a logistic regression model. A hierarchical non-negative garrote constrained estimation method is proposed. Second, the quality-process relationships for scalar offline setting variables, functional *in situ* process variables, and manufacturing quality responses are studied in Chapter 3. A functional graphical model that can integrate functional variables in a graphical model is proposed and investigated.

Third, the quantitative and qualitative quality responses are jointly modeled with scalar offline setting variables and functional *in situ* process variables in Chapter 4. A functional quantitative and qualitative model is proposed and investigated. Finally, I summarize the research contribution and discuss future research directions in Chapter 5.

The proposed methodologies have broad applications in manufacturing processes with functional variables, and are demonstrated in a crystal growth process with multiple functional variables (Chapter 2), a plasma spray process with multiple scalar and functional variables (Chapter 3), and an additive manufacturing process called fused deposition modeling with quantitative and qualitative quality responses (Chapter 4).

Synergistic Modeling of Advanced Manufacturing Processes with Functional Variables

Hongyue Sun

GENERAL AUDIENCE ABSTRACT

Advanced manufacturing has attracted much attention in recent years. One unique requirement in advanced manufacturing is that the entire product lifecycle needs to be optimized to satisfy the customer needs. Thanks to the advancement of sensing and information technology, various types of manufacturing data are collect, which provide a great opportunity for real-time, proactive quality assurance. At the current status, there is a lack of data analytics methods to analyze these manufacturing data, based on which effective decisions and actions can be made to improve the advanced manufacturing quality and efficiency. Among these sensor data, the continuously measured functional variables during the manufacturing processes, which can represent the *in situ* process conditions and rich product performance information, are widely encountered. In this dissertation, I will focus on the modeling of manufacturing processes with *in situ* process (functional) variables, and integrating these functional variables and other measured variables for the manufacturing modeling.

In particular, multiple functional variables, functional variables and scalar offline setting variables, and quantitative and qualitative quality variables are modeled in advanced manufacturing. After an introduction in Chapter 1, three research tasks are investigated. First, a functional variable selection problem is studied in Chapter 2 to identify the significant functional variables as well as their features in a logistic regression model for product quality condition classification. Second, the quality-process relationships for scalar offline setting variables, functional *in situ* process variables, and manufacturing quality responses are studied in Chapter 3.

A functional graphical model that can integrate functional variables in a graphical model is proposed and investigated. Third, the quantitative and qualitative quality responses are jointly modeled with scalar offline setting variables and functional *in situ* process variables in Chapter 4. A functional quantitative and qualitative model is proposed and investigated. Finally, I summarize the research contribution and discuss future research directions in Chapter 5.

The proposed methodologies have broad applications in manufacturing processes with functional variables, and are demonstrated in a crystal growth process with multiple functional variables (Chapter 2), a plasma spray process with multiple scalar and functional variables (Chapter 3), and an additive manufacturing process with quantitative and qualitative quality responses (Chapter 4).

ACKNOWLEDGEMENTS

First, I would like to express my whole hearted acknowledge and gratitude to Professor Ran Jin, my advisor, for the supervision, support and encouragement during my graduate study. Without his great guidance and care, I could not complete my dissertation. I will never forget his help and support throughout the past five years during my graduate study. I would like to thank my committee members, Professor Jaime A. Camelio, Professor Xinwei Deng, Professor Zhenyu (James) Kong and Professor William H. Woodall for their insightful suggestions, supervisions and support during my graduate study.

I would like to thank the valuable suggestions, supervisions and considerations from scholars in the academic society of Manufacturing, Quality and Statistics and beyond, including Professor Jianjun Shi, Professor Chuck Zhang and Dr. Kan Wang from Georgia Tech; Professor Yuan Luo from Northwestern University; Professor Kaibo Wang from Tsinghua University; Professor Prahalada Rao from University of Nebraska–Lincoln; Professor Shuai Huang from University of Washington; and Professor Kimberly P. Ellis, Professor Zhen He, Professor Yili Hong, Professor Leanna L. House, Professor Blake N. Johnson, Professor Inyoung Kim, Professor Nathan Lau and Professor Joel Nachlas from Virginia Tech.

I would also like to thank my fellow students, colleagues and friends for the support, encouragement and friendship during my graduate study, including but not limited to: Mr. Xiaoyu Chen, Mr. Jooneun Choi, Mr. Abhishek Kar, Mr. Qing Lan, Ms. Jingran Li, Mr. Yifu Li, Mr. Chen'ang Liu, Mr. Jia Liu, Mr. Shuai Luo, Ms. Karuniya Mohan, Mr. Gongzhuang Peng, Mr. Fangzhou Sun, Ms. Wenmeng Tian, Ms. Anqi Wang, and Mr. Lening Wang. In addition, I would

like to acknowledge National Science Foundation and several other industrial sponsors for the support and collaboration in my research.

Finally, I want to thank my parents and other family members for the unconditional support and love, which encourage me to come across the difficulties throughout my career and life.

Table of Contents

List of Figures

List of Tables

Chapter 1. Introduction

1.1. Motivation

Modern manufacturing systems equipped with advanced sensing technology have created a data-rich environment. Such an environment provides abundant information for manufacturing processes, leading to a great opportunity for data-driven decision making in smart manufacturing. However, the data-rich environment also poses great challenges for transforming data to effective decision-making towards quality and efficiency excellence [1]. This is primarily due to the lack of methods to analyze the heterogeneous types of data from different sources. For example, data collected from manufacturing processes have various formats such as scalar data, time series data, spatial correlated data and spatial-temporal data. The latter three types of data are presented as either functions over time or functions over space, which are called functional variables. These functional variables, if collected during the manufacturing processes, can represent the *in situ* process conditions with rich manufacturing process information. The integration of the functional variables with other measured variables in manufacturing processes modeling will advance the modeling performance, thus facilitate better decision-making. Therefore, it calls for systematic methods to model functional variables for manufacturing processes.

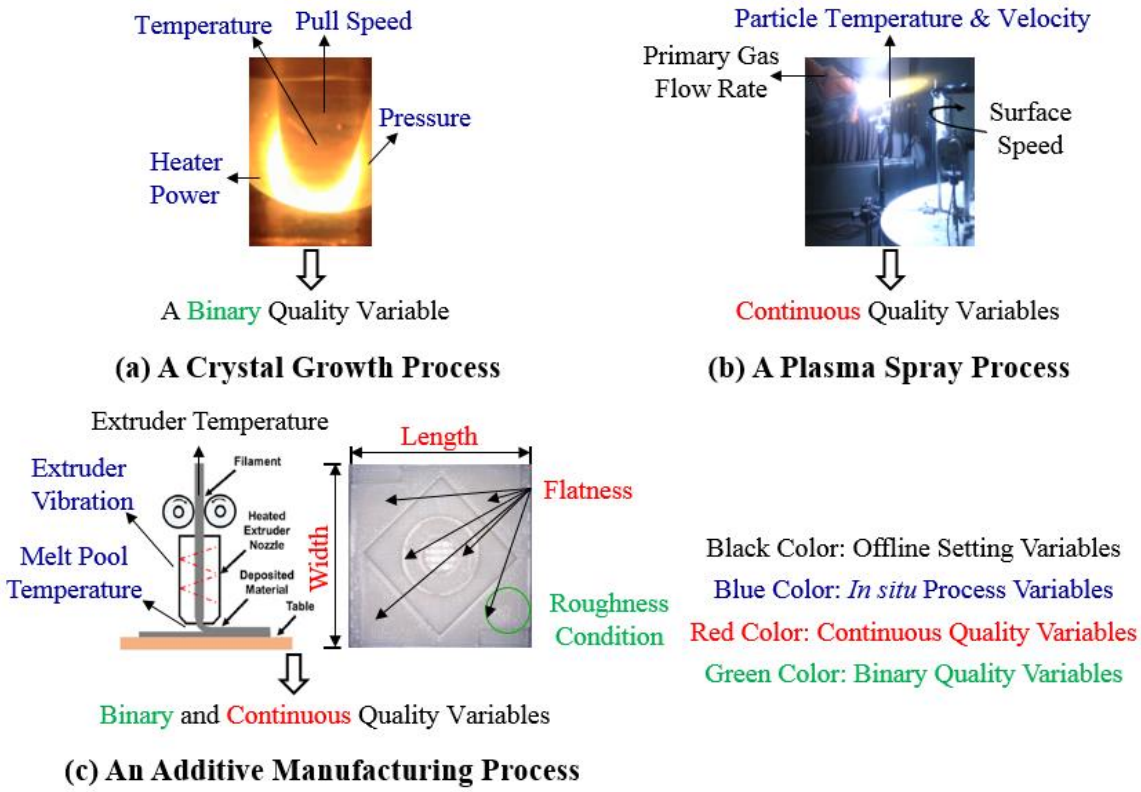

Figure 1.1. Motivating Manufacturing Processes in this Dissertation [2]

Functional variables are widely encountered in various manufacturing processes (Figure 1.1). For example, functional *in situ* process variables, such as ingot pull speed and heater power, are measured during the production of a crystal growth manufacturing process (Figure 1.1 (a)) [3-5]. This process is the first step in the entire semiconductor manufacturing processes, and determines the initial quality of semiconductor products. Therefore, it is important to model this process. However, there are still several types of process defects which would cause significant loss. How to identify the significant functional variables and their features for ingot quality modeling is a challenging variable selection problem due to the complex functional variable structures. For another example, both offline setting variables (scalar variables) and *in situ* process variables (functional variables) are measured to investigate the quality-process relationships in a plasma spray process (Figure 1.1 (b)). The understanding of variable

relationships is important to provide guidelines for better surface coating properties in the plasma spray process. Currently, it is unclear how the *in situ* process variables interact with offline setting variables during the quality modeling [6, 7]. In addition, in Additive Manufacturing (AM) processes, both Quantitative and Qualitative (QQ) quality variables could be used to characterize the part quality (Figure 1.1 (c)) [2, 8, 9]. For instance, the geometrical deviation from the nominal design value is a quantitative quality variable, and the surface condition judgment is a qualitative quality variable. The underlying association between the QQ quality variables, and their relationships with offline setting variables and *in situ* process variables remain unknown. A common challenge for the aforementioned processes is how to model the functional variables for the manufacturing processes characterization. The objective of this dissertation is to advance the knowledge on synergistic modeling of manufacturing processes by investigating the significance of functional measurements and their features.

1.2. State-of-the-Art

In quality engineering, there are some methods that use functional variables for variation reduction in manufacturing processes. In Statistical Process Control (SPC), different models are proposed to characterize the functional/profile variables and monitor the corresponding statistics. See Kim *et al.* for linear regression models [10], Qiu *et al.* for nonparametric methods [11], and Jensen *et al.* for mixed effect models [12]. Comprehensive reviews of profile monitoring can be found in [13-15]. Recently, monitoring methods based on images and spatial data [16, 17], and network data [18] are also developed. To model the functional variables in manufacturing processes, Jin and Shi proposes to model the tonnage signal with wavelet analysis [19]. Paynabar *et al.* proposes to model a continuous response for the vehicle comfort study via a hierarchical variable selection technique [20]. Huang models the growth of nanowire via Bayesian

hierarchical modeling [21]. Kong *et al.* study the end-point detection problem in chemical mechanical planarization process via a nonlinear sequential Bayesian framework [22]. These methods address the modeling of functional variables for manufacturing quality control, but they do not focus on modeling and selection of significant variables or features for heterogeneous types of data.

In statistical modeling and data analytics, general-purpose variable selection and modeling methods are proposed. For instance, to identify the significant variables, the best subset selection [23], forward/backward regression [24], and stepwise regression [24] can be used. But these methods are computationally intensive and limited to the number of variables. Recently, several penalization approaches are used for variable selection. Among these methods, the Lasso uses an l_1 penalty for model complexity penalization [25], the Non-Negative Garrote (NNG) rescales the model parameters by non-negative nuisance factors and constraint on the summation of these nuisance factors [26, 27], the Smoothly Clipped Absolute Deviation (SCAD) uses a non-convex penalty for model complexity penalization [28], and the Elastic Net (EN) uses an weighted l_1 and l_2 penalty for model complexity penalization [29]. The above penalization methods can only select individual variables. For variable selection with group structure, the above penalization methods may not perform well [30]. To address the group variable structure, Group Lasso and composite absolute penalties are proposed [30, 31]. Though these methods usually have better performance than traditional variable selection methods, they can only select the group as a whole and cannot select individual features within the group [20, 32]. For statistical modeling, a variety of statistical models, such as classification and regression tree, probabilistic graphical models, are developed [33]. These models are efficient in modeling the input-output

relationships with heterogeneous types of data in various applications. However, they cannot handle the functional variables as input.

1.3. Objectives

The focus of this dissertation is on synergistic modeling of advanced manufacturing processes with heterogeneous types of variables, especially functional variables. Figure 1.2 provides an illustration of the research strategy. In the synergistic modeling, the knowledge from domain knowledge, statistics, optimization, signal processing, etc. will be integrated. In particular, the "synergistic" strategy is emphasized by extracting informative features through the integration of multiple functional *in situ* process variables, functional *in situ* process variables and offline setting variables, or QQ quality variables. These data from different sources can borrow strength from each other and yield better modeling performance [34]. The objectives of this dissertation include:

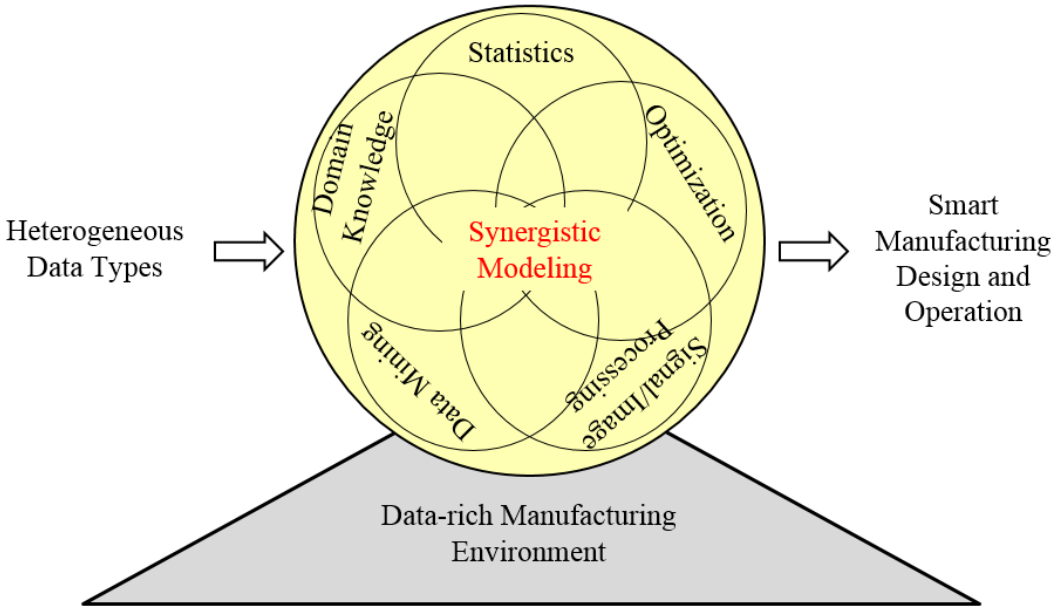

Figure 1.2. An Illustration of the Synergistic Modeling Research Strategy

1) to investigate the functional variable selection problem for manufacturing processes quality modeling, where both the significant functional variables and the significant features in the functional variables can be identified;

2) to study the modeling of the quality variables with offline setting variables and *in situ* process variables via a functional graphical model, where the measurement data and prior knowledge are integrated in the graphical modeling; and

3) to study the modeling of the QQ quality responses with offline setting variables and *in situ* process variables via a functional QQ model, where the QQ responses are jointly modeled.

1.4. Organization of the Dissertation

The rest part of this dissertation is organized as follows. In Chapter 2, a functional variable selection technique is proposed for a logistic regression and demonstrated with a crystal growth process. In Chapter 3, a functional graphical model is developed to characterize the relationships among offline setting variables, *in situ* process variables, and quality responses. The methodology is demonstrated in a plasma spray process. Chapter 4 discusses the joint modeling of QQ responses in AM with offline setting variables and *in situ* process variables via a functional QQ model. Chapter 2 is based on an earlier published paper in IISE Transactions [5]. Chapter 3 is based on an earlier accepted paper in IEEE Transactions on Automation Science and Engineering [7]. Chapter 4 is based on an earlier submitted paper in IEEE Transactions on Automation Science and Engineering [9].

Chapter 2. Logistic Regression for Crystal Growth Process Modeling through Hierarchical Nonnegative Garrote based Variable Selection

2.1. Introduction

Wafer manufacturing is an important upstream process for many high-tech products, such as computer electronics, automatic control devices, solar cells, etc. Such a manufacturing process consists of many stages, including crystal growth, wire slicing, etching, lapping, polishing, etc. The crystal growth process is the first step to produce a silicon ingot, which determines the initial quality for downstream products. Therefore, it is extremely important to control the quality at this stage.

The majority of crystal ingots are grown by Czochralski crystal growth processes (CZ processes) in industry [35]. A successful CZ process is maintained at extremely high temperature for more than 60 hours. The process can be divided into the following phases [36, 37]. First, the polycrystalline silicon is melted in a silica crucible. Then, a precisely oriented seed crystal is dipped into the melt. By jointly controlling of thermal gradient and pulling speed, the ingot grows to the desired diameter. Afterwards, the ingot is slowly pulled upwards and rotated simultaneously. Such a pulling and rotation process will last for more than 20 hours, which is called the “body growth phase”. This body growth phase is the most important phase during a CZ process, since the majority part of an ingot is grown in this phase. Finally, the ingot finishes its growth after a tailing phase. The above ingot growth process takes place in industrial CZ

furnaces as shown in Figure 2.1 (a) [4]. Inside the furnace, the structure and operation conditions in the hot zone are critical for the ingot growth (Figure 2.1 (b), [3]).

Due to the high energy consumption and long cycle time in the CZ process, any quality defect of the ingot would result in great waste of energy, time and cost. The quality defects include microscopic defects and macroscopic defects [36]. Examples of microscopic defects are void, interstitial, dislocation, etc., which will affect the electronic and mechanical properties of the downstream products [38]. The macroscopic defects are more severe and may cause the failure of the entire growth process. In such a situation, the manufacturer has to discard the nonconforming segments of the ingot, or re-melt the material and repeat the growth process, which leads to further waste. Among these macroscopic defects, polycrystalline defect is the most frequently observed type. Polycrystalline defect refers to the phenomenon that the desired monocrystalline ingot becomes polycrystalline. Once a segment of the ingot becomes polycrystalline, the entire segment will be discarded [3]. Thus, it is critical to reduce this type of quality defect during the manufacturing. In the literature, defects analysis in crystal growth mainly focuses on microscopic defects [36, 39-41]. In this chapter, we focus on polycrystalline defect modeling during the body growth phase, since the majority of polycrystalline defect appears in this phase.

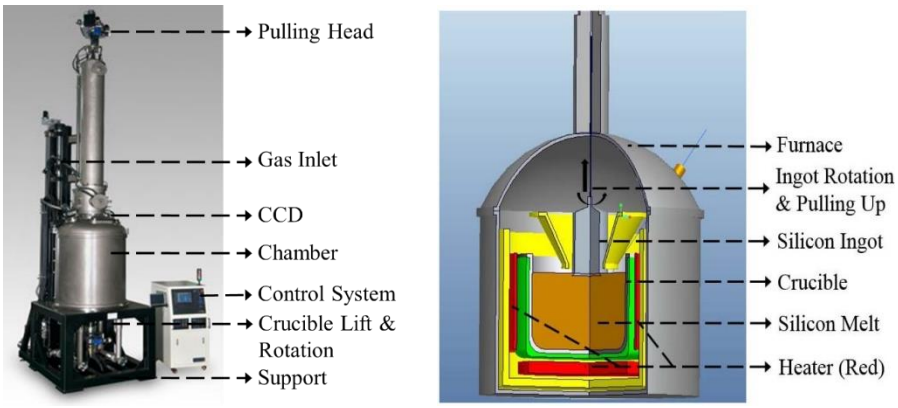

(a) Furnace (b) Internal Structure of the Chamber (Hot Zone)

Figure 2.1. Schematic of a Crystal Growth Furnace [3, 4]

To model the polycrystalline defect, we use a binary variable as the indicator for polycrystalline defect, and propose a logistic regression model to model the binary quality variable (response) with the functional *in situ* process variables (predictors). Engineering perceptions suggest that the features of the *in situ* process variables should be captured, because sudden changes of these process variables are potential root causes for polycrystalline defect. Therefore, we adopt wavelet analysis for each *in situ* process variable. Wavelet analysis is selected because it performs well in extracting features from local time and frequency [42]. Thus, all the wavelet coefficients of an *in situ* process variable form a group of features. In this chapter, the wavelet coefficients of a process variable are called "features" or "local features" and one process variable has a "group" of corresponding features. The objective of this research is to identify both key *in situ* process variables and their significant features. Therefore, a logistic regression with Hierarchical Non-Negative Garrote (HNNG) based variable selection is proposed.

The NNG is a shrinkage method for estimating a parsimonious model [26]. The NNG is first proposed for variable selection in linear models. Makalic and Schmidt develop NNG for logistic regression models [27]. The consistency in prediction and variable selection of the NNG is studied in [43]. However, none of the existing NNG based variable selection methods can address the aforementioned two-level (*in situ* process variable level and feature level) variable selection problem in a logistic regression model. In this chapter, the newly proposed HNNG method can identify significant groups (representing *in situ* process variables) as well as local features (representing wavelet coefficients from the *in situ* process variables) to predict the binary response. The advantages of the HNNG method lie in several aspects. First, the proposed HNNG method performs variable selection for significant groups and features simultaneously.

Second, the computation issues are addressed by quadratic approximation of the objective function. Third, the polycrystalline defect can be predicted in a timely manner based on the measurements. Specifically, we divide the measurements into windows with binary quality labels given by the domain expert. In each time window, wavelet analysis is adopted for the measurements and the corresponding wavelet coefficients are treated as predictors in the logistic regression. Therefore, the model can predict whether the ingot becomes polycrystalline for each window.

The rest part of this chapter is organized as follows. In Section 2.2, the state-of-the-art for CZ process modeling, variable selection, and wavelet analysis are reviewed. Section 2.3 illustrates the proposed method and the computation algorithm. We demonstrate the effectiveness of the proposed method in prediction and variable selection by using simulations and a case study in Sections 2.4 and 2.5, respectively. Finally, conclusions and future research are discussed in Section 2.6.

2.2. Research Background

2.2.1. Crystal Growth Processes Modeling

Engineering models are available for simulation and defect analysis of CZ processes. Simulation models mainly focus on predicting thermal field distribution for equipment design. Such models are typically based on Partial Differential Equations (PDE) describing the growth dynamics [44-46]. Müller proposes the concept of reverse simulation, which aims at controlling a certain kind of defect given the defect-process relationships [47]. In most cases, these simulation models are solved offline based on finite element methods. The performance of simulation models depends on the engineering assumptions, boundary conditions and accuracy of the material properties characterization. These models can be hardly adopted for polycrystalline modeling with potential

online prediction requirements. Another category of models focuses on microscopic defects, which typically models the distribution of the microscopic defects with process variables. Voronkov concludes that the ratio of crystal pulling speed and magnitude of temperature gradient above the solid-liquid interface determines the formation of point defects [40]. The formation of larger scale defects, such as oxidation-induced stacking fault ring are also modeled. Comprehensive reviews for defect modeling are available in [39, 41]. However, these models focus on the microscopic defects, and there are limited engineering-driven models to predict the polycrystalline defect quantitatively.

Researchers also attempt to model the CZ processes by using statistics, optimization or data mining methods. For instance, time series analysis for the dynamic properties of striations in the ingot is explored [48, 49]. Back-propagation, regularization and perceptron neural networks are used for the ingot striations pattern predictions. In addition, a genetic algorithm, coupled with thermal PDE, is used for the optimization of CZ furnace heat shield configuration [50]. For another example, Avci and Yamacli use Artificial Neural Network (ANN) to modify the PDE describing defect concentration [51]. Such a method yields good defect concentration prediction accuracy.

2.2.2. Variable Selection Methods

To model a binary quality variable with functional process variables, one can formulate this problem as a classification problem. Data mining methods, for instance, linear discriminant analysis, support vector machines, classification and regression tree, and random forests can be applied. See details in [33]. Functional logistic regression model can also be used to link the binary response and functional predictors [52]. In this chapter, we adopt the latter approach. To improve the model performance as well as interpretability, different kinds of variable selection

methods have been proposed. These methods include subset and stepwise regression [53], Lasso [25], NNG [26, 27], SCAD [28], and EN [29]. For variable selection with group structure, the penalization methods introduced above may not perform well. To address the group variable structure, Yuan and Lin propose Group Lasso [30]. Zhao *et al.* propose the flexible composite absolute penalties [31]. Meier *et al.* study the group variable selection for logistic regression via Group Lasso (GrpLasso) [54]. Though these methods usually have better performance than traditional methods, they can only select the group as a whole and cannot select individual features within the group [55].

To deal with the functional variable selection problem, Huang *et al.* propose Group Bridge (GrpBridge) [55]. However, GrpBridge penalty is not always differentiable and tends to be inconsistent for feature selection [56]. Zhou and Zhu propose Hierarchical Lasso (HLasso), which penalizes the coefficients by two levels of l_1 penalty [32]. Paynabar *et al.* point out that Zhou and Zhu's method may fall into a local optimum [20]. They propose a hierarchical NNG for group variable selection in linear regression by firstly identifying the important groups, and then the important features within the selected groups in two steps. They demonstrate that hierarchical NNG performed well in prediction and variable selection for linear regression models. In this chapter, we explore the functional variable selection for a logistic regression via HNNG. The advantage of HNNG is that it can select important groups and features simultaneously in one step. Besides, the hierarchical NNG method by Paynabar *et al.* focuses on linear regression models [20], while we focus on logistic regression models.

2.2.3. Wavelet Analysis

In this study, wavelet analysis is used to transform a functional variable into a group of wavelet features. Wavelet analysis is a multi-resolution analysis tool that can provide both localized time

and frequency information [42]. We use wavelet analysis so that the features from local time and frequency can represent the subtle changes of *in situ* process variables, which might lead to polycrystalline defects from engineering perception. Wavelet analysis has been widely adopted in engineering applications for quality improvement. For instance, Jin and Shi apply wavelet analysis to the force signal in a stamping process for data compression [57]. Jin and Shi further adopt wavelet analysis for fault diagnosis in the stamping process [19]. Other applications include nano-machining [58], a forging process [59], structural health monitoring [60], antenna [61], a rolling process [62] and an engine assembly process [63].

2.3. Proposed Method

2.3.1. Overview of the Proposed Method

An overview of the proposed method is shown in Figure 2.2. Based on the Proportional-Integral-Derivative (PID) control loops of the CZ process, the potentially important process variables are selected for the modelling. Wavelet analysis is then adopted for each process variable. After that, we use HNNG based logistic regression to predict the binary response based on groups of wavelet coefficients. Finally, the proposed method is compared with other benchmark methods.

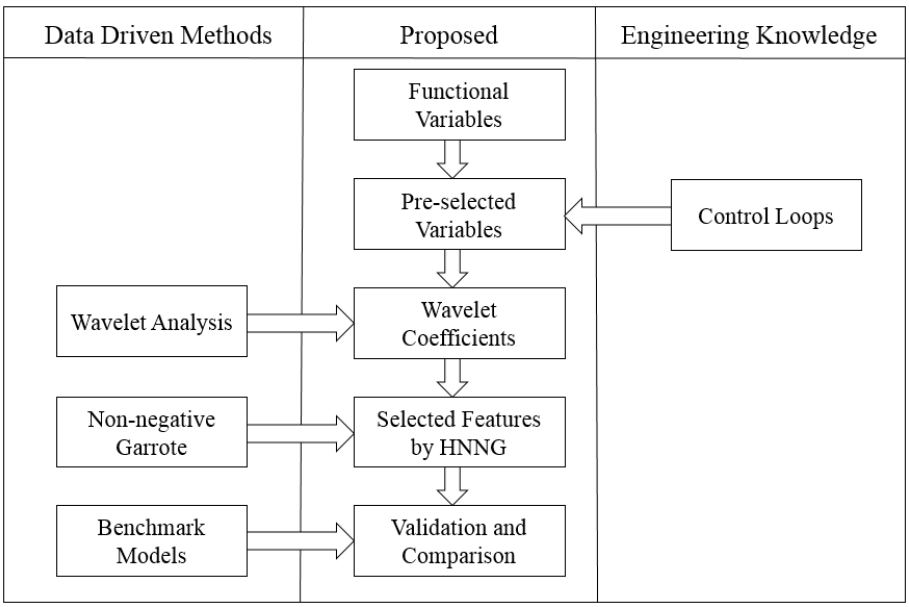

Figure 2.2. Overview of the Proposed Functional Variable Selection Method

2.3.2. Data Structure

Assuming that we have p functional process variables to be modeled, and the number of dilations in wavelet analysis is set to be m. After wavelet decomposition, we have m levels of detail coefficients and one level of coarse coefficients. The original process variable is formulated in the structure shown in Table 2.1, where $p_1, p_2, \ldots, p_m$ and p_c are the number of wavelet coefficients in each level. We denote $P_j = \sum_{i=1}^{m} p_i + p_c$ to be the number of features in the *j*-th process variable, and $P = \sum_{j=1}^{p} P_j$ to be the total number of features for p process variables. For each sample, there will be *P* predictors with structure shown in Table 2.1 and one binary response y_i. In total, there are n samples for modeling.

Table 2.1. Data Structure after Wavelet Decomposition

Detail Level 1	Detail Level 2	…	Detail Level m	Coarse Level
$x_{1,1}\ x_{2,1}\ \ldots\ x_{p_1,1}$	$x_{1,2}\ x_{2,2}\ \ldots\ x_{p_2,2}$	…	$x_{1,m}\ x_{2,m}\ \ldots\ x_{p_m,m}$	$x_{1,c}\ x_{2,c}\ \ldots\ x_{p_c,c}$

2.3.3. HNNG based Logistic Regression Model

The logistic regression model has the form illustrated in Eq. (2.1)

$$logit(E[y_i|\boldsymbol{x}_i]) = log\frac{p(\boldsymbol{x}_i)}{1-p(\boldsymbol{x}_i)} = \boldsymbol{x}_i{}^T\boldsymbol{\beta}, i = 1, \ldots, n, \quad (2.1)$$

where y_i is the binary response for the *i*-th sample, with $y_i = 0$ indicating a conforming growth sample, and $y_i = 1$ indicating a polycrystalline growth sample; $p(\boldsymbol{x}_i)$ is the probability that the *i*-th sample is polycrystalline (i.e., $y_i = 1$); $\boldsymbol{x}_i = \left(\boldsymbol{x}_{1,i}{}^T, \boldsymbol{x}_{2,i}{}^T, \ldots, \boldsymbol{x}_{p,i}{}^T\right)^T = (x_{1,1,i}, x_{2,1,i}, \ldots, x_{P_1,1,i}, x_{1,2,i}, x_{2,2,i}, \ldots, x_{P_2,2,i}, \ldots, x_{1,p,i}, x_{2,p,i}, \ldots, x_{P_p,p,i})^T$ is the predictor vector for the *i*-th sample, where $x_{k,j,i}$ is the *k*-th feature in the *j*-th group for the *i*-th sample. In the above notations, there are p groups of process variables and P_j features in each process variable. $\boldsymbol{\beta} =$

$(\beta_1{}^{(1)},\ \beta_2{}^{(1)}, \dots, \beta_{P_1}{}^{(1)}, \beta_1{}^{(2)}, \beta_2{}^{(2)}, \dots, \beta_{P_2}{}^{(2)}, \dots, \beta_1{}^{(p)}, \beta_2{}^{(p)}, \dots\ ,\ \beta_{P_p}{}^{(p)})^T$ is model coefficient vector with $\beta_k{}^{(j)}$ the coefficient for the *k*-th feature in the *j*-th group.

As discussed above, the NNG can be used to enforce a parsimonious model. It reparametrizes the model coefficient vector $\boldsymbol{\beta} = \boldsymbol{\theta} \cdot \widetilde{\boldsymbol{\beta}}$, where $\boldsymbol{\theta} = (\theta_1^{(1)},\ \theta_2^{(1)}\ \dots, \theta_{P_1}^{(1)}, \theta_1^{(2)},\ \theta_2^{(2)}\ \dots, \theta_{P_2}^{(2)},\ \dots, \theta_1^{(p)},\ \theta_2^{(\mathrm{p})}\ \dots, \theta_{P_p}^{(p)})^T$ is the shrinkage vector (with each element non-negative) to encourage variable selection, and $\theta_k^{(j)}$ the shrinkage factor for the *k*-th feature in the *j*-th group; the "$\cdot$" stands for element-wise multiplication; and $\widetilde{\boldsymbol{\beta}}$ is an initial estimate for model coefficients, which can be estimated by Maximum Likelihood Estimation (MLE). If $\theta_k^{(j)} = 1$, the corresponding coefficient $\beta_k{}^{(j)}$ will be estimated as the initial estimate. When $\theta_k^{(j)} = 0$, the corresponding coefficient shrinks to zero, and the predictor will not be selected in the model. To perform variable selection with the hierarchical group structure shown in Table 2.1, some adjustments have to be made. Specifically, we design two levels of constraints and minimize the negative log-likelihood through the following optimization problem

$$min\ L(\boldsymbol{\beta}) = -log\left\{\prod_{i=1}^{n}\left[p(\boldsymbol{x}_i)^{y_i}\left(1-p(\boldsymbol{x}_i)\right)^{1-y_i}\right]\right\}, \tag{2.2}$$

$$\text{subject to: } \beta_k^{(j)} = \theta_k^{(j)}\tilde{\beta}_k{}^{(j)}, \theta_k^{(j)} \geq 0,\ \forall j,\ k,$$

$$\sum_{k=1}^{P_j}\theta_k^{(j)} \leq \gamma_j, 0 \leq \gamma_j \leq P_j,$$

$$\sum_{j=1}^{p}\gamma_j \leq M, 0 \leq M \leq P,$$

where γ_j is the shrinkage factor for the *j*-th group; and $\boldsymbol{\gamma} = \left(\gamma_1,\ \gamma_2,\ \dots\ ,\ \gamma_p\right)^T$ is the shrinkage vector for different groups. The optimization problem will determine the optimal $\boldsymbol{\theta}$ and $\boldsymbol{\gamma}$ to minimize the objective function. In this optimization problem, we have several constraints. $\beta_k^{(j)} = \theta_k^{(j)}\tilde{\beta}_k{}^{(j)},\ \theta_k^{(j)} \geq 0,\ \forall j,\ k$ are the constraints for NNG to encourage general

variable selection. The first level of constraints $\sum_{k=1}^{P_j} \theta_k^{(j)} \leq \gamma_j,\ 0 \leq \gamma_j \leq P_j$ controls the number of features selected within the group. The upper limit of γ_j is set to be P_j, which is the number of coefficients in each group. The second level of constraints $\sum_{j=1}^{p} \gamma_j \leq M,\ 0 \leq M \leq P$ controls the number of groups selected. The upper limit of M is set to be P, which is the total number of coefficients. These upper limits are recommended to be used if no prior knowledge on variable importance is available. The intuition behind these selections is to allow the least squares estimation of the model coefficients in the feasible region (i.e., when $\theta_k^{(j)} = 1$ for all k and j). If the group level shrinkage γ_j becomes zero, then all feature coefficients in the j-th group will be zero, which indicates that the j-th process variable is not significant, vice versa. If the feature level shrinkage $\theta_k^{(j)}$ becomes zero, then the k-th feature in the j-th group will not be significant, vice versa. Here M is a tuning parameter which can be selected by Bayesian Information Criterion (BIC), the validation data set, or Cross Validation (CV) [33].

To facilitate fast computation for Eq. (2.2), we adopt a similar approach to Deng and Jin [64] and use a second-order Taylor expansion at the current estimate of $\boldsymbol{\beta}$ to approximate the objective function and update this approximation iteratively. After Taylor expansion, the objective function has quadratic form shown in Eq. (2.3)

$$min\ L(\boldsymbol{\beta}) = {}^{1}/_{2}\left(\widetilde{\boldsymbol{Y}} - \boldsymbol{X}\boldsymbol{\beta}\right)^{T}\boldsymbol{W}\left(\widetilde{\boldsymbol{Y}} - \boldsymbol{X}\boldsymbol{\beta}\right), \tag{2.3}$$

where $\boldsymbol{W} = \text{diag}\left(p(\boldsymbol{x}_1)\left(1 - p(\boldsymbol{x}_1)\right),\ \ldots,\ p(\boldsymbol{x}_n)\left(1 - p(\boldsymbol{x}_n)\right)\right)$ is an $n \times n$ diagonal matrix; and $\widetilde{\boldsymbol{Y}} = \boldsymbol{X}\widetilde{\boldsymbol{\beta}} + \boldsymbol{W}^{-1}(\boldsymbol{Y} - \boldsymbol{p})$, $\boldsymbol{X} = (\boldsymbol{x}_1, \ldots, \boldsymbol{x}_n)^T$, $\boldsymbol{Y} = (y_1, \ldots, y_n)^T$, $\boldsymbol{p} = \left(p(\boldsymbol{x}_1),\ \ldots,\ p(\boldsymbol{x}_n)\right)^T$. This quadratic programming guarantees a global optimum and a brief derivation is provided in Appendix A. In this way, our method can select the significant groups and features

simultaneously with computational issues addressed. The optimal solution to minimize Eq. (2.3) can be obtained by following Algorithm 2.1.

Algorithm 2.1.

Step 1. Compute the initial estimate $\widetilde{\boldsymbol{\beta}}$, choose the range of tuning parameter M, and set the initial values for $\boldsymbol{\theta}$ and $\boldsymbol{\gamma}$;

Step 2. Solve for the $\boldsymbol{\beta}$ with the objective functions defined in Eq. (2.3), and denote the current $\boldsymbol{\beta}$ as $\boldsymbol{\beta}^j$ at the j-th iteration;

Step 3. Check the convergence. The problem converges if $\left\|\boldsymbol{\theta}^j - \boldsymbol{\theta}^{j-1}\right\| < \delta$. If not, update $\widetilde{\boldsymbol{\beta}}=\boldsymbol{\beta}^j$ and go back to Step 2. δ is a predetermined threshold, e.g., $\delta = 10^{-3}$.

Some practical suggestions for the initial values selection in Algorithm 2.1 are provided as follows. First, the initial estimates should not contain many zero terms. In our problem, the ridge regression coefficients are used as initial estimates. Such initial estimates are also recommended by Yuan and Lin [30] and Makalic and Schmidt [27]. Second, the tuning parameter M varies from a small value (e.g., 0.1) to the total number of coefficients under study. Third, due to the quadratic approximation of Eq. (2.2), the optimization will reach to the global optimum. The initial values of $\boldsymbol{\theta}$ and $\boldsymbol{\gamma}$ will not affect the optimal solutions. The initial values of $\boldsymbol{\theta}$ and $\boldsymbol{\gamma}$ in this chapter are set as 1's.

2.4. Simulation

To evaluate the prediction and variable selection performance of the proposed method, we conduct simulations under different scenarios. For each scenario, the simulation procedure follows the steps listed in Figure 2.3.

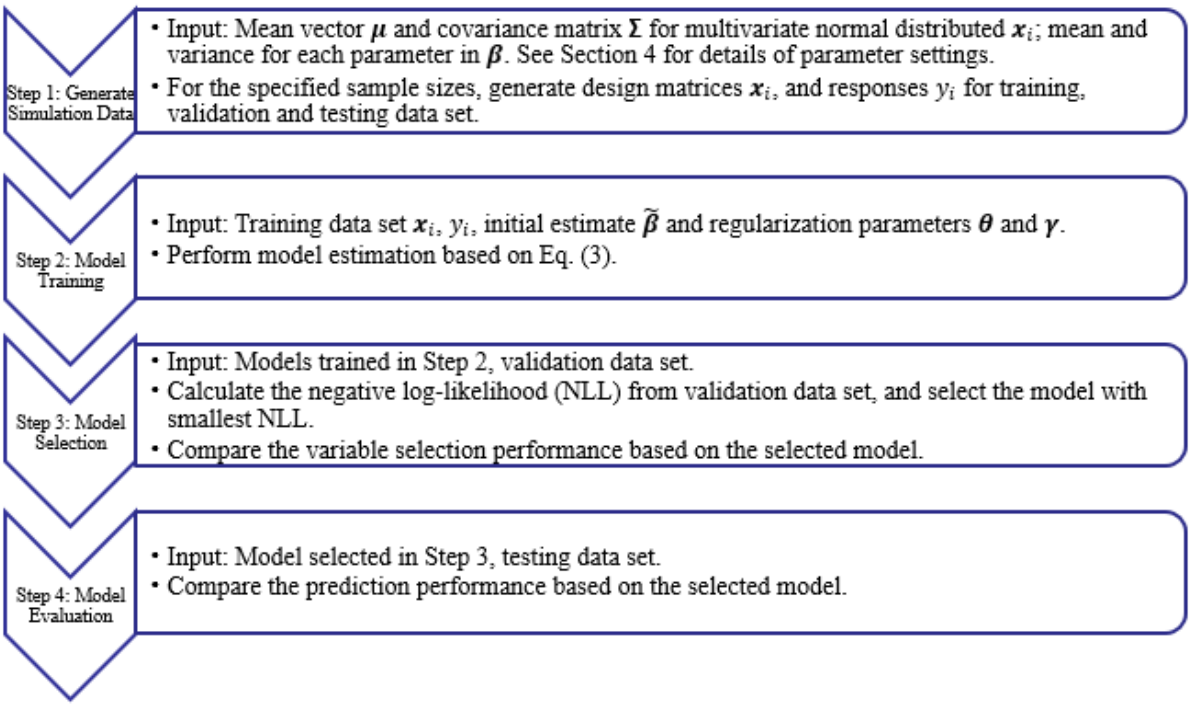

Figure 2.3. The Simulation Procedure in Functional Variable Selection

In the simulation, the response y_i follows binominal distribution

$$y_i = \begin{cases} 1 & w.p.\ p(\boldsymbol{x}_i) \\ 0 & w.p.\ 1 - p(\boldsymbol{x}_i) \end{cases}, \tag{2.4}$$

where $p(\boldsymbol{x}_i) = \frac{e^{{x_i}^T \boldsymbol{\beta}}}{1+e^{{x_i}^T \boldsymbol{\beta}}}$ and "$w.p.$" stands for "with probability". The predictors follow multivariate normal distribution with mean vector $\boldsymbol{\mu}$=($\mathbf{0}$, $\mathbf{0}$, …, $\mathbf{0}$) and covariance matrix $\boldsymbol{\Sigma}=\begin{bmatrix} \boldsymbol{\rho}_{11} & \boldsymbol{\tau}_{12} & \cdots & \boldsymbol{\tau}_{1p} \\ \boldsymbol{\tau}_{12} & \boldsymbol{\rho}_{22} & \cdots & \boldsymbol{\tau}_{2p} \\ \cdots & \cdots & \cdots & \cdots \\ \boldsymbol{\tau}_{1p} & \boldsymbol{\tau}_{2p} & \cdots & \boldsymbol{\rho}_{pp} \end{bmatrix}$, which are used to represent the wavelet coefficients of functional process variables. $\boldsymbol{\rho}_{ii}$ is the covariance matrix within a group and $\boldsymbol{\tau}_{ij}$ is the covariance matrix among groups. The number of groups is set to be 4 and the number of features in each group is set to be 5. In total, we have 20 predictors. To evaluate the performance of the proposed method, we test its performance by varying sample size, correlation structure and density of predictors.

Specifically, denote the sample sizes for training data sets, validation data sets and testing data sets as n_{tr}, n_{va}, and n_{te}, we choose n_{tr} to be 20, 100, 200, and set $n_{va} = n_{tr}$ and $n_{te} = 2n_{tr}$. These training, validation and testing data sets are generated from the same model as shown in Eq. (2.4). The covariance matrix of predictors within and among groups are set to be $\boldsymbol{\rho}=\begin{bmatrix} 1 & \rho^{|i-j|} & ... & \rho^{|i-j|} \\ \rho^{|i-j|} & 1 & ... & \rho^{|i-j|} \\ ... & ... & ... & ... \\ \rho^{|i-j|} & \rho^{|i-j|} & ... & 1 \end{bmatrix}$ and $= \begin{bmatrix} \tau & \tau^{|i-j|+1} & ... & \tau^{|i-j|+1} \\ \tau^{|i-j|+1} & \tau & ... & \tau^{|i-j|+1} \\ ... & ... & ... & ... \\ \tau^{|i-j|+1} & \tau^{|i-j|+1} & ... & \tau \end{bmatrix}$, respectively, where i and j are the row and column indices of the matrix $\boldsymbol{\rho}$ and $\boldsymbol{\tau}$. Two levels of correlation are selected for ρ and τ, and there are four combinations for the correlation structure. Specifically, the within group correlation coefficient ρ is set to be 0 and 0.6, and between group correlation coefficient τ is set to be 0 and 0.3. The density (denoted as *den.*) represents the proportion of significant predictors in the underlying model, and is set to be 10% and 40%. The coefficient for a significant predictor $\beta_k^{(j)}$ follows normal distribution $N(\mu_j, 0.1)$, and $\mu_j = 1, 1.3, 1.6, 1.9$, respectively, for the four groups of coefficients. In summary, there are 3 levels of sample size, 4 combinations of covariance structure, and 2 levels of density. In total, 24 scenarios of simulation settings are evaluated.

We compare our proposed method with Logistic Regression (LR), Lasso, Ridge, NNG, GrpLasso, and HLasso methods for the binary response prediction. We use the training data set to obtain the regression models, and use the validation data set for the tuning parameter selection. The model with the selected tuning parameter is used for variable selection comparison. We use a threshold to determine whether the coefficient is significant or not. If the magnitude (absolute value) of the coefficient is larger than the threshold, then the corresponding predictor is considered as significant. Specifically, the threshold is set to be 10^{-6}. Then we compare misclassification errors of the testing data set (called "testing error") for the proposed model and

all benchmark models. The above modeling process is repeated 50 times for each scenario. Figure 2.4 shows some simulation results (testing errors and overall variable selection errors) when the training sample size is 100 and $\rho = 0.6, \tau = 0$. More detailed simulation results (such as testing errors, Type I variable selection errors, Type II variable selection errors, and overall variable selection errors) as well as their definitions are described in Appendix B. In Figure 2.4, the bars represent the average errors over 50 simulation replicates under the same setting. The horizontal axis represents the benchmark methods and the proposed HNNG methods. Testing error is the error for the testing data. Overall variable selection error is calculated as the percentage of total incorrectly selected variables in the final estimated model among all predictors.

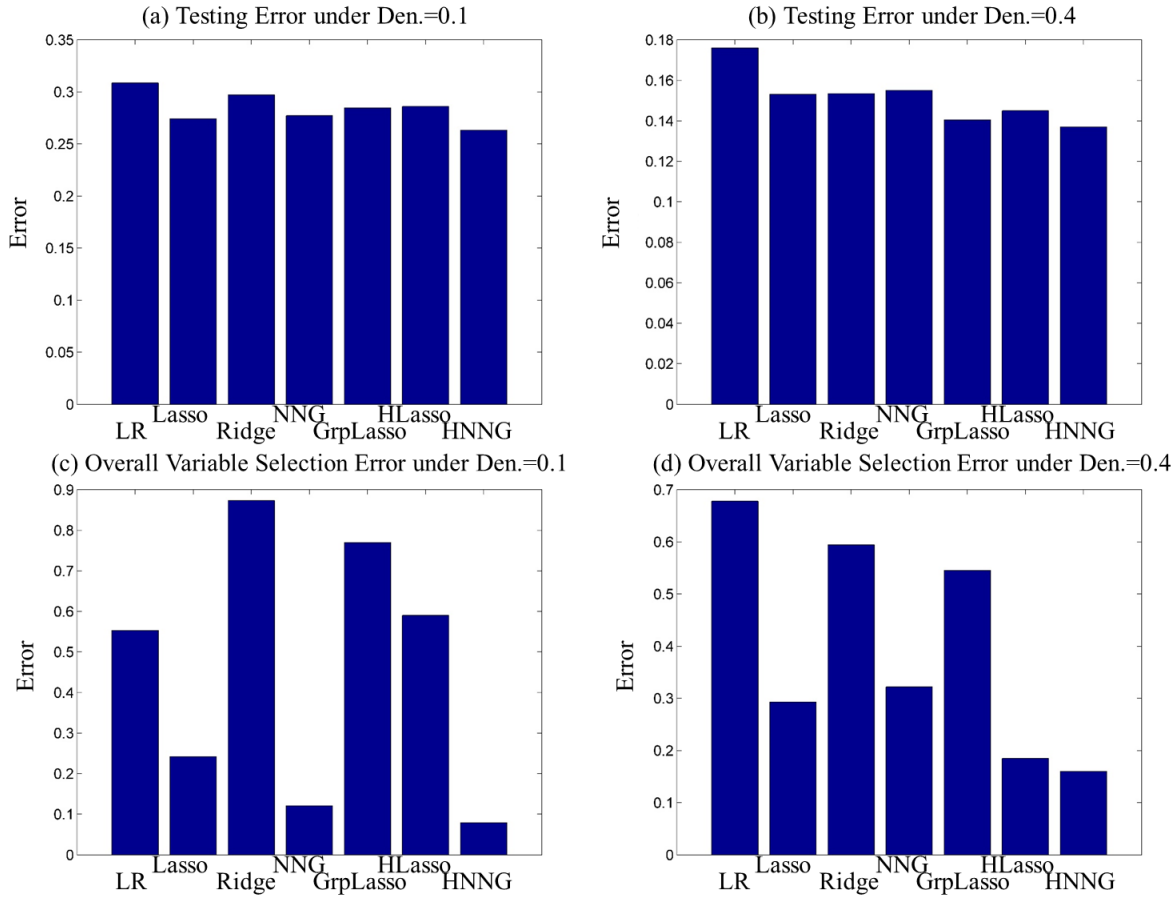

Figure 2.4. A Summary of Simulation Results over 50 Replications (a) Average Testing Errors under n_{tr}=100 $den.$=0.1 $\rho = 0.6$ $\tau = 0$; (b) Average Testing Errors under n_{tr}=100 $den.$=0.4 $\rho = 0.6$ $\tau = 0$; (c) Average Overall Variable Selection Errors under n_{tr}=100 $den.$=0.1 $\rho = 0.6$ $\tau = 0$; (d) Average Overall Variable Selection Errors under n_{tr}=100 $den.$=0.4 $\rho = 0.6$ $\tau = 0$

The simulation results are summarized as follows. When the sample size is small, GrpLasso has the best prediction performance, but HNNG is comparable, especially when the density is small. When the sample size becomes larger, the performance of HNNG is among the best. For variable selection performance, Lasso, NNG and HLasso perform well in variable selection when the sample size is small, but HNNG is comparable. When the sample size becomes larger, GrpLasso can identify the important features, but the corresponding Type II error (i.e., percentage of insignificant variables being selected in the final estimated model) is large since it selects all features in a significant group. HLasso performs well when the density is large. HNNG has comparable Type I variable selection error (i.e., percentage of significant variables not being selected in the final estimated model) and performs best for the Type II variable selection error under most settings. The overall variable selection performance of HNNG is among the best. The proposed method also has good variable selection performance for moderate sample size when the underlying model is sparse.

In summary, our proposed method outperforms the benchmark methods in terms of prediction performance when the sample size is large or the underling model is sparse. The proposed method can also eliminate insignificant predictors and outperforms the benchmark methods in terms of variable selection under the above situations. This is mainly because the HNNG can capture the hierarchical variable structure, and can be easily formulated as linear constraints in the optimization problem.

2.5. Case Study

We further use the proposed method to analyze the real data from a CZ process for single-crystal growth. 14 ingots (9 conforming ingots and 5 polycrystalline ingots) grown from the same furnace are used for the modeling. We select four key process variables based on the process built-in PID control algorithms: (1) heater power, which is the power supplied to the furnace to affect the temperature gradient in the furnace, (2) Set Point (SP) value, which is the temperature measurement by a thermocouple near the heater, (3) pull speed, which is the pulling speed of the crystal, and (4) furnace pressure, which is the pressure measurement of the furnace. These process variables need to be jointly controlled. For instance, if the thermal gradient at the interface is too large, the residual stress in the ingot will be large and the defect density will increase [39, 40]. On the other hand, if the thermal gradient is too small, the silicon melt will solidify at a slow rate and the corresponding growth speed will be slow. In addition, the larger the thermal gradient, the larger the ingot diameter tends to be; while higher pulling speed leads to smaller ingot diameter. As a result, the thermal gradient and pulling speed should be jointly adjusted for obtaining a target ingot diameter.

Figure 2.5 shows a few standardized process variables of a conforming batch and a polycrystalline batch. Each point in the figure represents the average of measurement over an hour. The sampling rate of the process variables is 1 measurement per minute. Notice that growth time of the polycrystalline batch is shorter than the conforming batch, because the process has to be stopped once polycrystalline defect is observed (the polycrystalline defect was recorded by an operator at around the 11^{th} hour in this example). From Figure 2.5, it is clear that the key process variables are functional variables and it is hard to distinguish between the polycrystalline batch and the conforming batch directly from these averaged measurements. Thus,

it is necessary to look into the detailed features of the measurements, and predict the polycrystalline in a timely manner.

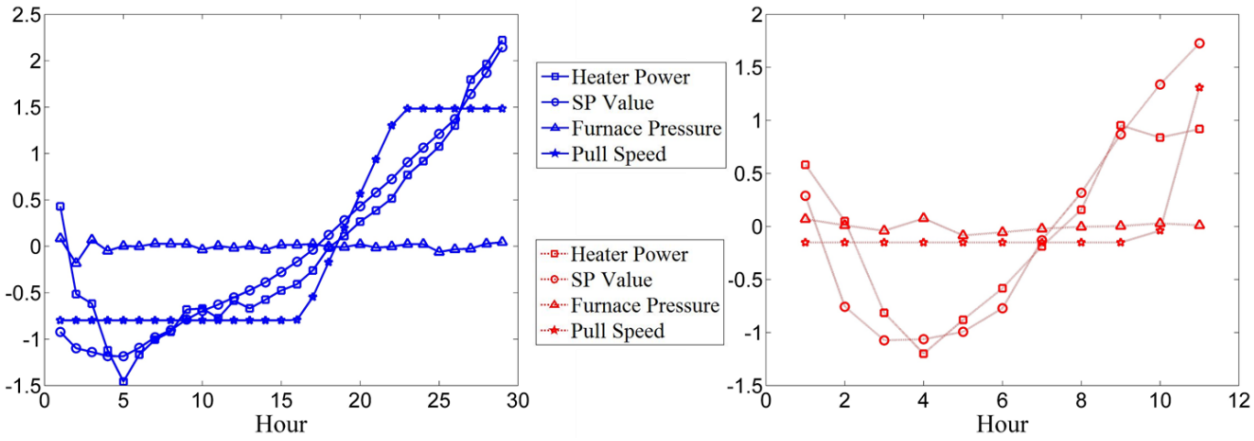

(a) A Conforming Batch (b) A Polycrystalline Batch

Figure 2.5. Selected Standardized Process Variables in a CZ Process

The selected process variables are standardized and then truncated into 15-minute windows. For each ingot, we select the window of the first 15-minute data points as the first sample, and label the window based on the quality of the ingot for that period of time. Then we select the window of the next 15-minute data points as the second sample, and label it. Thus, we can partition the whole batch of the data set into windows. After the truncation, these windows are regarded as separate samples modeled by Eq. (2.1). In this case, we can predict if the ingot becomes polycrystalline every 15 minutes. This is a significant improvement over the current practice, where the polycrystalline defect is detected by visual inspections performed by experienced operators. For each window, we perform wavelet analysis for each process variable with Daubechies 4 (db4) wavelet basis. The number of dilations is selected to be four, which is the maximum available dilations for a 15-minute window. Interested readers can refer to Ganesan *et al.* on how to select the number of dilations [58]. As a result, we process the raw data and turn it into 108 features as predictors and 435 samples in the modeling.

To evaluate the prediction performance, we use leave-one-out CV. In iterations, we use the data of all the 15-minute windows from 13 out of 14 ingots to estimate the model and perform variable selection. Then we evaluate the classification error based on the data of all the 15-minute windows of the ingot that is not used for model training (i.e., the left-out ingot). The average classification error of these left-out ingots is called "CV Error" and is used for model prediction performance evaluation. In the evaluation, the predicted binary response is compared with the real quality response labeled by domain expert. The tuning parameter M is selected by BIC.

Table 2.2. CV Error in the Crystal Growth Case Study

	LR	Lasso	Ridge	NNG	GrpLasso	HLasso	HNNG
Overall Classification Error	0.0785	0.0958	0.0805	0.0824	0.0671	0.0728	**0.0632**
Type I Classification Error	0.0581	0.0710	0.0409	0.0516	0.0366	0.0538	**0.0323**
Type II Classification Error	0.2456	0.2983	0.4035	0.3333	0.3158	**0.2281**	0.3158

Table 2.3. Variable Selection Results in the Crystal Growth Case Study

	LR	Lasso	Ridge	NNG	GrpLasso	HLasso	HNNG
Average Number of Groups Selected	4	4	4	3	2	1	2
Average Number of Features Selected	60	8.4285	17.5714	9.1429	28.9286	27	5.5714

The overall classification error, Type I classification error and Type II classification error are summarized in Table 2.2. The overall classification error is defined as the percentage of total misclassified samples. Type I classification error is defined as the percentage of conforming samples classified as polycrystalline samples, and Type II classification error is defined as the percentage of polycrystalline samples classified as conforming samples. The cut-off probability for the logistic regression prediction is selected to be 0.5. The selection of cut-off probability will influence the errors, and other cut-off probabilities can be selected based on one's needs. In Table 2.2, the model with the best prediction performance is highlighted in bold. We conclude

that the proposed method has the smallest overall classification error and Type I classification error. In summary, our proposed method can successfully identify polycrystalline defect while maintain the smallest overall error. Note that HNNG has larger Type II classification error than HLasso, and is comparable to Lasso, NNG and GrpLasso. One possible reason is that the sample sizes of the two classes are unbalanced. Specifically, the number of conforming samples is 378, and the number of nonconforming samples is 57. The variable selection results are summarized in Table 2.3. The proposed method selects moderate number of groups while it has the smallest number of features selected. The coefficients selected by HNNG come from the coarse levels of heater power and SP value, which implies that the changes in thermal field are responsible for polycrystalline defect in the production for case study. The detailed information of the selected local features is available in Appendix C.

2.6. Conclusions of Functional Variable Selection

A crystal growth process is the first step in semiconductor manufacturing industry, which suffers from the polycrystalline defect. In the current practice, a huge amount of polycrystalline ingots are discarded, and a lot of energy and time are wasted in the rework stage.

With abundant observational data available, we propose a logistic regression model with HNNG based variable selection to extract important features from functional *in situ* process variables. The method encourages variable selection in hierarchical group structure for a binary response, where each group represents a functional process variable and each predictor in the group is a wavelet coefficient reflecting local time and frequency information. The model performance is compared with benchmark methods, such as Lasso, NNG, GrpLasso and HLasso, when sample size, correlation structure and density of predictors are varied. The proposed method is better than benchmark methods in terms of prediction and variable selection, when the sample size is

large or the underlying model is sparse. The proposed method also performs well for the real data set from a crystal growth process.

It is worth mentioning that the functional variable selection is a general variable selection method for *in situ* process variables, and can be widely applied to situations with functional variables measured. As the sensor network become more and more complex, it is important to select, among the different sensors in the sensor network, the most important sensor channels for the manufacturing quality modeling. Moreover, the process monitoring and control can be performed based on the functional variable selection.

Chapter 3. Functional Graphical Models for a Plasma Spray Process Modeling

3.1. Introduction

Graphical models are powerful tools to model the underlying relationships among variables in various systems. The graphical models have been applied to a variety types of systems such as healthcare [65, 66], social science [67, 68] and manufacturing systems [69, 70]. In a graphical model, *nodes* represent the variables, while *edges* between nodes characterize the relationships among variables. The nodes and variables are used interchangeably in this chapter. An edge connecting two nodes indicates that the nodes are conditionally dependent with other variables. By specifying the conditional dependence among the variables, a graphical model essentially decomposes a multivariate distribution of a set of variables into a few conditional distributions [71]. Each conditional distribution consists of a subset of variables, which is in much lower dimension than the joint distribution. In other words, while many systems consist of multivariate variables whose joint distribution is difficult to derive, graphical models provide a flexible and interpretable approach to build the multivariate system model in a bottom-up fashion. By exploiting the "graphical representation" of the variables, the estimation problem of the joint distribution becomes the estimation problem of a few low-dimensional conditional distributions. For more details about graphical models, refer to [71, 72].

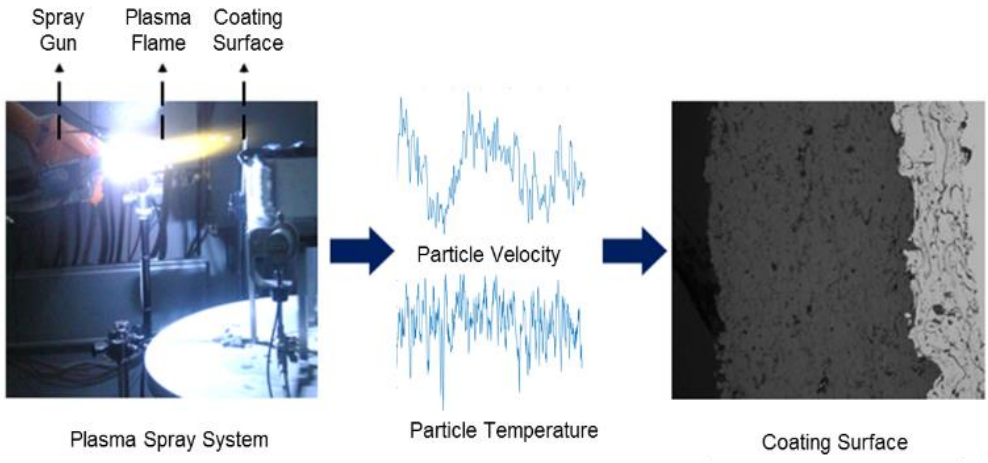

Figure 3.1. A Schematic Illustration of a Plasma Spray Process [6]

Despite being a powerful type of model, existing graphical models cannot be directly used to model a system with functional variables, which is widely encountered in manufacturing. For example, a plasma spray process generates coating layers on engineering surfaces to prevent the potential wear and corrosion. This manufacturing technology has been widely used in aerospace, automobile, and biomedical implants applications [6, 73]. Figure 3.1 shows a schematic illustration of a plasma spray process, where the coating particles are melted or semi-melted by the plasma formed in the spray gun, and propelled to the coating surface. Complex physical, chemical, and mechanical processes take place in the plasma spray process. There are many potential factors which can affect the coating properties, and an adequate model for the plasma spray process is lacking due to the process complexity and variability of the *in situ* process variables [73, 74]. Some *in situ* process variables, such as particle velocity and particle temperature, are measured as functional variables over time. These functional variables reflecting important process conditions will be used to model the plasma spray process. This is an important step to address the on-demand manufacturing needs for mass personalization, as the variable relationships of *in situ* process variables and the coating properties reflect the manufacturing process itself, which may remain the same for different specifications and quality

targets. If a graphical model is adopted to model the plasma spray process, the graphical model should be able to characterize the relationships among scalar variables and functional variables. It is worth pointing out that, the "process map" was widely used to link the coating properties with particle velocity, particle temperature, and other offline setting variables. This "process map" can also provide a recommended range for a particular setting variable for desired coating properties [75, 76]. But the technique is essentially a qualitative graphic representation of the relationships of variables. It lacks the capacity to characterize the features of the particle velocity and particle temperature in functional form, and quantify their effects on coating properties.

In this chapter, we aim to extend the scalar version of graphical models to functional graphical models for manufacturing. A naïve way to achieve this objective is to derive summary statistics (e.g., mean or standard deviation) from the functional variables, and then treat the summary statistics as scalar variables in appropriate existing graphical models. However, this approach ignores the structure in the functional variables and may oversimplify the problem. To mitigate this challenge, we propose to use functional data analysis to characterize the variation patterns of the functional variables, which is incorporated in the functional graphical model. In particular, we will investigate a directed graphical model, Bayesian Network (BN), in this chapter. The structure of a BN is a *Directed Acyclic Graph* (DAG), which is composed of acyclic directed arcs between nodes. If there is a directed arc from a variable X to another variable Y, then X is called a *parent* of Y, and Y is called a *child* of X. Two nodes which share a common child are called *spouses*. In many applications, the ordering of variables can be obtained from domain knowledge [77-81], which greatly facilitate the learning of the BN by reducing the number of possible graphical model structures in these applications. For example, the final coating properties can be affected by offline setting variables, such as power supply and carrier gas speed,

and *in situ* process variables reflecting the particle conditions, such as particle velocity and particle temperature. Meanwhile, the *in situ* process variables will also be affected by offline setting variables. With the *variable orderings*, the learning of BN can be reformulated as a sequential identification of the parent variables for each variable. Particularly, the distribution of each variable conditional on its parent variables takes the form as a regression model for multivariate Gaussian systems. Thus, a regression-type parameterization can be used for BN [65, 66].

In the proposed functional graphical model, we adopt the functional data analysis and represent a functional variable using basis expansion. Since the basis expansion provides a space to characterize the functional variables, each measurement of the functional variables can be converted to a vector of the basis expansion coefficients. When the regression-type of parameterization is used, the estimation of the graphical model becomes the regression modeling of each node with its potential parents. To identify the parents with limited sample size, we use the penalized regression with a combination of l_1 norm penalty and a *difference from the mean* penalty. While the l_1 norm penalty has been widely used in the literature, we introduce the difference from the mean penalty tailored for the functional variables. This is because the elements in a functional variable tend to have similar relationships with a certain parent variable. Such a penalization has been studied in multi-task learning literature [82, 83]. In addition, a Fast Iterative Shrinkage-Thresholding Algorithm (FISTA) is adopted for the model estimation. Simulation studies and a case study from a plasma spray process are used to demonstrate the performance of the proposed method.

The rest part of this chapter is organized as follows. In Section 3.2, the state-of-the-art graphical models learning approaches are reviewed. In Section 3.3, the proposed functional graphical

modeling method is discussed. The proposed method is demonstrated with simulation studies and a case study in a plasma spray process in Sections 3.4 and 3.5, respectively. Finally, Section 3.6 concludes this chapter.

3.2. Research Background

A variety of models are used for manufacturing systems improvement, such as regression models [5, 20, 84], state space models [85-89], graphical models [69, 70] and data mining methods [90-92]. Among these methods, graphical models provide a flexible and interpretable approach for building system models in a bottom-up fashion, and will be adopted in this chapter.

To learn a graphical model, one can adopt constraint-based methods, search and score based methods, and hybrid methods. Constraint-based methods learn the graphical model via conditional independence tests. If a pair of nodes is independent in the test, then the edge between the nodes will be removed in the final graph. The major drawbacks of constraint-based methods are: 1) the selection of threshold value in the conditional independence tests is arbitrary, 2) the number of conditional independence tests to be performed is large for high dimensional problems, and 3) the error will be inflated for a large number of conditional independence tests [66, 72]. In search and score based methods, a score is used to quantify the fitness of a graphical model, and local search and optimization method is used to find the best score by varying the graph structure. Since the number of potential graph structures increases exponentially with the number of nodes, the exhaustive search for high dimensional problems is computationally expensive [66, 72]. Inexact search methods, such as genetic algorithm [93] and ant colony optimization [94], can be used instead, but the solutions from these methods can be trapped into a local optima.

The hybrid methods reduce the search space for search and score based methods via constraint-based reasoning [95]. For example, Sparse Candidate (SC) algorithm assumes the maximum number of parents for each node to be a small constant *k* [96]. However, it is hard to determine the maximum number of parents, and the assumption that all nodes have the same maximum number of parents may not hold. For another example, max-min hill-climbing algorithm identifies potential parents and children (neighbors) for each node via conditional independence tests, and then performs the search in the potential neighbors [97]. Such an approach does not perform well in high dimensional settings [66].

In recent years, a kind of hybrid method is widely used for learning graphical models in high dimensional settings via penalized regression based methods [66, 80, 81, 98-101]. The basic idea is to learn the penalized conditional log-likelihood of each variable given other variables in order to find its parent variables. For example, an l_1-penalized regression technique is introduced in neighborhood selection of each node for undirected Gaussian graphical models [80, 99]. It is shown that the neighborhood selection method is consistent [99]. The l_1-penalization is also used to learn the structure for directed Gaussian graphical models [77, 98]. The basic procedure firstly learns the Markov blanket for each node, and then learns the directed graph by some local search methods. Huang *et al.* propose a novel penalization approach to learn the directed Gaussian graphical model structure and coefficients in one step [66]. The penalized regression approach is also applied for learning an Ising graphical models by l_1-penalized logistic regressions [102]. A group Lasso penalized regression approach is proposed for learning a mixed graphical model with both continuous and discrete variables [103].

The existing methods are developed for graphical models with only scalar variables, which cannot be used to model the aforementioned systems with both scalar variables and functional

variables. The challenge we aim to address in this chapter stems from the fact that many variables in the BN are functional variables, such as the *in situ* process variables in manufacturing. Therefore, a functional graphical model is proposed to attack the problem.

3.3. Proposed Method

3.3.1. Overview of the Proposed Method

A functional graphical model is proposed for modeling with both scalar and functional nodes in a multivariate Gaussian system. As we have mentioned, with the variable orderings, the learning of the graphical model can be simplified to sequential identification of the parent variables for each variable. The basic assumptions of the proposed method are that the functional variables can be represented through basis expansion, and the relationship among functional variables and scalar variables is stationary. Such a stationary assumption implies that the variable relationships in the system under study will not vary over time, which is generally true for manufacturing systems under normal operation. The variable relationships can be characterized as static models, where the model parameters are not changing over time. In a stationary system, the functional graphical model identifies the variable dependency (rather than the causal relationship) embedded in the measurement data collected during system operation. It should be emphasized that for a dynamic system, the variable relationship may change over time, and the corresponding graphical model structure may change dependent on the data. For the dynamic system, dynamic graphical models can be developed to handle the problem [104], which is out of the scope of the research in this chapter.

An overview of the proposed framework is illustrated in Figure 3.2. First, the observed data form scalar and functional nodes, which can be used as either predictors or responses in the regression models. These regression models will be trained sequentially following the variable orderings. If

the current node of interest is a scalar variable, then the scalar response regression will be used. If the current node of interest is a functional variable, then the functional response regression will be used. These scalar response regressions and functional response regressions form the basis for the functional graphical model. Penalizations will be used to control the overall model complexity and enhance the learning accuracy. Finally, the model coefficients will be estimated via FISTA.

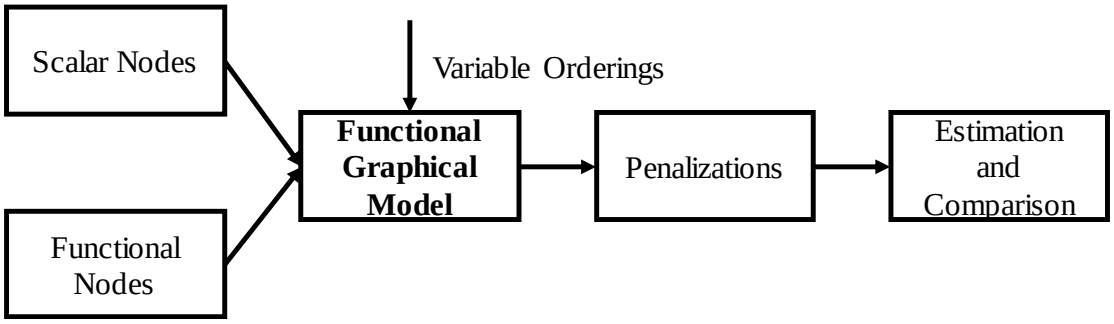

Figure 3.2. The Proposed Functional Graphical Modeling Framework

3.3.2. Graphical Models with both Functional and Scalar Nodes

Denote the scalar nodes as X_j, $j = 1,2,\cdots,p_s$, and the parents of a scalar node X_j as $PA(X_j)$. Denote functional nodes as $\boldsymbol{Y}_j$, $j = 1,2,\cdots,p_f$, and the parents of a functional node $\boldsymbol{Y}_j$ as $PA(\boldsymbol{Y}_j)$. p_s and p_f are the number of scalar nodes and functional nodes, respectively. Let $x_{j,i}$ be the i-th observation of the node X_j, and $y_{j,i}(t) = \left(y_{j,i,1},\cdots,y_{j,i,m}\right)^T$ be the i-th observation of the node $\boldsymbol{Y}_j$. $y_{j,i,t}$, $t = 1,\ldots m$ is the t-th element in the discrete realization of $y_{j,i}(t)$.

The characterization of the potential relationships among these variables lays the basis for any graphical model learning. In general, to characterize the relationships among a functional response node $\boldsymbol{Y}_j$ and its potential parents $PA(\boldsymbol{Y}_j)$, the following functional response regression model can be used [105]

$$y_{j,i}(t) = \sum_{r\in PA(\boldsymbol{Y}_j)} x_{r,i} w_{r,j}(t) + \sum_{r\in PA(\boldsymbol{Y}_j)} y_{r,i}(t) b_{r,j}(t) + e_{j,i}(t), t \in \Psi_j, \quad (3.1)$$

where $w_{r,j}(t)$ are the model coefficients for the *r*-th scalar parent of $\boldsymbol{Y}_j$, $b_{r,j}(t)$ are the model coefficients for the *r*-th functional parent of $\boldsymbol{Y}_j$, and $e_{j,i}(t) \sim N(0, \boldsymbol{\Sigma}_j)$ is the error term. Ψ_j denotes the time continuum of $\boldsymbol{Y}_j$. For example, a $\boldsymbol{Y}_j$ that belongs to the *in situ* process variables in a plasma spray process will be used as the functional response node in Eq. (3.1). An important assumption used in many functional regression models is that the functional coefficients, such as $b_{r,j}(t)$, can be represented by a set of basis functions [105]. In this chapter, we adopt this basis representation (such as spline and wavelet expansion). After applying basis expansion for the functional components in Eq. (3.1) with $\boldsymbol{\Theta}(\mathrm{t}) = \left(\theta_1(t), \theta_2(t), \ldots, \theta_K(t)\right)^T$, one can obtain $b_{r,j}(t) = \boldsymbol{\beta}_{r,j}{}^T \boldsymbol{\Theta}(t)$, $w_{r,j}(t) = \boldsymbol{\omega}_{r,j}{}^T \boldsymbol{\Theta}(t)$, and $e_{j,i}(t) = \boldsymbol{\varepsilon}_{j,i}{}^T \boldsymbol{\Theta}(t)$ [105]. Note that $\boldsymbol{\beta}_{r,j}, \boldsymbol{\omega}_{r,j}, \boldsymbol{\varepsilon}_{j,i} \in \mathrm{R}^{K\times 1}$. After the basis expansion, we have

$$y_{j,i}(t) = \sum_{r\in PA(\boldsymbol{Y}_j)} x_{r,i} \boldsymbol{\omega}_{r,j}{}^T \boldsymbol{\Theta}(t) + \sum_{r\in PA(\boldsymbol{Y}_j)} y_{r,i}(t) \boldsymbol{\beta}_{r,j}{}^T \boldsymbol{\Theta}(t) + \boldsymbol{\varepsilon}_{j,i}{}^T \boldsymbol{\Theta}(t), t \in \Psi_j. \quad (3.2)$$

The coefficients $\boldsymbol{\omega}_{r,j} = \left(\omega_{r,j,1}, \cdots, \omega_{r,j,K}\right)^T$ and $\boldsymbol{\beta}_{r,j} = \left(\beta_{r,j,1}, \cdots, \beta_{r,j,K}\right)^T$ in Eq. (3.2) can be estimated by minimizing the loss function

$$min\ \mathcal{L}\left(\boldsymbol{\omega}_{r,j}, \boldsymbol{\beta}_{r,j}, r \in PA(\boldsymbol{Y}_j)\right) = \sum_{i=1}^{n} \sum_{t\in\Psi_j} \Big(y_{j,i}(t) - \sum_{r\in PA(\boldsymbol{Y}_j)} x_{r,i} \boldsymbol{\omega}_{r,j}{}^T \boldsymbol{\Theta}(t) -$$

$$\sum_{r\in PA(\boldsymbol{Y}_j)} y_{r,i}(t) \boldsymbol{\beta}_{r,j}{}^T \boldsymbol{\Theta}(t)\Big)^2, \quad (3.3)$$

where n is the number of samples, and $\mathcal{L}(\cdot)$ is the loss function.

To characterize the relationships among a scalar response node X_j and its potential parents$PA(X_j)$, the following scalar response regression model can be used

$$x_{j,i} = \sum_{r\in PA(X_j)} x_{r,i} w_{r,j} + \sum_{r\in PA(X_j)} \int_{t\in\Psi_r} y_{r,i}(t) b_{r,j}(t) dt + \varepsilon_{j,i}, \quad (3.4)$$

where $w_{r,j}$ is the model coefficient for the *r*-th scalar parent of X_j, $b_{r,j}(t)$ are the model coefficients for the *r*-th functional parent of X_j, and $\varepsilon_{j,i} \sim N(0, \sigma_j^2)$ is the error term. Ψ_r denotes

the time continuum of $\boldsymbol{Y}_r$. For example, in the plasma spray process, an X_j that belongs to coating property will be selected as the scalar response node in Eq. (3.4). Similarly, basis expansion for $b_{r,j}(t)$ yields $b_{r,j}(t) = \boldsymbol{\beta}_{r,j}{}^T \boldsymbol{\Theta}(t)$. Therefore, Eq. (3.4) becomes

$$x_{j,i} = \sum_{r \in PA(X_j)} x_{r,i} w_{r,j} + \sum_{r \in PA(X_j)} \int_{t \in \Psi_r} y_{r,i}(t) \boldsymbol{\beta}_{r,j}{}^T \boldsymbol{\Theta}(t) dt + \varepsilon_{j,i}. \quad (3.5)$$

The coefficients $w_{r,j}$ and $\boldsymbol{\beta}_{r,j}$ can be estimated by minimizing the loss function

$$min\ \mathcal{L}\left(w_{r,j}, \boldsymbol{\beta}_{r,j}, r \in PA(X_j)\right) = \sum_{i=1}^{n} \Big(x_{j,i} - \sum_{r \in PA(X_j)} x_{r,i} w_{r,j} -$$

$$\sum_{r \in PA(X_j)} \sum_{t \in \Psi_r} y_{r,i}(t) \boldsymbol{\beta}_{r,j}{}^T \boldsymbol{\Theta}(t) \Big)^2. \quad (3.6)$$

3.3.3. Functional Graphical Models Learning Algorithm

The learning of the graphical model is equivalent to identifying the parent variables of each variable. In Huang *et al.* [66], a sparse learning formulation with l_1 norm has been proposed for robust learning that can scale-up to high-dimensional problems. We propose our learning method for functional graphical models within this framework. The primary difference of the proposed method and the one in the literature is that the functional variables are considered the first time in a graphical model. Moreover, the system can be better modeled by a combination of the l_1 norm and *difference from the mean* penalty for these functional variables with the computational issue addressed. We incorporate variable orderings to better specify the model structure. Denote the candidate parent variables of a scalar node X_j as $C(X_j)$, and candidate parent variables of a functional node $\boldsymbol{Y}_j$ as $C(\boldsymbol{Y}_j)$. Then, the functional graphical models learning can be decomposed into a sequence of sparse learning problems.

We propose to use a combination of the penalty methods. First, an l_1 norm is applied to encourage a parsimonious and interpretable model, and control the overall model complexity

$$\Omega_1(A) = \sum_{j=1}^{p} \left\| \boldsymbol{a}_j \right\|_1, \quad (3.7)$$

where $A = (\boldsymbol{a}_1, \cdots, \boldsymbol{a}_p)$ contains the model coefficients, and $\|\boldsymbol{a}_j\|_1$ is the l_1 norm for $\boldsymbol{a}_j = (a_{j,1}, \cdots, a_{j,K})^T$. Second, a functional node in the graphical model actually consists of multiple "scalar variables", i.e., each of the basis expansion coefficients is a scalar variable. In a stationary manufacturing process, the relationships between these scalar variables in a functional node and its parent node will be similar. Therefore, the basis expansion coefficients of the same functional node should have similar coefficients in the functional response regression model. Thus, the difference from the mean penalty is used to exploit this similarity to enhance the learning of the relationships among variables. Denote the number of basis expansion coefficients as *m* and the regression coefficients of the *t*-th basis expansion coefficient as $\boldsymbol{c}_t$. The penalty on the difference from the mean is defined as [82]

$$\Omega_2(C) = \sum_{t=1}^{m} \|\boldsymbol{c}_t - \boldsymbol{c}_{mean}\|_2^2 = \|\boldsymbol{CR}\|_F^2, \tag{3.8}$$

where $\boldsymbol{C} = (\boldsymbol{c}_1, \cdots, \boldsymbol{c}_m)$, $\boldsymbol{c}_{mean}$ is the mean coefficients vector over *m* basis expansion coefficients, $\|\boldsymbol{c}_t - \boldsymbol{c}_{mean}\|_2$ is the l_2 norm for $\boldsymbol{c}_t - \boldsymbol{c}_{mean}$, $\|\boldsymbol{CR}\|_F$ is the Frobenius norm for $\boldsymbol{CR}$, and $\boldsymbol{R} = \begin{bmatrix} 1-\frac{1}{m} & -\frac{1}{m} & \cdots & -\frac{1}{m} \\ -\frac{1}{m} & 1-\frac{1}{m} & \cdots & -\frac{1}{m} \\ \vdots & \vdots & \ddots & \vdots \\ -\frac{1}{m} & -\frac{1}{m} & \cdots & 1-\frac{1}{m} \end{bmatrix}$. This penalty tends to force the similarity of model coefficients for the basis expansion coefficients belonging to the same functional variable.

By adding the penalties to the loss functions Eqs. (3.3) and (3.6), the model coefficients can be estimated by minimizing the penalized loss functions in the following two scenarios:

a) If the current node is a functional node

$$min\ \mathcal{L}\left(\boldsymbol{\omega}_{r,j}, \boldsymbol{\beta}_{r,j}, r \in C(\boldsymbol{Y}_j)\right) + \lambda_{1,j}\left(\sum_{r\in C(\boldsymbol{Y}_j)}\|\boldsymbol{\omega}_{r,j}\|_1 + \sum_{r\in C(\boldsymbol{Y}_j)}\|\boldsymbol{\beta}_{r,j}\|_1\right) + \lambda_{2,j}\left(\|\boldsymbol{W}_j\boldsymbol{R}\|_F^2 + \|\boldsymbol{B}_j\boldsymbol{R}\|_F^2\right). \tag{3.9}$$

b) If the current node is a scalar node

$$min\ \mathcal{L}\left(w_{r,j}, \boldsymbol{\beta}_{r,j}, r \in C(X_j)\right) + \lambda_{3,j}\left(\sum_{r\in C(X_j)}|w_{r,j}| + \sum_{r\in C(X_j)}\left\|\boldsymbol{\beta}_{r,j}\right\|_1\right), \tag{3.10}$$

where $\boldsymbol{W}_j = \left(\boldsymbol{\omega}_{1,j}, \cdots, \boldsymbol{\omega}_{r,j}, \cdots, \boldsymbol{\omega}_{n_y,j}\right)^T$ and $\boldsymbol{B}_j = \left(\boldsymbol{\beta}_{1,j}, \cdots, \boldsymbol{\beta}_{r,j}, \cdots, \boldsymbol{\beta}_{n_y,j}\right)^T$ are the model coefficients, and n_y is the number of candidate parents for $\boldsymbol{Y}_j$. The penalty $\left\|\boldsymbol{B}_j\boldsymbol{R}\right\|_F^2$ is included under the assumption that the system under study is a stationary system, and the relationship between a functional node and its functional parent is similar at different time instances. For a dynamic system, dynamic graphical models can be developed to capture the system dynamics [104]. $\lambda_{1,j}$ and $\lambda_{3,j}$ are the tuning parameters that control the model complexity, and $\lambda_{2,j}$ is the tuning parameter that controls the coefficients similarity across elements in a functional node. Note that when $\lambda_{2,j} = 0$, the problem will be reduced to the penalized regression based method used in the literature [66]. These tuning parameters can be selected by minimizing BIC, prediction error in a validation data set, or prediction error in CV [33].

The functional variables in a high dimensional space will pose challenges to the learning of the functional graphical model. To perform a pair-wise model estimation in Eqs. (3.9) and (3.10), black-box convex optimization methods could be applied. However, computation via black-box methods will be time consuming [106]. In recent years, proximal algorithms are shown to be effective for solving high dimensional problems [83, 107, 108]. In this chapter, the FISTA is adopted. The FISTA is suitable for solving the objective function that is composed of a smooth convex function and a nonsmooth convex penalization term, as shown in Eqs. (3.9) and (3.10). The key subroutine in FISTA is to compute the proximal operator that admits a closed-form solution, and update the optimization solution iteratively. See Beck and Teboulle for more details [108].

3.4. Simulation

In the simulation, the proposed functional graphical model (denoted Proposed) is compared with two benchmark models. In the first benchmark model, the elements (i.e., basis expansion coefficients) in a functional node are separately modeled (denoted Benchmark Separate Node) via Eq. (3.10). In the second benchmark model, the summary statistics (i.e., mean and standard deviation) of a functional variable are modeled (denoted Benchmark Summary Statistics) via Eq. (3.10). Note that a scalar response node will be modeled in a same way via Eq. (3.10) in the proposed and benchmark models. Therefore, only functional response nodes are simulated and compared in the simulation studies. To evaluate the performance of the proposed model versus the benchmark models under different scenarios, intensive simulation studies are performed. Several important factors that usually affect the prediction and variable selection accuracy of graphical models are selected. The factors investigated in the simulation studies include: 1) *density*, which is the proportion of significant coefficients in the underlying model for each response node; 2) *sample size*, which is the training sample size for each response node; 3) *overlap*, which is the proportion of overlap samples across elements in a functional node. This factor is investigated since the missing data are frequently encountered for on-line sensor data, and the systems may vary due to the change of machine status and raw material, which may lead to the variation of samples across elements in a functional node; 4) *correlation*, which controls the correlation in the design matrix (detailed form will be given later); 5) *Signal-to-Noise Ratio (SNR)*, which is the ratio of variance of the response and noise term; and 6) *SNR group difference*, which is the difference of SNR among different functional variables. The detailed settings and meanings for the above factors are listed in Table 3.1. In total, 144 combinations of simulation scenarios are studied.

Table 3.1. Simulation Factors Settings for Functional Graphical Models

Factors	Levels	Meanings
Density	Level 1: 0.1 Level 2: 0.2	Proportion of significant coefficients in the underlying model
Sample size	Level 1: 10 Level 2: 60	Training sample size
Overlap	Level 1: none Level 2: half Level 3: all	Overlap of samples across elements in a functional node
Correlation	Level 1: 0.3 Level 2: 0.55 Level 3: 0.8	ρ that governs the covariance matrix of design matrix
SNR	Level 1: 10 Level 2: 1	Ratio of variance of the response and noise term
SNR group difference	Level 1: none Level 2: rescaling by a factor u~[0.2,2]	Difference of SNR among different functional variables

The simulation data are generated by mimicking Eq. (3.2) with

$$\boldsymbol{y}_{k,i} = \boldsymbol{x}_{k,i}^{T}\boldsymbol{\beta}_k + \boldsymbol{\varepsilon}_{k,i}, \tag{3.11}$$

where $\boldsymbol{y}_{k,i} = \left(y_{k,i,1}, \cdots, y_{k,i,m}\right)$ is the response of the i-th sample at the k-th functional response node, and $\boldsymbol{x}_{k,i} = \left(x_{k,i,1}, \cdots, x_{k,i,p}\right)^{T}$ is the input of the i-th sample at the k-th node, m is the total number of elements in the functional node and p is the total number of inputs. The elements in $\boldsymbol{y}_{k,i}$ are used to represent the basis expansion coefficients in the i-th realization of the functional variable, and the elements in $\boldsymbol{x}_{k,i}$ are used to represent the i-th realization of candidate parent variables of $\boldsymbol{y}_{k,i}$. It is also possible to simulate the functional variables first and then convert the functional variables to basis expansion coefficients. Both simulation strategies will not change the nature of the problem. Here, $\boldsymbol{x}_{k,i} \sim N(\boldsymbol{\mu}_{\boldsymbol{x}}, \boldsymbol{\Sigma})$, where $\boldsymbol{\mu}_{\boldsymbol{x}} \in \mathrm{R}^{p\times 1}$ is a zero vector, and $\boldsymbol{\Sigma} \in \mathrm{R}^{p\times p}$ with the (i, j)-th element $\Sigma_{i,j} = \rho^{|i-j|}$. ρ is a constant that controls the correlation level among inputs. $\boldsymbol{\beta}_k = \left(\boldsymbol{\beta}_{k,1}, \cdots \boldsymbol{\beta}_{k,m}\right)$ is a $p \times m$ matrix of model coefficients. The j-th column of $\boldsymbol{\beta}_k$ is $\boldsymbol{\beta}_{k,j} = \left(\beta_{k,j,1}, \cdots, \beta_{k,j,p}\right)^{T}$ that characterizes the relationships between the candidate parent

variables and the *j*-th element in the functional variable. In the simulation, $\boldsymbol{\beta}_{k,j} = \boldsymbol{\beta}_{k,0} + \boldsymbol{\tau}_k + \boldsymbol{\theta}_{k,j}$, $\boldsymbol{\beta}_{k,0}$ is the mean coefficient vector, $\boldsymbol{\tau}_k$ is a perturbation term for the *k*-th node, and $\boldsymbol{\theta}_{k,j}$ is a perturbation term for the *j*-th column of $\boldsymbol{\beta}_k$. $\boldsymbol{\tau}_k$ controls the difference of coefficients among functional nodes, and $\boldsymbol{\theta}_{k,j}$ controls the difference of coefficients within a functional node. The scale of $\boldsymbol{\theta}_{k,j}$ is much smaller than $\boldsymbol{\tau}_k$. $\boldsymbol{\beta}_{k,j}, \boldsymbol{\beta}_{k,0}, \boldsymbol{\theta}_{k,j}, \boldsymbol{\tau}_k \in \mathrm{R}^{p\times 1}$. $\boldsymbol{\varepsilon}_{k,i} \in \mathrm{R}^{1\times m}$ is the error term that follows $N(\mathbf{0}, \sigma^2 diag(1,1,\cdots,1))$. The error term can be used to represent the difference between the basis expansion coefficients (i.e., $\boldsymbol{y}_{k,i}$) and the "perfect" basis expansion coefficients (i.e., $\boldsymbol{y}_{k,i} - \boldsymbol{\varepsilon}_{k,i}$) that fits perfectly for the functional variable.

The detailed settings in the simulation studies are: the dimension of input p is 50, the number of functional nodes k is 5, and number of elements m in each functional node is 100. Therefore, there will be 5 or 10 significant variables in the model, depending on the density level in Table 3.1. The sample size of the training data set is 10 or 60, as specified in Table 3.1. The number of samples in the validation and testing data set is twice of that of the training data set. If the factor overlap is set to level "none" or "all", the samples across elements in a functional node will be totally different or the same. The data generation for the level "half" of overlap works as follows: for two consecutive elements i and j in a functional node, the second half of i and the first half of j will have the same set of samples. The settings of other factors can be easily found based on their definitions in Table 3.1. The simulation data are generated for 100 replications of the data set, and the average model performance over these 100 replications is reported. For example, the simulation model for the first element in the first node with all factors in Table 3.1 set at level 1 is

$$y_{1,i,1} = -0.1018x_{1,i,5} + 0.1080x_{1,i,7} + 0.7256x_{1,i,32} + 0.5538x_{1,i,41} - 0.2197x_{1,i,46} + \varepsilon_{1,i,1}.$$

The proposed functional graphical model (specifically, functional response node regression) is applied to the simulation data. The tuning parameters are selected by the validation data set, i.e., the tuning parameters that lead to the smallest prediction error for the validation data set will be selected. Due to the limited space, only several representative results are provided to show the effect of each factor on the prediction performance. Detailed results for the 144 scenarios are available in Table D1 in Appendix D. In Figure 3.3, a comparison of the Root Mean Square Error (RMSE) of the proposed method and the benchmark methods is provided. For Proposed and Benchmark Separate Node (SN), the RMSE is calculated from 1) the reconstructed functional variable $\hat{\mathbb{y}}_{k,i}$ that is reconstructed based on the predicted basis expansion coefficients $\hat{\boldsymbol{y}}_{k,i}$, and 2) the underlying functional variable $\mathbb{y}_{k,i}$ that is reconstructed based on the "perfect" basis expansion coefficients (i.e., $\boldsymbol{y}_{k,i} - \boldsymbol{\varepsilon}_{k,i}$). The spline basis functions used in the case study are used during the reconstruction. The RMSE is calculated as $\sqrt{\frac{1}{n}\sum_{i=1}^{n}\left(\frac{1}{m}\sum_{t=1}^{m}\left(\hat{\mathbb{y}}_{t,k,i} - \mathbb{y}_{t,k,i}\right)^2\right)}$, where $\hat{\mathbb{y}}_{t,k,i}$ is the t-th element of the reconstructed functional variable $\hat{\mathbb{y}}_{k,i}$, $\mathbb{y}_{t,k,i}$ is the t-th element of the underlying functional variable, m is the number of elements in the functional variable and n is the number of samples. For Benchmark Summary Statistics (SS), the RMSE is calculated based on the same formula but $\hat{\mathbb{y}}_{t,k,i}, \forall t$ is substituted by the predicted mean value of the functional variable.

In Figure 3.3, the testing RMSEs of the first functional node by varying the six factors in Table 3.1 are provided. Other functional nodes have similar performance as the first functional node. The horizontal axis shows the factor under study, and the vertical axis shows the average testing RMSE over 100 replications. The smaller RMSE is, the better a model performs. The simulation factors under study in the plots are represented by "~" in Figure 3.3 (a)-(f), and the levels of other factors are represented by 1, 2 or 3 as specified in Table 3.1. For example, [~, 1, 1, 1, 1, 1]

means the density is under study, while sample size, overlap, correlation, SNR and SNR group difference are fixed at level 1.

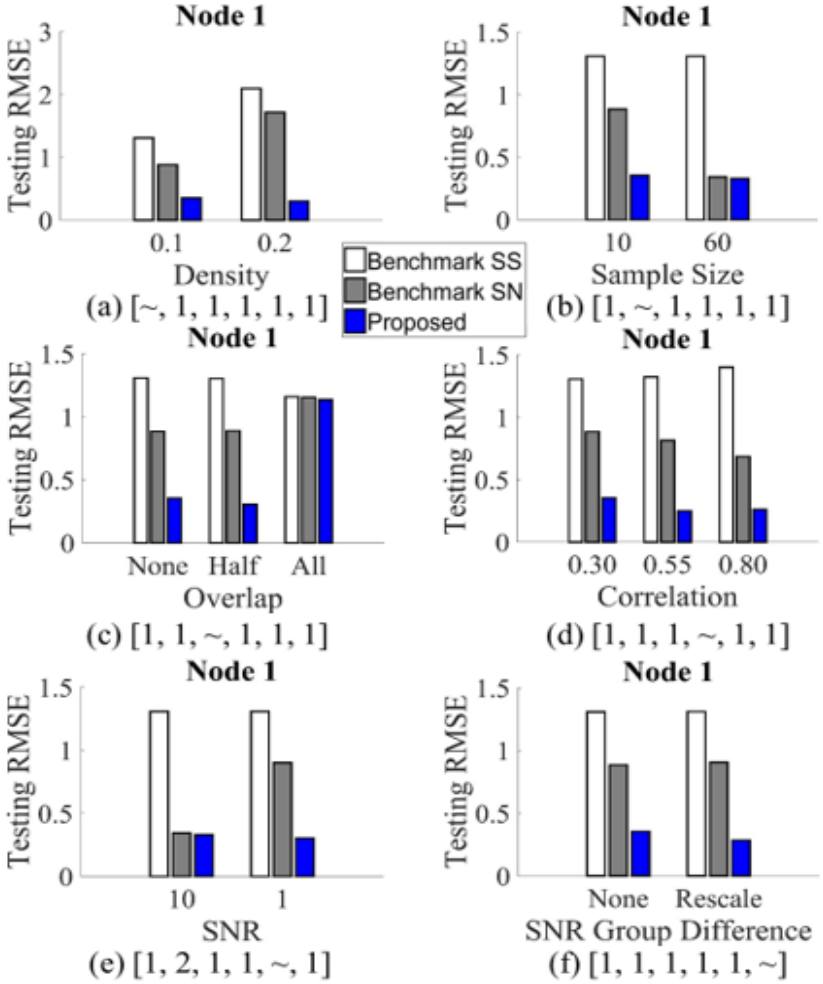

Figure 3.3. Effects of Simulation Factors on RMSE (The factor level combinations are provided in (a)-(f), where numerical values represent factor levels specified in Table 3.1 and "~" represents that the factor is under comparison. SS: Summary Statistics; SN: Separate Node.)

Based on the simulation studies shown in Figure 3.3, the following observations can be obtained at the specified levels: 1) the proposed method outperforms the benchmark methods regardless of density (Figure 3.3 (a)). 2) The proposed method outperforms the benchmark methods when the sample size is small. Proposed and Benchmark Separate Node tend to perform comparable when the sample size is large (Figure 3.3 (b)). 3) The proposed method outperforms the benchmark

methods when the samples across elements in a functional node do not overlap, or partially overlap (half overlap). The proposed and benchmark methods tend to perform comparable when the samples across elements in a functional node totally overlap (Figure 3.3 (c)). 4) The proposed method outperforms the benchmark methods regardless of correlation levels (Figure 3.3 (d)). 5) The proposed method outperforms the benchmark methods when the SNR is small. Proposed and Benchmark Separate Node tend to perform comparable when the SNR is large (Figure 3.3 (e)). 6) The proposed method outperforms the benchmark method regardless of SNR group difference specified in Table 3.1 (Figure 3.3 (f)). See Table D1 in Appendix D for results at all 144 scenarios. In summary, the proposed method is better than the benchmark methods because the elements in a functional node can borrow strength from each other in model estimation. This strength is obvious when the sample size is small, the samples across elements in a functional node do not totally overlap, or the measurement is noisy (SNR is small). The proposed and benchmark methods (especially Benchmark Separate Node) tend to become comparable when the sample size is large, the samples across elements in a functional node totally overlap, or the SNR is large.

The corresponding variable selection performance in the six scenarios over 100 replications is illustrated in Figure 3.4. The variable selection accuracy is defined as the proportion of variables successfully selected or eliminated in the final models compared with the underlying models. In Figure 3.4, the horizontal axis shows the factor under study, and the vertical axis shows the average variable selection accuracy. From Figure 3.4, the proposed method outperforms the benchmark method in terms of variable selection when the sample size is small, the samples across elements in a functional node do not totally overlap, or the SNR is small. Detailed results for the 144 scenarios are available in Table D2 in Appendix D. In the appendix, the proportion of

significant variables being selected (i.e., true positive rate) and proportion of insignificant variables being eliminated (i.e., true negative rate) are also provided in Tables D3-D4.

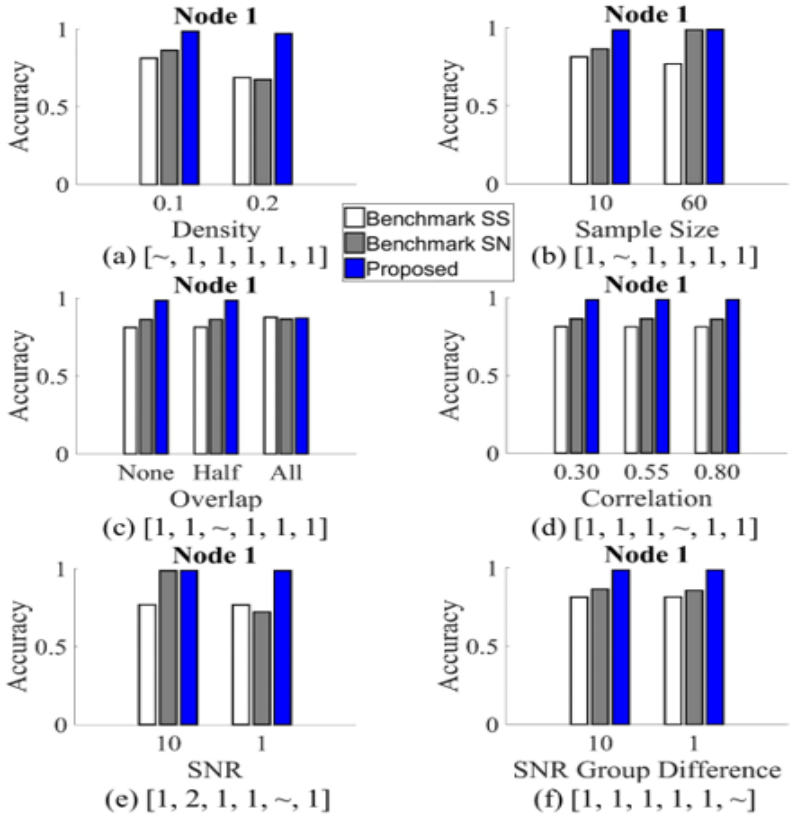

Figure 3.4. Effects of Simulation Factors on Variable Selection Accuracy (The factor level combinations are provided in (a)-(f) with the same meaning as those in Figure 3.3. SS: Summary Statistics; SN: Separate Node.)

As an illustration, the actual model structure that is used to simulate the data (Figure 3.5 (a)), the model structure learned by the proposed method (Figure 3.5 (b)), the model structure learned by Benchmark Separate Node (Figure 3.5 (c)), and the model structure learned by Benchmark Summary Statistics (Figure 3.5 (d)), are compared in Figure 3.5. The color of the heat map represents the number of times a variable being selected over 100 replications. If the learned structure has a similar heat map with the actual model structure (Figure 3.5 (a)), then this learned model structure can successfully represent the underlying models. From Figure 3.5, the proposed

method can successfully identify the underlying model structures, whereas the benchmark methods have some problems for model estimation due to the large correlation and small SNR in the scenario [2, 2, 1, 3, 2, 2] represented in Figure 3.5. The factor combinations have similar interpretations as before, i.e., numerical values in the square brackets represent factor levels specified in Table 3.1.

In summary, the proposed method outperforms the benchmark methods when the sample size is small, the samples across elements in a functional node do not totally overlap, or the SNR is small. The proposed and benchmark methods tend to perform comparable when the sample size is large, the samples across elements in a functional node totally overlap, or the SNR is large in the simulation studies. This result makes our proposed functional graphical model valuable. This is because larger sample size, totally overlapped functional nodes and larger SNR requires more experimental runs, better design with complete data sets and better sensors in manufacturing, which would significantly increase the cost and time for data collection in manufacturing.

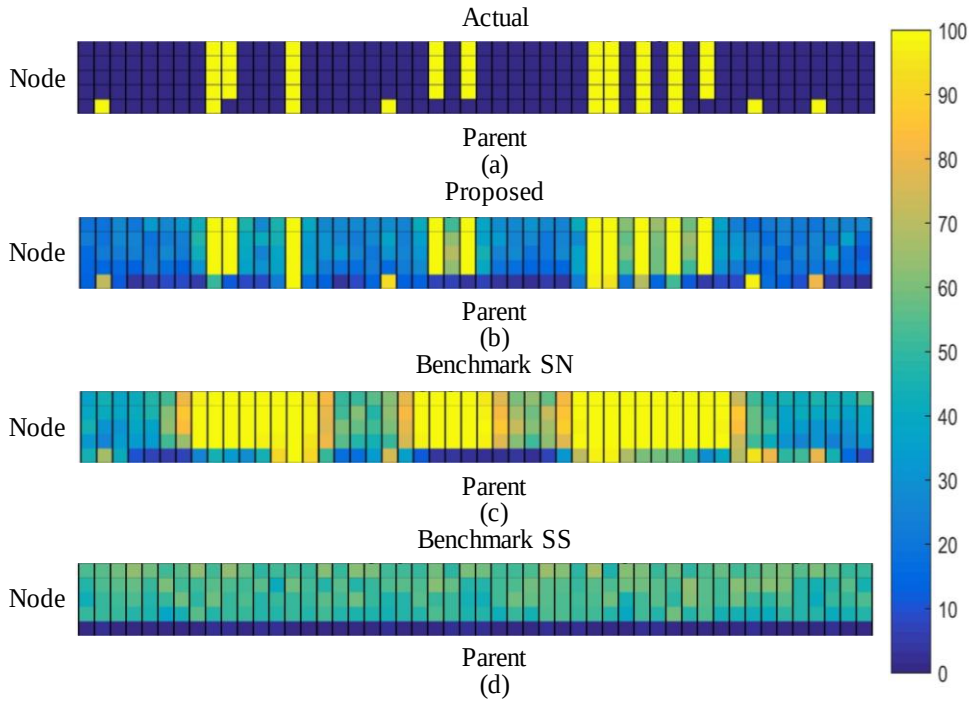

Figure 3.5. Model Structure Learned by the Proposed Method and Benchmark Methods under [2, 2, 1, 3, 2, 2] ((a)-(d) are separately the underlying model structure and model structures learned from the proposed and benchmark methods)

3.5. Case Study

A plasma spray process is used to demonstrate the modeling performance of the proposed method. The offline setting variables, *in situ* process variables, and coating property variables are measured for the modeling of this process. The details of these variables are provided in Table 3.2. After the preprocessing, there are 36 scalar variables generated from offline setting variables, 2 functional variables each with 186 basis expansion coefficients after spline expansion, and 3 scalar quality response variables. All details about the plasma spray process discussed here can be found in [6].

Table 3.2. Data Structure in the Thermal Spray Case Study

Variables	Meanings	Categories
Stand-off distance	Distance of the torch from the substrate	Setting
Surface speed	The line speed of rotated substrate	Setting

Current	The current input of the torch	Setting
Primary gas flow rate	The flow rate of primary gas forming the plasma	Setting
Secondary gas flow rate	The flow rate of secondary gas forming the plasma to improve plasma thermal conductivity	Setting
Carrier gas flow rate	The flow rate of carrier gas for particles	Setting
Powder flow rate	The flow rate of powder	Setting
Traverse rate	The traverse speed of torch	Setting
Particle velocity	Average velocity at the measurement area	*In situ*
Particle temperature	Average temperature at the measurement area	*In situ*
Hardness	Quantify how hard the surface is	Response
Deposition rate	Quantify the amount of material deposited per unit time	Response
Porosity	Quantify the proportion of porous area in the surface	Response

The proposed functional graphical model is applied to the plasma spray process. The scalar variables generated from the offline setting variables are standardized, and the quality response variables are centralized prior to the modeling. For Proposed and Benchmark Separate Node, the standardized basis expansion coefficients in the functional variables are used. For Benchmark Summary Statistics, the standardized summary statistics (mean and standard deviation) are used. 8, 12, or 16 samples are randomly sampled as the training data set from all 40 samples. The training sample size is varied to test the effect of sample size on the model performance. 12 samples are randomly sampled as the validation data set, and 12 samples are randomly sampled as the testing data set. The training, validation and testing data set do not overlap. The training data set is used to fit the functional graphical model, and the validation data set is used for tuning parameters selection. The model performance is evaluated by the testing data set. The above random sampling and modeling process is repeated for 100 times. The average RMSEs for the testing data set over 100 replications and the standard errors of the RMSEs (in parenthesis) are summarized in Table 3.3. The RMSEs for the functional nodes are calculated based on the method described in the simulation study, where the predicted functional variables are

reconstructed based on the predicted basis expansion coefficients in Proposed and Benchmark Separate Node. The RMSEs for the scalar nodes are calculated based on the predicted and measured centralized quality response variables. In Table 3.3, the smaller RMSEs (better modeling performance) are highlighted in bold. F1 and F2 represent functional nodes (i.e., *in situ* process variables) particle velocity and particle temperature, respectively. And S1-S3 represents scalar nodes (i.e., offline setting variables): hardness, deposition rate, and porosity.

Table 3.3. RMSEs of Testing Data for Case Study (F: functional node; S: scalar node; Prop.: proposed method; Bench.: benchmark method; SN: separate node; SS: summary statistics)

		F1	F2	S1	S2	S3
Training sample size 8	Prop.	**10.068 (0.320)**	**46.440 (1.154)**	2.702 (0.068)	0.171 (0.004)	1.134 (0.024)
	Bench. SN	10.368 (0.318)	48.198 (1.106)	2.702 (0.068)	0.171 (0.004)	1.134 (0.024)
	Bench. SS	12.081 (0.374)	50.449 (1.147)	2.950 (0.072)	0.193 (0.006)	1.310 (0.032)
Training sample size 12	Prop.	**9.632 (0.264)**	**40.236 (0.819)**	2.572 (0.054)	0.155 (0.003)	1.023 (0.019)
	Bench. SN	9.925 (0.265)	41.733 (0.828)	2.572 (0.054)	0.155 (0.003)	1.023 (0.019)
	Bench. SS	10.919 (0.295)	43.319 (0.940)	2.825 (0.080)	0.180 (0.005)	1.129 (0.024)
Training sample size 16	Prop.	**9.147 (0.258)**	**38.227 (0.719)**	2.378 (0.040)	0.151 (0.003)	1.038 (0.019)
	Bench. SN	9.361 (0.249)	39.569 (0.715)	2.378 (0.040)	0.151 (0.003)	1.038 (0.019)
	Bench. SS	10.200 (0.265)	40.824 (0.783)	2.584 (0.073)	0.172 (0.004)	1.165 (0.024)

From Table 3.3, the proposed functional graphical model has smaller RMSEs (highlighted in bold) than the benchmark methods for the functional response prediction. As the same size increases, the two methods tend to perform comparable in general. Note that Proposed and Benchmark Separate Node use the same model Eq. (3.10) for the scalar response node. Therefore, they have identical prediction performance in Table 3.3 for the scalar response

regressions (the last 3 columns). Both Proposed and Benchmark Separate Node perform better (i.e., smaller RMSE) than Benchmark Summary Statistics where mean and standard deviation are used as inputs.

A final graphical model structure learned with training sample size 8 is shown in Figure 3.6 as an illustration. In Figure 3.6, the yellow, green and red nodes are used to separately present the offline setting variables, *in situ* process variables, and coating quality variables. The edges in Figure 3.6 are based on the average coefficients over elements in a functional node. Due to the confidentiality of the exact data set, the variables shown in Figure 3.6 are randomly encoded and the detailed relationships of the physical variables cannot be disclosed.

In summary, the proposed functional graphical model can successively construct the graph structure with better prediction accuracy than the benchmark models.

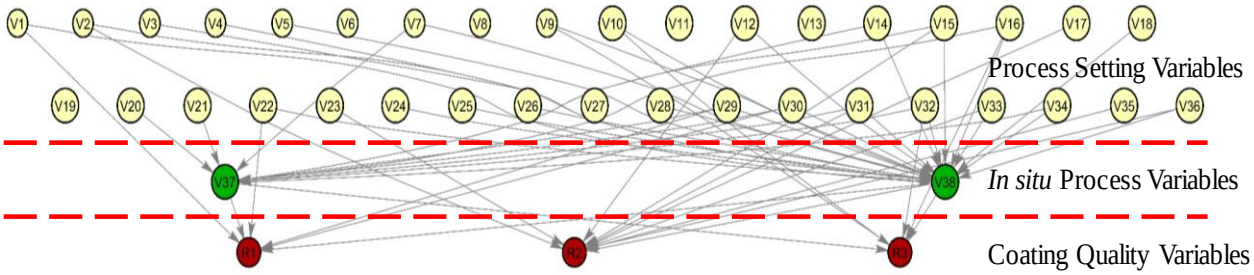

Figure 3.6. Functional Graphical Model Structure for a Plasma Spray Process (The yellow, green and red nodes are used to present the offline setting variables, *in situ* process variables, and coating quality variables, respectively.)

In summary, the proposed functional graphical model can successively construct the graph structure with better prediction accuracy than the benchmark model.

3.6. Conclusions of Functional Graphical Models

Graphical models are useful to represent conditional relationships among variables in systems, but they cannot be directly applied to systems with functional variables. On the other hand, many

manufacturing processes have functional variables, such as the plasma spray process that has been studied in this chapter. This process has functional variables measured to present the *in situ* manufacturing process conditions. To include the *in situ* information in modeling is critical since it allows the direct modeling of the manufacturing process rather than products for future mass personalization.

In this chapter, a functional graphical modeling method is proposed to learn the variable relationships by integrating methodologies from functional data analysis, graphical models, and sparse learning. We further develop the computational procedures to learn the model with known variable orderings from domain knowledge. It is shown that the proposed method outperforms the benchmark methods when the sample size is small, the samples across elements in a functional node do not totally overlap, or the SNR is small in the simulation studies. The proposed method also outperforms the benchmark methods in the case study of the plasma spray process. This functional graphical modeling approach is valuable for learning the high-dimensional variable relationships with functional variables, and provides a straight forward representation of the variable relationships.

Chapter 4. Functional Quantitative and Qualitative Models for Quality Modeling in a Fused Deposition Modeling Process

4.1. Introduction

AM fabricates a part by printing materials layer by layer from a Computer Aided Design (CAD) file, thus enables flexible part geometry and reduces material wastes. Compared with the traditional subtractive manufacturing processes, AM can eliminate the time-consuming fixture and tool design steps. Therefore, it can significantly reduce the tooling and assembly cost, as well as the product development life cycle [109-111].

AM processes have shown their capability in various industries, such as aerospace, automobile, and healthcare [112-115]. For instance, maxillofacial, neurosurgical and orthopedic medical parts are fabricated with stereolithography and Fused Deposition Modeling (FDM) [112]. Commercial and military aircraft parts are fabricated with selective laser sintering [113]. However, most of these applications are still in the proof-of-concept phase, and several challenges need to be solved before the industrial applications of AM. Among these challenges, the product quality modeling and assurance is a key issue [109, 110].

We focus on the AM product quality modeling for a FDM AM process in this chapter. A schematic of a desktop FDM printer is shown in Figure 4.1 [2]. The process fabricates a part by successively printing layers of molten plastic filament on the substrate with the following procedures [2, 115]. First, the offline machine setting process variables (such as bed temperature, layer thickness, etc.) are specified. Then, the filament heated over its glass transition temperature

is extruded out of the extruder. The extruded material cools down and solidifies when it reaches the substrate. The extruder travels over the substrate to form the desired cross-section profile for the current layer. Finally, the base plate moves down one layer, and the next layer is deposited. These successive layers solidify and bond together to form the part. In a FDM process, the part quality variables are affected by offline setting variables, machine precision, material shrinkage, external environment, etc. These quality variables should be controlled to meet the design specifications.

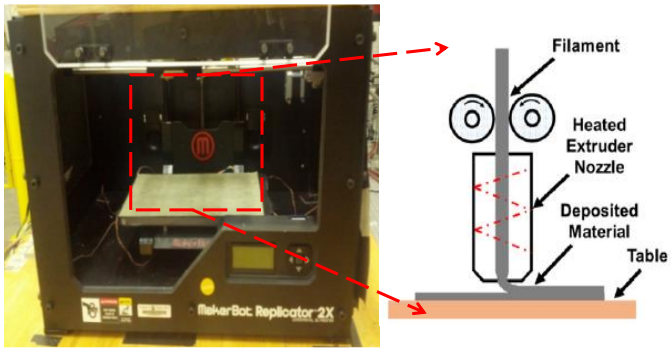

Figure 4.1. A Schematic Illustration of a Desktop FDM Printer [2]

To improve the part quality, the effects of various offline setting variables, such as feed rate, flow rate, build orientation, layer thickness, extruder temperature, raster angle, etc., on the part quality are studied [2, 116]. These quality variables can be quantitative or qualitative, such as dimensional accuracy [117-119], surface roughness (condition) [120-122], presence or number of voids [123-125], and presence of missing features [126, 127]. In most of the published works, these part quality variables are investigated separately based on the scalar offline setting variables. Limited attention is paid to the association of the QQ types of part quality variables, and their relationships with the functional *in situ* process variables. Recently, it is demonstrated that the model prediction performance is improved over separate modeling of each response, if a joint modeling procedure for the QQ responses is adopted in a wafer lapping process [64]. But this work is limited to model the *in situ* process variables. On the other hand, Rao *et al.*

developed a real time sensing system for a FDM process [2]. With the help of the sensing system, *in situ* process variables such as the vibration at the extruder and bed, and the temperature at the melt pool and bed can be collected [2]. It is shown that these *in situ* process variables are informative for predicting whether the FDM part will fail or not [2, 128]. Therefore, the *in situ* process variables should also be considered in the modeling of a FDM process.

In this chapter, we focus on the analysis of the association of the QQ quality variables in a FDM process. These quality variables are modeled by both offline setting variables and *in situ* process variables via functional QQ models. The functional QQ models are widely applicable for the modeling of quantitative quality variables in AM, such as dimensional accuracy and mechanical property, and qualitative quality variables, such as surface roughness condition and missing features. The contributions of this chapter mainly lie on integration of functional *in situ* process variables into the QQ modeling framework [64]. In addition, a hierarchical variable selection method (i.e., hierarchical non-negative garrote (HNNG)) is used to identify not only which *in situ* process variables are significate in the modeling, but also which features of these *in situ* process variables are significant. Such a functional variable selection approach is demonstrated in a logistic regression model for a binary defect indicator in a crystal growth process [5], and a linear regression model for a continuous comfort score in a vehicle ingress/egress comfort study [20]. However, this functional variable selection method is never reported for functional QQ models with both QQ responses and functional predictors in the models. The unique features from the FDM process allow us to explore this new functional QQ modeling methods.

The rest of the chapter is organized as follows. The state-of-the-art for FDM quality improvements, and the QQ responses modeling are reviewed in Section 4.2. In Section 4.3, the proposed functional QQ models are introduced. Simulation studies and a case study in a FDM

process are used to demonstrate the effectiveness of the proposed method in Sections 4.4 and 4.5, respectively. Finally, conclusions are made in Section 4.6.

4.2. Research Background

4.2.1. Fused Deposition Modeling Quality Improvements

In this section, we first review the studies on quality improvement for quality variables in FDM processes, and then review the existing monitoring and control works on FDM processes.

Various quantitative quality response variables in FDM, such as mechanical property and dimensional accuracy, are widely studied. For instance, Fodran *et al.* investigate the effect of air gap, layer thickness and filament width on tensile stress, tangent modulus and part strength in qualitative experimental studies [129]. Matas proposes stiffness and strength models based on first principles [130]. For dimensional accuracy, Sood *et al.* use Taguchi methods for length, width, thickness and diameter modeling, and find that different quality variables have different optimal offline setting variable conditions [117]. Boschetto and Bottini propose a geometrical model for the prediction of FDM part irregularity and dimensional accuracy [119]. Geometrical models are proposed for surface roughness characterization based on offline setting variables [120, 121, 131]. Statistical and data mining methods, such as Analysis of Variance (ANOVA), Taguchi methods and Artificial Neural Network (ANN), are also applied for the quality modeling and improvements in FDM [118, 132, 133]. See also [122, 134, 135]. On the other hand, the qualitative quality variables in FDM, such as presence or number of voids and missing features are also studied. For instance, Agarwala *et al.* investigate various strategies, such as improving feed filament quality, optimizing build environment temperature and adjusting process variables, to reduce or eliminate the presence of voids [123]. Rodriguez *et al.* conclude that the fiber gap and flow rate strongly affect the presence and number of voids [124]. See also

[126, 127], and a recent review in [116].

In this chapter, we focus on the FDM part dimensional accuracy and surface roughness condition modeling. The dimensional accuracy can be measured by easily accessible tools such as calipers, while the surface roughness needed to be measured by contact or non-contact methods. In contact method (such as using a profilometer [119]), a stylus is dragged on the part surface, which may damage the part surface. Non-contact method is nondestructive, but professional equipment, such as confocal microscopy, is needed. The public FDM users may not have access to professional non-contact equipment or even profilometer for surface roughness measurement. In addition, for the situation of in situ quality assessment of roughness, one cannot measure roughness based on profilometer or microscope during the printing. However, the users can easily observe part surface appearance, and provide a quick judgement of the surface roughness condition. Therefore, we treat surface roughness as a binary indicator based on the go/no-go judgement. Note that the proposed method can be generally applied to situations with quantitative and qualitative responses, and is not limited to the modeling of dimensional accuracy and surface roughness condition.

Recently, *in situ* process monitoring and control of AM processes attract many attentions [109-111, 136]. The majority of research and review for the monitoring and control are on metal based AM processes [110, 111, 137]. For the FDM process, Dinwiddie *et al.* use an infrared camera to monitor the temperature distribution of the extrusion process, where the temperature distribution was useful for modifying the part design [138]. Kousiatza and Karalekas embed fiber Bragg grating sensors and thermocouples at different layers of a FDM part for *in situ* strain field and temperature profile monitoring, and showed that the sample location with regard to the building platform will significantly affect the strain and temperature [139]. Rao *et al.* build a real time

sensing system to capture the vibration, temperature and video of the printing process [2]. These *in situ* process variables can help monitor whether the part will fail or not [2, 128]. Shrinkage is a phenomenon that affects the dimensional accuracy of the FDM parts, and the offline shape shrinkage compensation is studied by various scholars to control the part shape to target [140-142].

The aforementioned works discover many important facts about the quality variables in FDM, but fail to consider the association of both the QQ types of quality variables and their relationships with the offline setting variables and *in situ* process variables systematically. QQ models are powerful in exploring the association of heterogeneous quality response variables, which are adopted in this chapter.

4.2.2. Quantitative and Qualitative Responses Modeling

The QQ responses are widely encountered in biomedical and healthcare systems, and manufacturing systems [64, 143-145]. Traditionally, the QQ responses are modeled separately [85, 91, 146-148]. The separate modeling usually fails to keep track of the association of these heterogeneous responses, and may lead to inferior performance compared with joint modeling of QQ responses [64, 145].

The analysis of the QQ responses starts with the correlation study [143, 149]. To model the QQ responses, Catalano and Ryan use a continuous latent variable for a binary response, and assume a joint Gaussian distribution for the latent variable and the continuous variable [150]. Fitzmaurice and Laird incorporate covariates in a marginal model for the responses [151]. The purposes of the above models are for independence testing and model estimation, but not for variable selection for a parsimonious and interpretable model.

Deng and Jin propose the QQ models for joint modeling of QQ responses by a constrained likelihood estimation, where the significant variables can be identified [64]. The authors applied the QQ models to a lapping process where wafer total thickness variation is modeled as a quantitative response and site total indicator reading is modeled as a binary qualitative response [64]. It is shown that joint modeling of the QQ responses can improve the model estimation and model prediction performance for the lapping process with scalar variables as model input, compared with the separate modeling approach [64]. In this chapter, we generalize the QQ models to functional QQ models so that the functional *in situ* process variables can be modeled as predictors. Moreover, the HNNG constraint is used and generalized in the functional QQ models to select not only which functional variables, but also which features in the functional variables are important for the QQ responses [5].

4.3. Proposed Method

4.3.1. Overview of the Proposed Method

The proposed method is illustrated in Figure 4.2. The scalar offline setting variables and functional *in situ* process variables are processed and used as input for the functional QQ models. In the functional QQ models, ridge regression estimator is used as initial estimator [5], and HNNG constraint enforces the model sparsity. Finally, the functional QQ models are compared with the benchmark models, where the QQ responses are modeled separately. The functional QQ models can serve as the basis for future monitoring and control of AM processes.

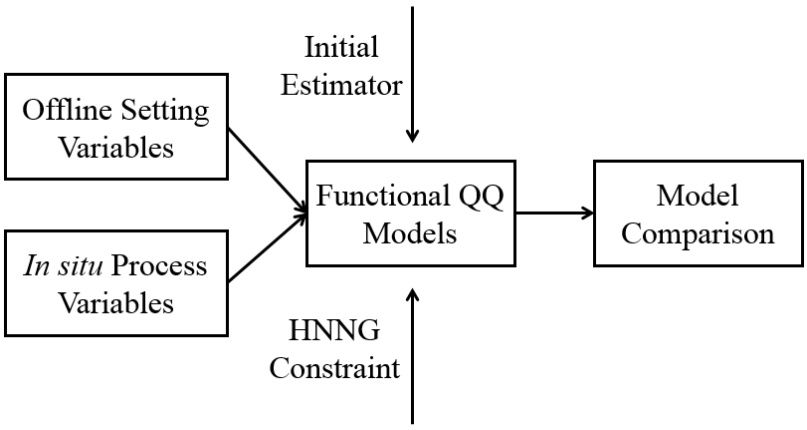

Figure 4.2. The Proposed Functional Quantitative and Qualitative Modeling Framework

4.3.2. Functional Quantitative and Qualitative Models

Denote the data for the *i*-th sample $\boldsymbol{x}_i = \left(\boldsymbol{x}_i^S; \boldsymbol{x}_i^F\right) = (x_{1,i}^S; \dots; x_{q,i}^S; \boldsymbol{x}_{1,i}^F; \dots; \boldsymbol{x}_{p,i}^F)$, where $\boldsymbol{x}_i^S$ represents the scalar offline setting variables and $\boldsymbol{x}_i^F$ represents the (discretized realization of) functional *in situ* process variables. $x_{k,i}^S$ is the *k*-th process setting variable (such as extruder temperature in FDM), and $\boldsymbol{x}_{j,i}^F$ is the *j*-th *in situ* process variable (such as melt pool temperature in FDM), $k = 1, \dots, q$ and $j = 1, \dots, p$. We use ";" to represent the column-wise concatenation. Without loss of generality, we consider the problem with one quantitative response $y_i \in R$ (e.g., dimensional accuracy in the FDM process), and one qualitative (binary) response $z_i \in \{0,1\}$ (e.g., surface roughness condition in the FDM process, where z_i=1 represents bad surface roughness condition).

Following a similar spirit of QQ models for scalar variables [64], the functional QQ models use a functional logistic regression for the binary response z_i, and functional linear regressions for the continuous response y_i conditional on the binary response z_i

$$logit(E[z_i|\boldsymbol{x}_i]) = log\left(\frac{p(\boldsymbol{x}_i)}{1-p(\boldsymbol{x}_i)}\right) = \left(\boldsymbol{x}_i^S\right)^T \boldsymbol{\gamma}^S + \int x_{1,i}^F(t)\, \tilde{\gamma}_1^F(t)dt + \cdots + \int x_{p,i}^F(t)\, \tilde{\gamma}_p^F(t)dt, \quad (4.1)$$

$$(y_i|z_i = m) = \left(\boldsymbol{x}_i^S\right)^T \boldsymbol{b}^{S(m)} + \int x_{1,i}^F(t)\, \tilde{b}_1^F(t)^{(m)}dt + \cdots + \int x_{p,i}^F(t)\, \tilde{b}_p^F(t)^{(m)}dt + \varepsilon^{(m)}, m = 0,1,$$

(4.2)

where $\boldsymbol{\gamma}^S = (\gamma_1^S, \dots, \gamma_q^S)^T$ and $\boldsymbol{b}^{S^{(m)}} = \left(b_1^{S^{(m)}}, \dots, b_q^{S^{(m)}}\right)^T$, $m = 0, 1$, is a vector of coefficients for scalar variables in the functional logistic regression and functional linear regressions, respectively. $\tilde{\gamma}_j^F(t)$ and $\tilde{b}_j^F(t)^{(m)}$, $j = 1, \cdots, p, m = 0,1$, is the coefficient for the *j*-th functional variable in the functional logistic regression and functional linear regressions, respectively. Assume the error distribution does not depend on m, i.e., $\varepsilon^{(m)} \sim N(0, \sigma^2)$, $m = 0, 1$ [64].

The functional variables are measured over time, and usually have high dimensions. To address the high dimensionality issue, various basis expansion techniques, such as spline expansion, Fourier transform and wavelet analysis are widely adopted [152]. We apply the basis expansion to the functional coefficients in this chapter. Denote the orthogonal basis as $\boldsymbol{\theta}(t) = \left(\theta_1(t), \theta_2(t), \dots, \theta_K(t)\right)^T$, we have $\tilde{\gamma}_j^F(t) = \left(\boldsymbol{\gamma}_j^F\right)^T \boldsymbol{\theta}(t)$, $\tilde{b}_j^F(t)^{(m)} = \left(\boldsymbol{b}_j^{F^{(m)}}\right)^T \boldsymbol{\theta}(t)$, $m = 0,1$, after the basis expansion. $\boldsymbol{\gamma}_j^F$ and $\boldsymbol{b}_j^{F^{(m)}}$, $m = 0,1$, is a vector of the basis expansion coefficients for $\tilde{\gamma}_j^F(t)$ and $\tilde{b}_j^F(t)^{(m)}$, respectively. Therefore, Eqs. (4.1) and (4.2) become

$$logit(E[z_i|\boldsymbol{x}_i]) = log\left(\frac{p(\boldsymbol{x}_i)}{1-p(\boldsymbol{x}_i)}\right) = \left(\boldsymbol{x}_i^S\right)^T \boldsymbol{\gamma}^S + \sum_{j=1}^p \sum_{t\in\Psi} x_{j,i}^F(t) \left(\boldsymbol{\gamma}_j^F\right)^T \boldsymbol{\theta}(t), \tag{4.3}$$

$$(\mathrm{y}_i|\mathrm{z}_i = m) = \left(\boldsymbol{x}_i^S\right)^T \boldsymbol{b}^{S^{(m)}} + \sum_{j=1}^p \sum_{t\in\Psi} x_{j,i}^F(t) \left(\boldsymbol{b}_j^{F^{(m)}}\right)^T \boldsymbol{\theta}(t) + \varepsilon^{(m)}, m = 0,1, \tag{4.4}$$

where Ψ is the time continuum of the corresponding functional variables. Re-organizing the above expression, we have

$$log\left(\frac{p(\mathbb{x}_i)}{1-p(\mathbb{x}_i)}\right) = \boldsymbol{x}_i{}^T \phi \boldsymbol{\eta} = \mathbb{x}_i{}^T \boldsymbol{\eta}, \tag{4.5}$$

$$(\mathrm{y}_i|\mathrm{z}_i = m) = \mathbb{x}_i{}^T \boldsymbol{\beta}^{(m)} + \varepsilon^{(m)}, m = 0, 1, \tag{4.6}$$

where $\phi = diag\left(I_{q\times q}, \boldsymbol{\theta}(t)^T, \cdots, \boldsymbol{\theta}(t)^T\right)$, $\mathbb{x}_i = (\boldsymbol{x}_i{}^T \phi)^T$, $\boldsymbol{\eta} = (\boldsymbol{\gamma}^S; \boldsymbol{\gamma}^F) = \left(\eta_1; \cdots; \eta_q; \boldsymbol{\eta}_{q+1}; \cdots; \boldsymbol{\eta}_{q+p}\right)$ and $\boldsymbol{\gamma}^F = \left(\boldsymbol{\gamma}_1^F; \dots; \boldsymbol{\gamma}_p^F\right)$. Note that there are q scalar variables and p

functional variables. Similarly, $\boldsymbol{\beta}^{(m)} = \left(\boldsymbol{b}^{S^{(m)}}; \boldsymbol{b}^{F^{(m)}}\right) = (\beta_1{}^{(m)}; \cdots; \beta_q{}^{(m)}; \boldsymbol{\beta}_{q+1}{}^{(m)}; \cdots; \boldsymbol{\beta}_{q+p}{}^{(m)})$ and $\boldsymbol{b}^{F^{(m)}} = \left(\boldsymbol{b}_1^{F^{(m)}}; \cdots; \boldsymbol{b}_p^{F^{(m)}}\right)$, $m = 0,1$. The coefficients for the j-th functional variable in the functional logistic and functional linear models have the form $\boldsymbol{\eta}_{q+j} = \left(\eta_{1,q+j}, \cdots, \eta_{P_{q+j},q+j}\right)^T$ and $\boldsymbol{\beta}_{q+j}{}^{(m)} = \left(\beta_{1,q+j}{}^{(m)}, \cdots, \beta_{P_{q+j},q+j}{}^{(m)}\right)^T$, $m = 0,1$, where P_{q+j} is the number of coefficients for the j-th functional variable. These P_{q+j} coefficients for a functional variable naturally form a group [30]. In total, we have $q + p$ groups of coefficients. For q scalar variables, the group size (i.e., number of coefficients in a group) is 1, and for the j-th functional variables, the group size is $P_{q+j}, j = 1, \cdots, p$.

Therefore, the proposed functional QQ models can be summarized to have the following form

$$z_i = \begin{cases} 1, \ with\ probability\ p(\mathbb{x}_i) \\ 0, \ with\ probability\ 1 - p(\mathbb{x}_i) \end{cases}, \tag{4.7}$$

$$(y_i|\mathrm{z}_i) \sim N\left(\mathrm{z}_i \mathbb{x}_i{}^T \boldsymbol{\beta}^{(1)} + (1 - \mathrm{z}_i)\mathbb{x}_i{}^T \boldsymbol{\beta}^{(0)}, \sigma^2\right), \tag{4.8}$$

where the continuous response is modeled as a conditional regression of the binary response. If the coefficients $\boldsymbol{\beta}^{(1)}$ and $\boldsymbol{\beta}^{(0)}$ are identical both in terms of significant sets and values, i.e., the two linear models are the same no matter what the value of z_i is, the QQ responses are independent. Otherwise, the QQ responses are associated, and the joint modeling of the QQ responses has the potential to provide better prediction performance over separate modeling of the responses [64].

The model coefficients in Eqs. (4.7) and (4.8) can be estimated by using MLE. However, the MLE is not feasible when the number of coefficients is larger than the sample size. Different penalties are proposed for this problem to learn a parsimonious and interpretable model [153]. When there are groups of coefficients, the group Lasso with $l_{1,2}$ penalty can be used for variable

selection [30]. However, the $l_{1,2}$ penalty in group Lasso can only select a group of coefficients as a whole and cannot select individual coefficients in the group [5, 20].

To address the variable selection problem for selecting not only which group but also which coefficient in the group (i.e., the bi-level variable selection problem [154]), the HNNG constraint is adopted for the functional QQ models. We use a constrained MLE approach for estimating the coefficients and learning a parsimonious and interpretable model. The model estimation can be solved by optimizing the objective function

$$min -2\,L\left(\boldsymbol{\eta}, \boldsymbol{\beta}^{(1)}, \boldsymbol{\beta}^{(0)}\right), \tag{4.9}$$

$$\text{s.t. } \left(\beta_{k,r}\right)^{(m)} = \left(\varphi_{k,r}\right)^{(m)}\left(\tilde{\beta}_{k,r}\right)^{(m)}, \eta_{k,r} = \tau_{k,r}\tilde{\eta}_{k,r}, m = 0,1,$$

$$\sum_{k=1}^{P_r} w_r\left(\varphi_{k,r}\right)^{(m)} \leq (\rho_r)^{(m)}, \sum_{k=1}^{P_r} w_r\tau_{k,r} \leq \rho_r, m = 0,1,$$

$$\left(\varphi_{k,r}\right)^{(m)} \geq 0, \tau_{k,r} \geq 0, (\rho_r)^{(m)} \geq 0, \rho_r \geq 0, m = 0,1,$$

$$\sum_{r=1}^{p+q}\left((\rho_r)^{(1)} + (\rho_r)^{(0)}\right) \leq M_1,$$

$$\sum_{r=1}^{p+q} \rho_r \leq M_2,$$

where $L\left(\boldsymbol{\eta}, \boldsymbol{\beta}^{(1)}, \boldsymbol{\beta}^{(0)}\right) = log\{\prod_{i=1}^{n} f(y_i|z_i)f(z_i)\} = log\{\prod_{i=1}^{n} f(z_i)\} + log\{\prod_{i=1}^{n} f(y_i|z_i)\}$ is the log-likelihood function, $\left(\tilde{\beta}_{k,r}\right)^{(m)}$ is the initial estimator of the *k*-th coefficient in the *r*-th variable in functional linear regressions, $m = 0,1$, and $\tilde{\eta}_{k,r}$ is the initial estimator of the *k*-th coefficient in the *r*-th variable in functional logistic regression. The initial estimator is taken as ridge regression estimator [5]. $\left(\varphi_{k,r}\right)^{(m)}$ and $\tau_{k,r}$ are non-negative shrinkage factors for general variable selection [26]. The second line of the constraints controls the number of coefficients selected in each group of coefficients, where w_r is a weight factor proportional to the group size of the *r*-th group of coefficients. Adding such a weight factor will avoid the situation that the coefficients in a larger group is more likely to be selected compared with the coefficients in a

smaller group [26]. In this chapter, $w_r = \sqrt{P_r}$, where P_r is the group size for the r-th group [30]. The constraints in the last two lines control the total number of groups selected for the functional linear regressions (controlled by M_1) and functional logistic regression (controlled by M_2), respectively.

It is worth pointing out that the unique formulation of the proposed functional QQ models over the QQ models for scalar variables [64] and the functional variable selection method [5] includes: 1) the functional predictors (*in situ* process variables) are modeled for the first time in the QQ modeling framework; 2) two tuning parameters M_1 and M_2 are used to separately control the complexity in the functional linear regressions and functional logistic regression; 3) the weight factor w_r is introduced to take the effect of group size into consideration during variable selection.

As mentioned, the HNNG constraint enforces the bi-level variable selection. This bi-level variable selection is fulfilled by the group level shrinkage factor $(\rho_r)^{(m)}$ or ρ_r, and the individual level shrinkage factor $\left(\varphi_{k,r}\right)^{(m)}$ or $\tau_{k,r}$. If the group level shrinkage factor $(\rho_r)^{(m)}$ or ρ_r equals to zero, then the current group will not be selected (all coefficients in this group will not be selected), vice versa. If the individual level shrinkage factor $\left(\varphi_{k,r}\right)^{(m)}$ or $\tau_{k,r}$ equals to zero, the current coefficient will not be selected, vice versa. The M_1 and M_2 are tuning parameters that can be selected by BIC, the prediction errors in CV or the prediction errors in validation data set [33]. To optimize the objective function in Eq. (4.9) directly is a challenging task, and a quadratic approximation technique is used [5, 64]. After the quadratic approximation, the problem in Eq. (4.9) is simplified to a quadratic programming problem with guaranteed convergence [5, 64]. In the following, both simulation studies and a case study in a FDM process are used to demonstrate the effectiveness of the proposed method.

4.4. Simulation

Denote $\boldsymbol{I}^{(1)}$ and $\boldsymbol{I}^{(0)}$ as the sets of significant coefficients in the underlying functional linear regressions (dependent on the binary response value), and $\boldsymbol{I}$ as the set of significant coefficients in the underlying functional logistic regression. To evaluate the performance of the functional QQ models, four scenarios are considered in the simulation [64]:

Scenario 1: the significant sets $\boldsymbol{I}^{(1)}$ and $\boldsymbol{I}^{(0)}$ are exactly the same, and the significant coefficients in $\boldsymbol{\beta}^{(1)}$ and $\boldsymbol{\beta}^{(0)}$ have similar values;

Scenario 2: the significant sets $\boldsymbol{I}^{(1)}$ and $\boldsymbol{I}^{(0)}$ do not overlap, but the significant coefficients in $\boldsymbol{\beta}^{(1)}$ and $\boldsymbol{\beta}^{(0)}$ have similar values;

Scenario 3: the significant sets $\boldsymbol{I}^{(1)}$ and $\boldsymbol{I}^{(0)}$ are exactly the same, but the significant coefficients in $\boldsymbol{\beta}^{(1)}$ and $\boldsymbol{\beta}^{(0)}$ have different values;

Scenario 4: the significant sets $\boldsymbol{I}^{(1)}$ and $\boldsymbol{I}^{(0)}$ do not overlap, and the signifiant coefficients in $\boldsymbol{\beta}^{(1)}$ and $\boldsymbol{\beta}^{(0)}$ have different values.

Furthermore, several factors are varied for the simualtion data generation under each scanario: 1) the number of variables in the underlying models, 2) the correlation structure for the model input, and 3) the density (percentage of significant coefficients) in the underlying models. See Table 4.1 for a summary of detailed settings of these factors and their meanings. Under each scenario, we have 16 combinations of simulation settings. And there are 64 simulation scenarios in total for the four scenarios.

Table 4.1. Simulation Setting for Functional QQ Models

Factors	Levels	Meanings
Number of variables	1: $p = 2, q = 4$ 2: $p = 4, q = 8$	p: number of functional variables q: number of scalar variables
Correlation structure	1: $\rho_1 = 0, \rho_2 = 0$ 2: $\rho_1 = 0.6, \rho_2 = 0$	ρ_1: within group correlation coefficient ρ_2: among group correlation coefficient

	3: $\rho_1 = 0, \rho_2 = 0.3$ 4: $\rho_1 = 0.6, \rho_2 = 0.3$	
Density	1: $den. = 0.2$ 2: $den. = 0.4$	Percentage of significant coefficients in the underlying models

For each simulation setting, the data are generated from Eqs. (4.5) and (4.6). Specifically, $\mathbb{x}_i \sim N(\boldsymbol{\mu}, \boldsymbol{\Sigma})$, where the mean vector $\boldsymbol{\mu} = (\mu_1; \ldots; \mu_q; \boldsymbol{\mu}_{q+1}; \ldots; \boldsymbol{\mu}_{q+p})$, $\mu_j, j = 1, \cdots, q$ is the mean for the *j*-th scalar variable, and $\boldsymbol{\mu}_{q+k}$ is the mean for the *k*-th functional variable. The number of coefficients in each functional variable is set to be 10, and $\boldsymbol{\mu}$ is set to be a zero vector. The covariance matrix $\boldsymbol{\Sigma} = diag(\boldsymbol{\Sigma}^S, \boldsymbol{\Sigma}^F)$, $\boldsymbol{\Sigma}^S = \boldsymbol{I}_{q \times q}$ is the covariance matrix for the scalar variables, $\boldsymbol{\Sigma}^F = \begin{bmatrix} \boldsymbol{\Sigma}_{11} & \ldots & \boldsymbol{\Sigma}_{1p} \\ \vdots & \ddots & \vdots \\ \boldsymbol{\Sigma}_{p1} & \ldots & \boldsymbol{\Sigma}_{pp} \end{bmatrix}$ is the covariance matrix for the functional variables. $\boldsymbol{\Sigma}_{rr} = \begin{bmatrix} 1 & {\rho_1}^{|i-j|} & \ldots & {\rho_1}^{|i-j|} \\ {\rho_1}^{|i-j|} & 1 & \ldots & {\rho_1}^{|i-j|} \\ \ldots & \ldots & \ldots & \ldots \\ {\rho_1}^{|i-j|} & {\rho_1}^{|i-j|} & \ldots & 1 \end{bmatrix}_{P_r \times P_r}$ is the within group covariance matirx for coefficients in the r-th functional variable. $\boldsymbol{\Sigma}_{rs} = \begin{bmatrix} \rho_2 & {\rho_2}^{|i-j|+1} & \ldots & {\rho_2}^{|i-j|+1} \\ {\rho_2}^{|i-j|+1} & \rho_2 & \ldots & {\rho_2}^{|i-j|+1} \\ \ldots & \ldots & \ldots & \ldots \\ {\rho_2}^{|i-j|+1} & {\rho_2}^{|i-j|+1} & \ldots & \rho_2 \end{bmatrix}_{P_r \times P_s}$ is the among group covariance matrix for coefficients in the r-th and s-th functional variable. Three data sets, training, validation and testing data sets of sample sizes $n_{tr} = 100$, $n_{va} = 100$, and $n_{te} = 200$ are generated for each setting. Note that one can also generate the simulation data by firstly generating the functional variables, and then using basis expansion to decompose the functional variables to form $\mathbb{x}_i$, but the nature of the problem will not change.

The model coefficients are generated as follows. For Scenarios 1 and 2, ${\boldsymbol{\beta}_0}^{(1)} \sim N(\boldsymbol{\mu}', \boldsymbol{I})$, $\boldsymbol{\mu}'$ has the same structure as $\boldsymbol{\mu}$. The scalar variables' coefficients in $\boldsymbol{\mu}'$ have mean 2, and the functional variables' coefficients in $\boldsymbol{\mu}'$ have mean $\mathbf{1}$, where $\mathbf{1}$ is a vector composed of 1's. $\boldsymbol{I}$ is an identity

matrix. The coefficients in $\boldsymbol{\beta}_0{}^{(0)}$ is generated by adding a small pertubation that follows $N(0, 0.1^2)$ to coefficients in $\boldsymbol{\beta}_0{}^{(1)}$. For Scenarios 3 and 4, $\boldsymbol{\beta}_0{}^{(1)}$ and $\boldsymbol{\beta}_0{}^{(0)}$ are generated independently from $N(\boldsymbol{\mu}', \boldsymbol{I})$ and $N(\boldsymbol{\mu}' + 3, \boldsymbol{I})$, respectively. For all scenarios, $\boldsymbol{\eta}_0 \sim \frac{1}{2} N(\boldsymbol{\mu}', \boldsymbol{I})$. The elements in the significant sets $\boldsymbol{I}^{(1)}$, $\boldsymbol{I}^{(0)}$ and $\boldsymbol{I}$ take binary values, and are randomly generated according to the conditions in Scenarios 1-4. Finally, $\boldsymbol{\beta}^{(1)}$, $\boldsymbol{\beta}^{(0)}$ and $\boldsymbol{\eta}$ are obtained by $\boldsymbol{\beta}^{(1)} = \boldsymbol{\beta}_0{}^{(1)} \cdot \boldsymbol{I}^{(1)}$, $\boldsymbol{\beta}^{(0)} = \boldsymbol{\beta}_0{}^{(0)} \cdot \boldsymbol{I}^{(0)}$, and $\boldsymbol{\eta} = \boldsymbol{\eta}_0 \cdot \boldsymbol{I}$, where $\cdot$ represents elementwise multiplication. Finally, $\varepsilon^{(m)} \sim N(0,1)$, $m = 0,1$.

We compare the proposed functional QQ models with benchmark models, where l_1 penalized functional linear regressions and an l_1 penalized functional logistic regression are separately used for modeling the quantitative and qualitative responses [155]. Under each simulation setting, 50 replications are performed. In each replication, the training data set is used for model estimation, the validation data set is used for tuning parameters selection, and the model prediction performance is evaluated with the testing data set. Specifically, the tuning parameters that yield the smallest prediction errors in the validation data set are selected for model prediction.

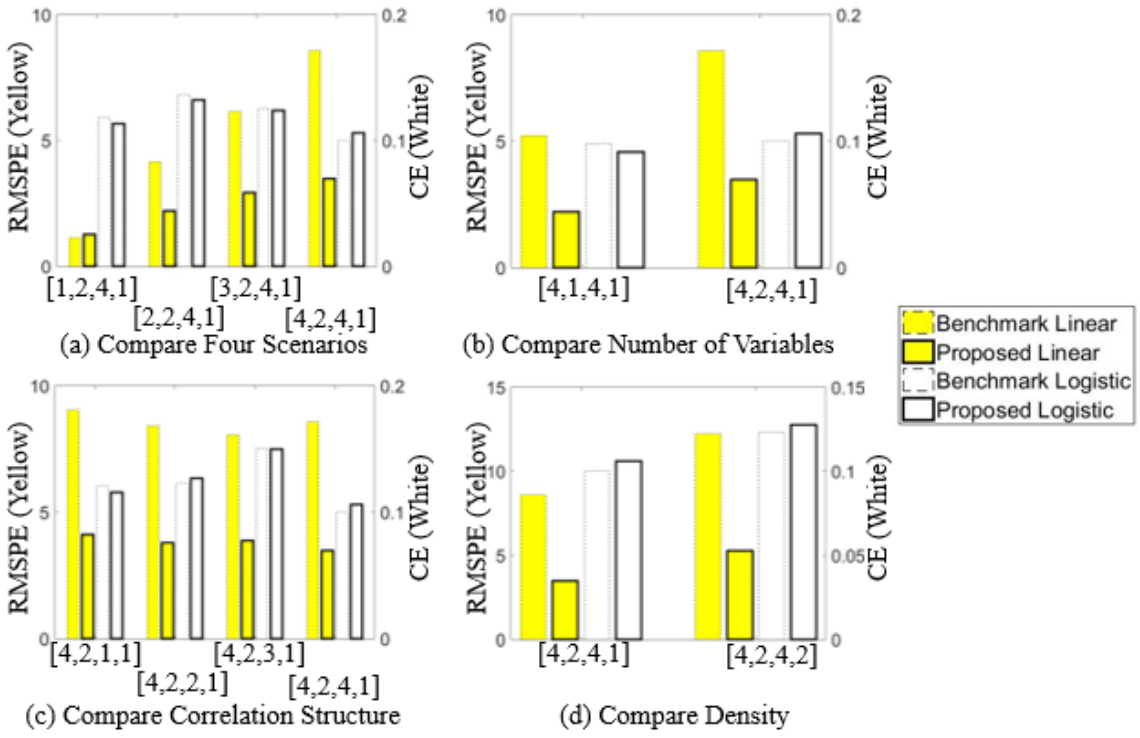

Figure 4.3. A Summary of Representative Simulation Average Testing RMSPE (Yellow) for the Quantitative Response and CE (White) for the Qualitative Response

Figure 4.3 shows comparisons of some representative average testing Root Mean Square Prediction Errors (RMSPE) for the quantitative response and Classification Errors (CE) for the qualitative response over 50 replications. The smaller the errors, the better the models perform. In each plot of Figure 4.3, the left vertical axis shows the scale for average RMSPE (Yellow), the right vertical axis shows the scale for average CE (White), and the horizontal axis shows different simulation settings. These simulation settings are indexed by the numbers in the parethnesis (see Table 4.1 for detailed values and meanings of these numbers). For instance, [1,1,4,2] represents the current simulation setting is for the first scenario, the first number of variables level ($p = 2, q = 4$), the fourth correlation structure level ($\rho_1 = 0.6, \rho_2 = 0.3$), and the second density level ($den. = 0.4$). A list of average testing RMSPE and CE over all simulation settings are provided in Table E1 in Appendix E. The major conclusions from the simulation

studies are: 1) For Scenario 1 (with the same levels in other factors), the benchmark models have comparable or slightly better prediction performance than functional QQ models (Figure 4.3 (a)); 2) For Scenarios 2-4 (with the same levels in other factors), the functional QQ models perform better than benchmark models for the quantitative response prediction, and the two approaches perform comparable for the qualitative response prediction (Figure 4.3 (a)); 3) When the number of variables or the proportion of significant coefficients in the underlying models increases, both the RMSPE in the proposed and benchmark models increase (Figure 4.3 (b) and (d)). And the advantage of the proposed models over benchmark models becomes more obvious under the above situations. The functional QQ models perform well under scenarios 2-4 since the underlying models for the quantatitative response at different conditions of the qualitative response are different, and the association of the QQ responses can be borrowed to enhance the model performance.

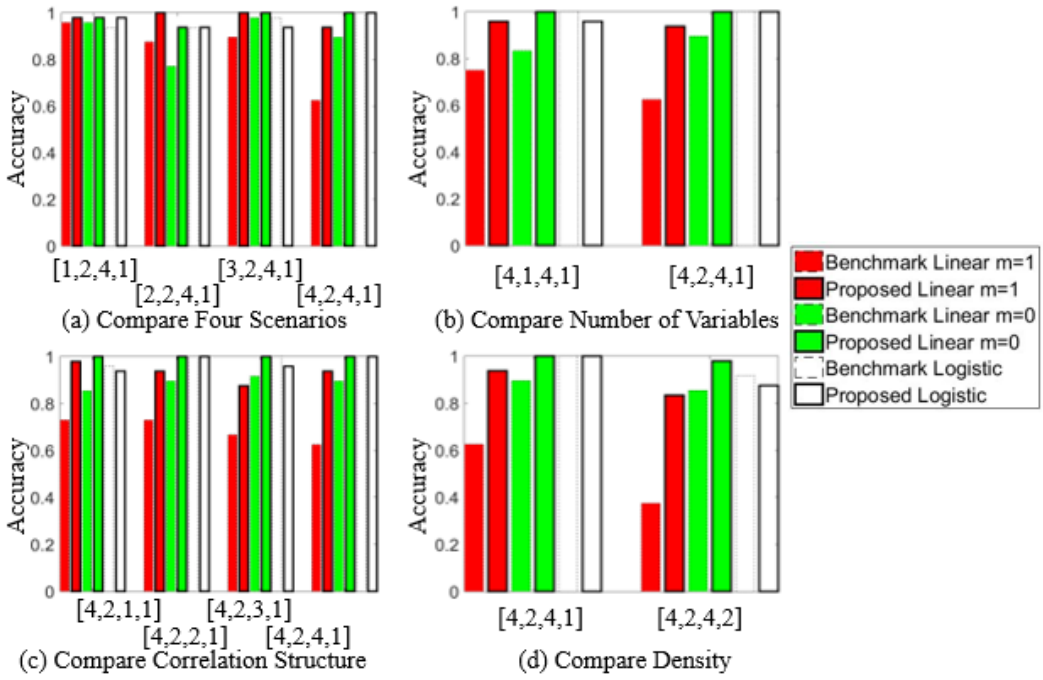

Figure 4.4. A Summary of Representative Simulation Average Variable Selection Accuracy Comparison

Figure 4.4 shows comparions of some representative average variable selection accuracy over 50 replications, where a variable is treated important if it is selected in more than half of the replications (i.e., 25 replications). The variable selection accuracy is calculated as the proportion of significant coefficients in the underlying model being selected or insignificant coefficients in the underlying model being eliminated. For benchmark linear regression, we compare the estimated model with the underlying $m = 1$ and $m = 0$ linear models to obtain the accuracy for "Benchmark Linear $m = 1$" and "Benchmark Linear $m = 0$", respectively. The vertical axis in each plot of Figure 4.4 represents the average variable selecton accuracy over 50 replications, and the horizontal axis has the same meaning as those in Figure 4.3. A list of overall variable selection accuracy, true positive rate (proportion of significant coefficients in the underlying model being selected) and true negative rate (proportion of insignificant coefficients in the underlying model being eliminated) over all simulation settings are provided in Tables E2-E4 in Appendix E. For the variable selection accuracy, the proposed models have better variable selection accuracy than benchmark models under Scenarios 2-4 (Figure 4.4 (a)). The variable selection accuracy (especially in the linear $m = 1$ model) tends to decrease when the number of variables or the proportion of significant coefficients in the underlying models increases, and the advantage of the proposed models is more obvious for these situations.

4.5. Case Study

The proposed functional QQ models are applied to the experimental data collected from a FDM process. In this process, a part modified from National Aerospace Standard (NAS) 979 standard testing part (Figure 4.5 (a)) is printed with Acrylonitrile Butadiene Styrene (ABS) material by MakerBot Replicator 2X [2]. During the experiment, three factors are varied: feed/flow ratio,

layer thickness and extruder temperature [2]. Other process variables, such as extruder travel path, filament diameter, etc. are kept constant.

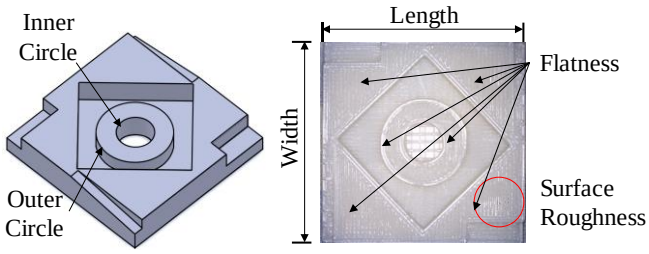

(a) FDM Test Part (b) FDM Printed Part

Figure 4.5. (a) FDM Test Part Modified from NAS 979 Standard Part [2] (b) FDM Printed Part and Representative Quality Variables

In total, we have 44 successfully printed parts, where *in situ* process variables are collected from the sensor network [2]. After the parts are printed (Figure 4.5 (b)), their dimensional accuracy is inspected by the Coordinate Measurement Machine (CMM). The dimensional accuracy variables measured include (Figure 4.5): part width, part length, diameter of the outer circle, top plane flatness, outer circle roundness, inner circle roundness, concentric of the two circles, coaxial of the two circles, run-out cylinderity of the outer circle. The surface roughness (go/no-go) is judged by domain experts, where the "no-go" samples are indexed by 1 and "go" samples are indexed by 0.

Since the part roughness judgement is only related to the surface and the dimensional accuracy is related to all layers but mainly determined by the layers close by the surface, we extract the segment of the *in situ* process variables that corresponded to the top several layers for the quality modeling. Specifically, the segments for the top three layers are extracted in this study, where the data for different layers are separated based on the part g-code. If the printing quality in between the layers can be measured, the corresponding *in situ* measurements for the quality variable can be extracted and used for the modeling. Figure 4.6 (a-c) shows the sensor system, and Figure 4.6

(d) shows an example of the three axes vibration signals at extruder and bed, and temperature signals at melt pool and bed. See the details of the sensor type, placement, etc. in [2]. In particular, The melt pool temperature is measured with IR temperature sensor (Exergen UIRT/C.4-440F) located at the extruder head pointing towards the melt pool (Figure 4.6 (a)), the vibration data are measured with tri-axis accelerometer (Analog Devices ADXL335) located at extruder arm and table respectively for extruder vibration and table vibration measurement (Figure 4.6 (b)-(c)), and the bed temperature is measured with thermocouples (Omega 5TC-GG-K-20-36) located at four corners of the printer bed (Figure 4.6 (c)). The vibration and bed temperature signals are measured at a sampling frequency of ~2.5 Hz, and the melt pool temperature signal is measured at a sampling frequency of 1 Hz. All signals are synchronized to the same frequency of 1 Hz in the analysis. Such a frequency combination has shown to be effective to reflect the FDM process condition [2, 128].

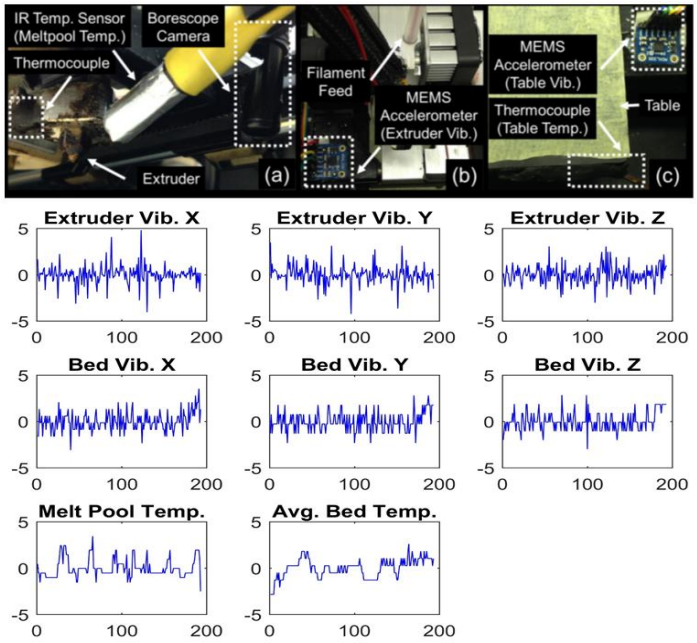

(d) An example of standardized *in situ* process variables.
(Vib.: Vibration, Temp.: Temperature, Avg.: Average)

Figure 4.1. (a-c) Sensor Placement in the Sensor Network [2]. (d) An Example of Standardized *in situ* Process Variables

For extruder and bed vibration, the Power Spectrum Density (PSD) is calculated based on the x-, y- and z-axis vibration measurements [156]. The PSD of vibration signal is widely used for machine condition monitoring and fault diagnosis [156]. The PSD of three axes is calculated as one variable since the vibration in all axes tends to affect the part quality, and we are interested in the effects of the entire vibration at the extruder and at the bed on the part quality. As a result, we have 86 features for extruder and bed vibration, separately. For melt pool temperature and average bed temperature, 56 features are generated with the spline basis expansion. The scalar offline setting variables and their two-way interactions are also considered, which include 6 features. In total, we have 290 features as model inputs. We take the first Principle Component (PC) of the dimensional accuracy variables measured by the CMM as the quantitative response, and the surface roughness condition as the qualitative (binary) response in the functional QQ models. The first PC is used as a composite quality indicator in this chapter to represent the overall part dimensional accuracy, and functional QQ models with multiple quantitative responses will be considered in the future work.

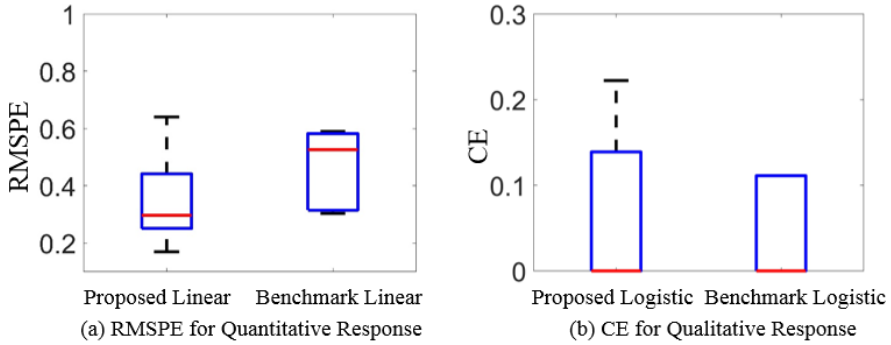

Figure 4.7. Boxplots of Testing RMSPE and CE for the Quantitative Response and Qualitative Response

We use two levels of 5-fold CV for tuning parameters selection and model evaluation, separately. 5-fold CV is used since the sample size in the case study is limited for generating a validation

data set for tuning parameters selection. Specifically, we first divide the samples approximately equally into 5 folds (first level CV), and select 4 of them as training data set. During the model fitting, the selected training data set is further divided approximately equally into 5 folds (second level CV). The tuning parameters are selected by the second level CV, i.e., the M_1 and M_2 yielding the smallest average testing errors in the second level CV are selected. The model performance is evaluated by the first level CV. The boxplots of the testing RMSPE and CE for the proposed models and benchmark models under the 5-fold CV are shown in Figure 4.7. From Figure 4.7, the functional QQ models have better prediction performance than the benchmark models for the quantitative response, and the two approaches have comparable performance for the qualitative response prediction. This is because the quantitative dimensional accuracy is modeled conditional on the qualitative surface roughness condition, and the functional linear regressions for the quantitative dimensional accuracy under different surface roughness condition are different (Figure 4.8). Therefore, the functional QQ models can yield better modeling performance by jointly model the QQ responses in the FDM process.

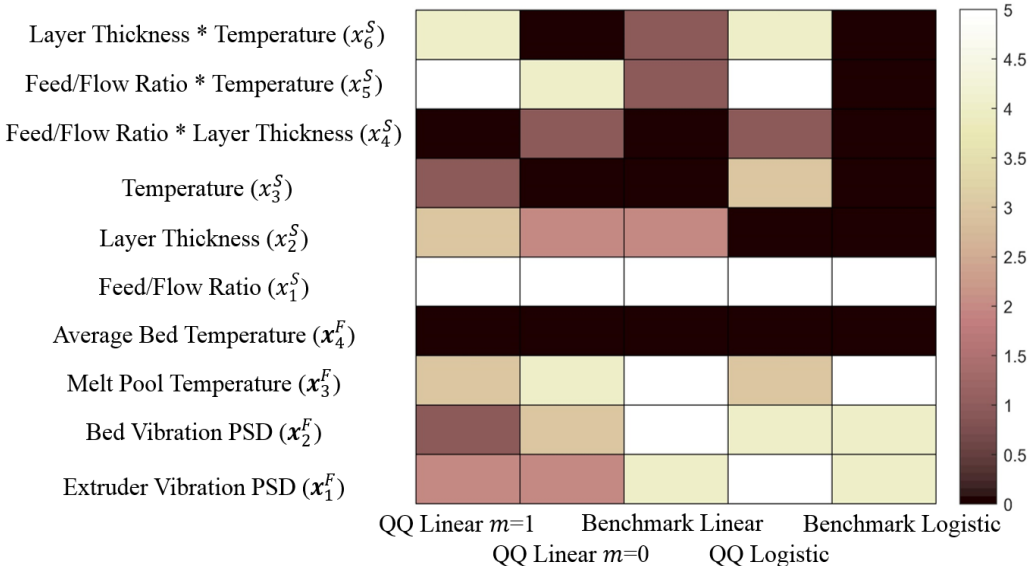

Figure 4.8. Number of Times a Variable Being Selected over 5-fold CV

Furthermore, a summary of the average selected variables over the 5-fold CV (first level CV) is shown in Figure 4.8. In Figure 4.8, an *in situ* process variable is regarded as selected if some elements in this *in situ* process variable is selected. Each column in Figure 4.8 represents a model, and each row represents a variable or two-way interaction between variables. The intensity (color bar) in Figure 4.8 shows the number of times a variable being selected in the 5-fold CV. From Figure 4.8, both offline setting variables and *in situ* process variables are important for the quality modeling, and the two linear models under different surface roughness conditions are different. Note that the conditional relationships between the qualitative response (surface roughness condition) and quantitative response (dimensional accuracy) in Eqs. (4.10)-(4.11) show the association among the QQ responses, but not causal relationships. The functional QQ models can enhance the prediction performance for the quantitative response based on this association (Figure 4.7 (a)), compared with the benchmark separate modeling of QQ responses. In particular, the feed/flow ratio governing the ratio of how fast the nozzle travels and how fast the material is extruded from the nozzle is very important for the part quality. The *in situ* process variables extruder vibration, bed vibration and melt pool temperature are important for modeling the dimensional accuracy and surface roughness condition (the last 3 rows in Figure 4.8). This is because the changes in extruder vibration, bed vibration, and temperature in the melt pool area are informative for the process condition. Moreover, the functional QQ models in the last CV fold for dimensional accuracy with the surface roughness at bad condition (m=1) and at good condition (m=0), and for surface roughness condition are shown in Eqs. (4.10), (4.11) and (4.12), respectively. The variable names in Eqs. (4.10)-(4.12) are available in Figure 4.8. For instance, $x_{3,55}^{F}$ refers to the 55-th elements in the melt pool temperature, and x_1^S refers to feed/flow ratio.

$$(y_i|z_i = 1) = -0.038x_{3,55}^{F} - 0.912x_1^S + 0.382x_2^S - 0.149x_5^S + 0.005x_6^S, \quad (4.10)$$

$$(y_i|z_i = 0) = 0.012x_{1,37}^F + 0.092x_{2,37}^F + 0.007x_{2,82}^F + 0.050x_{3,40}^F - 0.864x_1^S + 0.050x_2^S - 0.035x_5^S, \quad (4.11)$$

$$logit(E[z_i|\boldsymbol{x}_i]) = -1.328 - 0.291x_{1,15}^F + 0.754x_{1,53}^F + 0.692x_{2,3}^F + 0.240x_{2,20}^F + 0.488x_{3,40}^F - 1.283x_1^S + 0.378x_3^S - 0.142x_4^S - 1.202x_5^S + 0.671x_6^S, \quad (4.12)$$

These equations are helpful for the AM processes quality monitoring and control. For instance, one can monitor whether the surface roughness or dimensional accuracy is at a desired condition based on the offline setting variables and *in situ* process variables by control charts. Eqs. (4.10) and (4.11) can also be used for the dimensional accuracy control. Note that the model parameters will vary for different applications, and need to be refitted for other machines and applications.

4.6. Conclusions of Functional Quantitative and Qualitative Models

AM is a promising manufacturing process to produce flexible part, reduce material waste and product development life cycle. In the past decade, both industry and academia have investigated intensively to help with the wide deployment of AM applications. More investigations are still needed for quality control and assurance in AM processes. In this chapter, we investigate the heterogeneous types of quality responses in a FDM AM process. The dimensional accuracy (quantitative response) and surface roughness condition (qualitative response) are jointly modeled with both offline setting variables and *in situ* process variables. Functional QQ models are newly proposed to fulfill the above task.

It is demonstrated that the product quality responses can be better predicted by jointly considering the QQ responses, since the linear models for different surface roughness conditions are different (Figure 4.8). The offline setting variables feed/flow ratio, layer thickness, extruder temperature and their two-way interactions, and the *in situ* process variables extruder vibration, bed vibration and melt pool temperature are important for the part quality modeling. The functional QQ models are also evaluated in the simulation studies, and yield better prediction and variable selection results as long as the underlying linear models vary with different values

of the qualitative response.

The functional QQ models provide a method to simultaneously evaluate the quantitative and qualitative responses with *in situ* process variables and offline setting variables in a system, and can be used for the process monitoring and control for systems with QQ responses.

Chapter 5. Conclusions and Future Research

Advanced manufacturing needs to optimize the entire product lifecycle to satisfy the evolving and diverse customer requirements. To achieve this goal, one needs to investigate the real time data and information embedded in manufacturing. Thanks to the development of sensing and information technology, heterogeneous types of variables are collected in manufacturing processes to reflect the process conditions. Among different types of variables, functional *in situ* process variables are measured in real time during the manufacturing processes. These functional variables provide great opportunity for data-driven modeling, monitoring and control of the manufacturing processes to achieve the system resilience and flexibility. However, these functional variables also bring challenges for the manufacturing processes data analytics. Currently, there is a lack of systematic methodology to address the modeling of heterogeneous types of variables in advanced manufacturing processes.

In this dissertation, several problems on modeling of heterogeneous types of variables are addressed. In particular, the following methodologies are proposed:

1) A functional variable selection methodology is proposed to select the important *in situ* process variables and their local features for a binary quality indicator. This method formulates the prediction of binary quality indicator as a classification problem, and uses logistic regression model for the classification. To simultaneously select the *in situ* process variables and their local features, an HNNG constraint is proposed (Section 2.3.3) with the computational issue solved by a second order Taylor expansion of the objection function [64]. The merits of the functional variable selection method are demonstrated in both simulation studies and a case study in a crystal growth manufacturing process by comparing with benchmark methods such as Lasso, NNG, GrpLasso and HLasso. The proposed method performs well when the number of training

samples is sufficient or the underlying model is sparse in the simulation studies, and performs well in the case study.

2) A functional graphical model is proposed to learn the variable relationships among offline setting variables, *in situ* process variables, and continuous quality variables. The functional graphical model integrates the knowledge from graphical modeling and functional data analysis, so that functional nodes can be handled in the graphical model. Under a multivariate normal distribution assumption and known variable orderings, the conditional dependency of nodes in the graphical model can be learned by penalized regressions, where an l_1 norm is used for overall model complexity and a difference from the mean penalty is introduced for functional nodes (Eq. 3.8 in Section 3.3.3). The merits of the functional graphical model over the traditional scalar graphical models are demonstrated in both simulation studies and a case study in a plasma spray process. The proposed method performs well when the sample size is small, the SNR is small, or the samples across elements in a functional node do not totally overlap in the simulation studies, and performs well in the case study.

3) Functional QQ models are proposed to jointly model the QQ responses with offline setting variables and *in situ* process variables. Other than separately model the quantitative and qualitative responses in two models, the QQ models use a joint likelihood approach to model QQ responses in one model [64]. In addition to the offline setting variables, the *in situ* process variables are incorporated in the functional QQ models, and the HNNG constraint is used for functional variable selection. Compared with the HNNG in chapter 2, the effect of group size is considered in the HNNG constraint (since the model predictors include both scalar offline setting variables and functional *in situ* process variables), and two tuning parameters are separately tuned for the quantitative and qualitative responses model complexity (Eq. (4.9) in Section 4.3.2).

The merits of the proposed method over benchmark separate response modeling method are demonstrated in both simulation studies and a case study in a FDM AM process. The proposed method performs well when the relationships between the quantitative response and model predictors vary at different levels of qualitative response in simulation studies, and performs well in the case study.

The proposed methodologies are widely applied to advanced manufacturing processes, including semiconductor manufacturing, aero-engine manufacturing, and additive manufacturing. There are several future research topics that deserve to be investigated to enhance the capability of the proposed methodologies, including:

1) to address the class imbalance problem in the functional variable selection in Chapter 2, weighted logistic regression or new algorithms can be investigated [157]. The relationships between successive samples and the observational data from other crystal growth phases can be studied, where historical functional regression models can be used to describe the temporal relationships [158]. The computation issue for large scale problems (i.e., when the number of functional variables is large) can be addressed by designing computation efficient algorithms. For instance, instead of using quadratic programming, first-order algorithms such as proximal gradient method and accelerated proximal gradient method can be adopted [159]. Distributed computing can be used, by developing variants of Alternating Direction Method of Multipliers (ADMM) [159], to allocate the computation into different computing units.

2) In the functional graphical model in Chapter 3, the variables of interests come from different categories (offline setting variables, *in situ* process variables and quality response variables). The association of the variables within the same category of variables is not investigated. For examples, the *in situ* process variables may be associated with each other. To address this issue,

a chain graphical model [161] can be investigated, where both directed edges to represent the relationships for the variables among the categories and undirected edges to represent the correlation for the variables within a category. In addition, the functional graphical model can be generalized to handle the dynamic systems, where the model structure may change over time [104]. The learning of functional graphical model without the variable orderings can be studied. Moreover, Bayesian variants of the graphical modeling approaches can be explored by proposing novel priors to enforce the sparsity and coefficients similarity. Finally, online updating of the graphical model structures as new data streams are observed will be investigated.

3) For the functional QQ models, multiple quantitative or qualitative responses can be considered in the modeling, where multiple heterogeneous responses can borrow strength from each other during the modeling. For instance, in the FDM process, other than modeling the PC of the geometrical deviation variables, multiple quantitative responses can be modeled for each geometrical deviation variable. The hierarchical principle for the scalar factors and their two-way interactions can be included during the modeling. In addition, the situation with missing data in certain response will be tolerated in the joint modeling to increase the robustness of the framework. Moreover, the QQ models based monitoring and control will be investigated. Finally, the hierarchical relationships among the scalar offline setting variables, *in situ* process variables, and quality responses can be explored. Such hierarchical relationships can help answer the question of what combinations of heterogeneous variables should be used to balance the model prediction accuracy and sensor instrumentation cost.

References

[1] http://techonomy.com/2014/09/manufacturers-struggle-turn-data-insight/.

[2] P. K. Rao, J. P. Liu, D. Roberson, Z. J. Kong, and C. Williams, "Online real-time quality monitoring in additive manufacturing processes using heterogeneous sensors," *Journal of Manufacturing Science and Engineering*, vol. 137, no. 6, pp. 061007, 2015.

[3] J. Zhang, W. Li, K. Wang, and R. Jin, "Process adjustment with an asymmetric quality loss function," *Journal of Manufacturing Systems*, vol. 33, no. 1, pp. 159-165, 2014.

[4] L. Zhu, C. Dai, H. Sun, W. Li, R. Jin, and K. Wang, "Curve monitoring for a single-crystal ingot growth process," *Proceedings of the 5th International Asia Conference on Industrial Engineering and Management Innovation (IEMI2014)*, E. Qi, Q. Su, J. Shen, F. Wu and R. Dou, eds., pp. 227-232: Atlantis Press, 2015.

[5] H. Sun, X. Deng, K. Wang, and R. Jin, "Logistic regression for crystal growth process modeling through hierarchical nonnegative garrote-based variable selection," *IIE Transactions*, vol. 48, no. 8, pp. 787-796, 2016.

[6] H. Sun, R. Jin, and B. Zimmerman, "Process Modeling and Mapping for a Plasma Spray Coating Process," *Proceedings of the 2015 Industrial and Systems Engineering Research Conference*, S. Cetinkaya and J. K. Ryan, eds., pp. 1797-1804, 2015.

[7] H. Sun, S. Huang, and R. Jin, "Functional graphical models for manufacturing process modeling," *IEEE Transactions on Automation Science and Engineering*, accepted, 2017.

[8] H. Sun, K. Wang, Y. Li, C. Zhang, and R. Jin, "Quality modeling of printed electronics in aerosol jet printing based on microscopic images," *Journal of Manufacturing Science and Engineering*, vol. 139, no. 7, pp. 071012, 2017.

[9] H. Sun, P. Rao, Z. J. Kong, X. Deng, and R. Jin, "Modeling quantitative and qualitative quality responses in additive manufacturing with offline setting and *in situ* process variables," *IEEE Transactions on Automation Science and Engineering*, under revision, 2016.

[10] K. Kim, M. A. Mahmoud, and W. H. Woodall, "On the monitoring of linear profiles," *Journal of Quality Technology*, vol. 35, no. 3, pp. 317-328, 2003.

[11] P. Qiu, C. Zou, and Z. Wang, "Nonparametric profile monitoring by mixed effects modeling," *Technometrics*, vol. 52, no. 3, pp. 265-277, 2010.

[12] W. A. Jensen, J. B. Birch, and W. H. Woodall, "Monitoring correlation within linear profiles using mixed models," *Journal of Quality Technology*, vol. 40, no. 2, pp. 167-183, 2008.

[13] W. H. Woodall, D. J. Spitzner, D. C. Montgomery, and S. Gupta, "Using control charts to monitor process and product quality profiles," *Journal of Quality Technology*, vol. 36, no. 3, pp. 309-320, 2004.

[14] W. H. Woodall, "Current research on profile monitoring," *Production*, vol. 17, no. 3, pp. 420-425, 2007.

[15] R. Noorossana, A. Saghaei, and A. Amiri, *Statistical analysis of profile monitoring*: John Wiley & Sons, 2011.

[16] F. M. Megahed, L. J. Wells, J. A. Camelio, and W. H. Woodall, "A spatiotemporal method for the monitoring of image data," *Quality and Reliability Engineering International*, vol. 28, no. 8, pp. 967-980, 2012.

[17] L. Wells, F. Megahed, C. Niziolek, J. Camelio, and W. Woodall, "Statistical process monitoring approach for high-density point clouds," *Journal of Intelligent Manufacturing,* vol. 24, no. 6, pp. 1267-1279, 2013.
[18] W. H. Woodall, M. J. Zhao, K. Paynabar, R. Sparks, and J. D. Wilson, "An overview and perspective on social network monitoring," *IISE Transactions,* vol. 49, no. 3, pp. 1-12, 2016.
[19] J. Jin, and J. Shi, "Automatic feature extraction of waveform signals for in-process diagnostic performance improvement," *Journal of Intelligent Manufacturing,* vol. 12, no. 3, pp. 257-268, 2001.
[20] K. Paynabar, J. Jin, and M. P. Reed, "Informative sensor and feature selection via hierarchical nonnegative garrote," *Technometrics,* vol. 57, no. 4, pp. 514-523, 2015.
[21] Q. Huang, "Physics-driven Bayesian hierarchical modeling of the nanowire growth process at each scale," *IIE transactions,* vol. 43, no. 1, pp. 1-11, 2010.
[22] Z. Kong, O. Beyca, S. T. Bukkapatnam, and R. Komanduri, "Nonlinear sequential Bayesian analysis-based decision making for end-point detection of chemical mechanical planarization (CMP) processes," *IEEE Transactions on Semiconductor Manufacturing,* vol. 24, no. 4, pp. 523-532, 2011.
[23] P. M. Narendra, and K. Fukunaga, "A branch and bound algorithm for feature subset selection," *IEEE Transactions on Computers,* vol. 26, no. 9, pp. 917-922, 1977.
[24] S. Derksen, and H. Keselman, "Backward, forward and stepwise automated subset selection algorithms: Frequency of obtaining authentic and noise variables," *British Journal of Mathematical and Statistical Psychology,* vol. 45, no. 2, pp. 265-282, 1992.
[25] R. Tibshirani, "Regression shrinkage and selection via the Lasso," *Journal of the Royal Statistical Society. Series B (Methodological),* vol. 58, no. 1, pp. 267-288, 1996.
[26] L. Breiman, "Better subset regression using the nonnegative garrote," *Technometrics,* vol. 37, no. 4, pp. 373-384, 1995.
[27] E. Makalic, and D. Schmidt, "Logistic regression with the nonnegative garrote," *AI 2011: Advances in Artificial Intelligence, Lecture Notes in Computer Science,* D. Wang and M. Reynolds, eds., pp. 82-91: Springer Berlin Heidelberg, 2011.
[28] A. Antoniadis, and J. Fan, "Regularization of wavelet approximations," *Journal of the American Statistical Association,* vol. 96, no. 455, pp. 939-955, 2001.
[29] H. Zou, and T. Hastie, "Regularization and variable selection via the Elastic Net," *Journal of the Royal Statistical Society. Series B (Statistical Methodology),* vol. 67, no. 2, pp. 301-320, 2005.
[30] M. Yuan, and Y. Lin, "Model selection and estimation in regression with grouped variables," *Journal of the Royal Statistical Society: Series B (Statistical Methodology),* vol. 68, no. 1, pp. 49-67, 2006.
[31] P. Zhao, G. Rocha, and B. Yu, "The composite absolute penalties family for grouped and hierarchical variable selection," *The Annals of Statistics,* vol. 37, no. 6A, pp. 3468-3497, 2009.
[32] N. F. Zhou, and J. Zhu, "Group variable selection via a hierarchical lasso and its oracle property," *Statistics and Its Interface,* vol. 3, no. 4, pp. 557-574, 2010.
[33] T. Hastie, R. Tibshirani, and J. Friedman, *The elements of statistical learning: data mining, inference, and prediction,* New York: Springer 2009.
[34] P. H. Foo, and G. W. Ng, "High-level information fusion: an overview," *Journal of Advances in Information Fusion,* vol. 8, no. 1, pp. 33-72, 2013.

[35] G. Fisher, M. R. Seacrist, and R. W. Standley, "Silicon crystal growth and wafer technologies," *Proceedings of the IEEE,* vol. 100, no. Special Centennial Issue, pp. 1454-1474, 2012.
[36] G. Dhanaraj, K. Byrappa, V. Prasad, and M. Dudley, *Springer handbook of crystal growth*: Springer Berlin Heidelberg, 2010.
[37] W. Zulehner, "Czochralski growth of silicon," *Journal of Crystal Growth,* vol. 65, no. 1–3, pp. 189-213, 1983.
[38] S. Mahajan, "Defects in semiconductors and their effects on devices," *Acta Materialia,* vol. 48, no. 1, pp. 137-149, 2000.
[39] T. Sinno, E. Dornberger, W. V. Ammon, R. A. Brown, and F. Dupret, "Defect engineering of Czochralski single-crystal silicon," *Materials Science and Engineering: R: Reports,* vol. 28, no. 5–6, pp. 149-198, 2000.
[40] V. V. Voronkov, "The mechanism of swirl defects formation in silicon," *Journal of Crystal Growth,* vol. 59, no. 3, pp. 625-643, 1982.
[41] R. A. Brown, Z. Wang, and T. Mori, "Engineering analysis of microdefect formation during silicon crystal growth," *Journal of Crystal Growth,* vol. 225, no. 2–4, pp. 97-109, 2001.
[42] S. G. Mallat, "A theory for multiresolution signal decomposition: the wavelet representation," *Pattern Analysis and Machine Intelligence, IEEE Transactions on,* vol. 11, no. 7, pp. 674-693, 1989.
[43] M. Yuan, and Y. Lin, "On the non-negative garrotte estimator," *Journal of the Royal Statistical Society. Series B (Statistical Methodology),* vol. 69, no. 2, pp. 143-161, 2007.
[44] J. J. Derby, and R. A. Brown, "Thermal-capillary analysis of Czochralski and liquid encapsulated Czochralski crystal growth: I. Simulation," *Journal of Crystal Growth,* vol. 74, no. 3, pp. 605-624, 1986.
[45] D. E. Bornside, T. A. Kinney, R. A. Brown, and G. Kim, "Finite element/Newton method for the analysis of Czochralski crystal growth with diffuse-grey radiative heat transfer," *International Journal for Numerical Methods in Engineering,* vol. 30, no. 1, pp. 133-154, 1990.
[46] P. A. Sackinger, R. A. Brown, and J. J. Derby, "A finite element method for analysis of fluid flow, heat transfer and free interfaces in Czochralski crystal growth," *International Journal for Numerical Methods in Fluids,* vol. 9, no. 4, pp. 453-492, 1989.
[47] G. Müller, "Experimental analysis and modeling of melt growth processes," *Journal of Crystal Growth,* vol. 237–239, Part 3, no. 0, pp. 1628-1637, 2002.
[48] T. Miyano, and A. Shintani, "Nonlinear analysis of complexities in striations of Czochralski silicon crystals," *Applied Physics Letters,* vol. 63, no. 26, pp. 3574, 1993.
[49] A. Shintani, T. Miyano, and M. Hourai, "A novel apporach to the characterization of growth striations in Czochralski silicon crystals," *Journal of The Electrochemical Society,* vol. 142, no. 7, pp. 2463-2469, 1995.
[50] T. Fühner, and T. Jung, "Use of genetic algorithms for the development and optimization of crystal growth processes," *Journal of Crystal Growth,* vol. 266, no. 1-3, pp. 229-238, 2004.
[51] M. Avci, and S. Yamacli, "Neural network reinforced point defect concentration estimation model for Czochralski-grown silicon crystals," *Mathematical and Computer Modelling,* vol. 51, no. 7-8, pp. 857-862, 2010.

[52] S. J. Ratcliffe, G. Z. Heller, and L. R. Leader, "Functional data analysis with application to periodically stimulated foetal heart rate data. II: Functional logistic regression," *Statistics in Medicine,* vol. 21, no. 8, pp. 1115-1127, 2002.
[53] A. J. Miller, *Subset selection in regression,* Boca Raton: Chapman & Hall/CRC, 2002.
[54] L. Meier, S. Van De Geer, and P. Bühlmann, "The group lasso for logistic regression," *Journal of the Royal Statistical Society: Series B (Statistical Methodology),* vol. 70, no. 1, pp. 53-71, 2008.
[55] J. Huang, S. Ma, H. Xie, and C. Zhang, "A group bridge approach for variable selection," *Biometrika,* vol. 96, no. 2, pp. 339-355, 2009.
[56] J. Huang, P. Breheny, and S. Ma, "A selective review of group selection in high-dimensional models," *Statistical Science,* vol. 27, no. 4, pp. 481-499, 2012.
[57] J. Jin, and J. Shi, "Feature-preserving data compression of stamping tonnage information using wavelets," *Technometrics,* vol. 41, no. 4, pp. 327-339, 1999.
[58] R. Ganesan, T. K. Das, and V. Venkataraman, "Wavelet-based multiscale statistical process monitoring: A literature review," *IIE Transactions,* vol. 36, no. 9, pp. 787-806, 2004.
[59] S. Zhou, and J. Jin, "Automatic feature selection for unsupervised clustering of cycle-based signals in manufacturing processes," *IIE Transactions,* vol. 37, no. 6, pp. 569-584, 2005.
[60] S. Bukkapatnam, J. Nichols, M. Seaver, S. Trickey, and M. Hunter, "A wavelet-based, distortion energy approach to structural health monitoring," *Structural Health Monitoring,* vol. 4, no. 3, pp. 247-258, 2005.
[61] M. K. Jeong, J. C. Lu, X. Huo, B. Vidakovic, and C. Di, "Wavelet-based data reduction techniques for process fault detection," *Technometrics,* vol. 48, no. 1, pp. 26-40, 2006.
[62] J. Li, J. Shi, and T.-S. Chang, "On-line seam detection in rolling processes using snake projection and discrete wavelet transform," *Journal of Manufacturing Science and Engineering,* vol. 129, no. 5, pp. 926-933, 2007.
[63] K. Paynabar, and J. Jin, "Characterization of non-linear profiles variations using mixed-effect models and wavelets," *IIE Transactions,* vol. 43, no. 4, pp. 275-290, 2011.
[64] X. Deng, and R. Jin, "QQ models: joint modeling for quantitative and qualitative quality responses in manufacturing systems," *Technometrics,* vol. 57, no. 3, pp. 320-331, 2015.
[65] P. J. Lucas, L. C. van der Gaag, and A. Abu-Hanna, "Bayesian networks in biomedicine and health-care," *Artificial Intelligence in Medicine,* vol. 30, no. 3, pp. 201-214, 2004.
[66] S. Huang, J. Li, J. Ye, A. Fleisher, K. Chen, T. Wu, and E. Reiman, "A sparse structure learning algorithm for Gaussian Bayesian network identification from high-dimensional data," *Pattern Analysis and Machine Intelligence, IEEE Transactions on,* vol. 35, no. 6, pp. 1328-1342, 2013.
[67] M. Jamali, and M. Ester, "A matrix factorization technique with trust propagation for recommendation in social networks," *Proceedings of the Fourth ACM Conference on Recommender Systems,* pp. 135-142: ACM New York, NY, USA, 2010.
[68] A. Ahmed, and E. P. Xing, "Recovering time-varying networks of dependencies in social and biological studies," *Proceedings of the National Academy of Sciences,* vol. 106, no. 29, pp. 11878-11883, 2009.
[69] L. Zeng, and S. Zhou, "Inferring the interactions in complex manufacturing processes using graphical models," *Technometrics,* vol. 49, no. 4, pp. 373-381, 2007.

[70] J. Li, and J. Shi, "Knowledge discovery from observational data for process control using causal Bayesian networks," *IIE Transactions,* vol. 39, no. 6, pp. 681-690, 2007.
[71] M. I. Jordan, and M. J. Wainwright, "Graphical models, exponential families, and variational inference," *Foundations and Trends® in Machine Learning,* vol. 1, no. 1–2, pp. 1-305, 2007.
[72] D. Koller, and N. Friedman, *Probabilistic graphical models: principles and techniques*: MIT press, 2009.
[73] P. Fauchais, J. R. Heberlein, and M. Boulos, *Thermal spray fundamentals,* New York: Springer, 2014.
[74] P. Fauchais, "Understanding plasma spraying," *Journal of Physics D: Applied Physics,* vol. 37, no. 9, pp. 86-108, 2004.
[75] M. Friis, and C. Persson, "Control of thermal spray processes by means of process maps and process windows," *Journal of Thermal Spray Technology,* vol. 12, no. 1, pp. 44-52, 2003.
[76] S. Sampath, X. Jiang, A. Kulkarni, J. Matejicek, D. L. Gilmore, and R. A. Neiser, "Development of process maps for plasma spray: case study for molybdenum," *Materials Science and Engineering: A,* vol. 348, no. 1–2, pp. 54-66, 2003.
[77] A. Shojaie, and G. Michailidis, "Penalized likelihood methods for estimation of sparse high-dimensional directed acyclic graphs," *Biometrika,* vol. 97, no. 3, pp. 519-538, 2010.
[78] W. Buntine, "Theory refinement on Bayesian networks," *Proceedings of the Seventh Conference on Uncertainty in Artificial Intelligence,* pp. 52-60: Morgan Kaufmann Publishers Inc., 1991.
[79] G. F. Cooper, and E. Herskovits, "A Bayesian method for the induction of probabilistic networks from data," *Machine learning,* vol. 9, no. 4, pp. 309-347, 1992.
[80] F. Li, and Y. Yang, "Using modified lasso regression to learn large undirected graphs in a probabilistic framework," *Proceedings of the National Conference on Artificial Intelligence*, pp. 801-807: AAAI Press, 2005.
[81] J. Z. Huang, N. Liu, M. Pourahmadi, and L. Liu, "Covariance matrix selection and estimation via penalised normal likelihood," *Biometrika,* vol. 93, no. 1, pp. 85-98, 2006.
[82] T. Evgeniou, and M. Pontil, "Regularized multi-task learning," *Proceedings of the 10th ACM SIGKDD International Conference on Knowledge Discovery and Data Mining*, pp. 109-117: ACM New York, NY, USA, 2004.
[83] J. Zhou, J. Chen, and J. Ye, "MALSAR: Multi-task learning via structural regularization," *Arizona State University*, 2011.
[84] J. Lawless, R. Mackay, and J. Robinson, "Analysis of variation transmission in manufacturing processes--Part I," *Journal of Quality Technology,* vol. 31, no. 2, pp. 131-142, 1999.
[85] J. Shi, *Stream of variation modeling and analysis for multistage manufacturing processes*: CRC press, 2006.
[86] Q. Huang, and J. Shi, "Stream of variation modeling and analysis of serial-parallel multistage manufacturing systems," *Journal of Manufacturing Science and Engineering,* vol. 126, no. 3, pp. 611-618, 2004.
[87] J. Liu, J. Jin, and J. Shi, "State space modeling for 3-D variation propagation in rigid-body multistage assembly processes," *Automation Science and Engineering, IEEE Transactions on,* vol. 7, no. 2, pp. 274-290, 2010.

[88] S. Zhou, Y. Chen, and J. Shi, "Statistical estimation and testing for variation root-cause identification of multistage manufacturing processes," *Automation Science and Engineering, IEEE Transactions on,* vol. 1, no. 1, pp. 73-83, 2004.
[89] D. Djurdjanovic, and J. Ni, "Stream-of-variation (SoV)-based measurement scheme analysis in multistation machining systems," *Automation Science and Engineering, IEEE Transactions on,* vol. 3, no. 4, pp. 407, 2006.
[90] R. Jin, and J. Shi, "Reconfigured piecewise linear regression tree for multistage manufacturing process control," *IIE Transactions,* vol. 44, no. 4, pp. 249-261, 2012.
[91] K. Liu, and S. Huang, "Integration of data fusion methodology and degradation modeling process to improve prognostics," *Automation Science and Engineering, IEEE Transactions on,* vol. 13, no. 1, pp. 344-354, 2016.
[92] S. Bukkapatnam, M. Malshe, P. Agrawal, L. Raff, and R. Komanduri, "Parametrization of interatomic potential functions using a genetic algorithm accelerated with a neural network," *Physical Review B,* vol. 74, no. 22, pp. 224102, 2006.
[93] P. Larrañaga, M. Poza, Y. Yurramendi, R. H. Murga, and C. M. Kuijpers, "Structure learning of Bayesian networks by genetic algorithms: A performance analysis of control parameters," *Pattern Analysis and Machine Intelligence, IEEE Transactions on,* vol. 18, no. 9, pp. 912-926, 1996.
[94] L. M. De Campos, J. M. Fernandez-Luna, J. A. Gámez, and J. M. Puerta, "Ant colony optimization for learning Bayesian networks," *International Journal of Approximate Reasoning,* vol. 31, no. 3, pp. 291-311, 2002.
[95] M. Schmidt, "Graphical model structure learning with l1-regularization," University of British Columbia, 2010.
[96] N. Friedman, I. Nachman, and D. Peér, "Learning Bayesian network structure from massive datasets: the sarse candidate algorithm," *Proceeding of the 15th Conference on Uncertainty in Artifitial Intelligence*, pp. 206-215: Morgan Kaufmann Publishers Inc., 1999.
[97] I. Tsamardinos, L. E. Brown, and C. F. Aliferis, "The max-min hill-climbing Bayesian network structure learning algorithm," *Machine Learning,* vol. 65, no. 1, pp. 31-78, 2006.
[98] F. Li, and Y. Yang, "Recovering genetic regulatory networks from micro-array data and location analysis data," *Genome Informatics,* vol. 15, no. 2, pp. 131-140, 2004.
[99] N. Meinshausen, and P. Bühlmann, "High-dimensional graphs and variable selection with the Lasso," *The Annals of Statistics,* vol. 34, no. 3, pp. 1436-1462, 2006.
[100] M. Yuan, and Y. Lin, "Model selection and estimation in the Gaussian graphical model," *Biometrika,* vol. 94, no. 1, pp. 19-35, 2007.
[101] J. Friedman, T. Hastie, and R. Tibshirani, "Sparse inverse covariance estimation with the graphical lasso," *Biostatistics,* vol. 9, no. 3, pp. 432-441, 2008.
[102] M. J. Wainwright, J. D. Lafferty, and P. K. Ravikumar, "High-dimensional graphical model selection using l1-regularized logistic regression," *Advances in NIPS 2006*, Vancouver, Canada, 2006, pp. 1465-1472.
[103] J. D. Lee, and T. J. Hastie, "Learning the structure of mixed graphical models," *Journal of Computational and Graphical Statistics* vol. 24, no. 1, pp. 230-253, 2015.
[104] K. P. Murphy, "Dynamic Bayesian networks: representation, inference and learning," University of California, Berkeley, 2002.
[105] J. O. Ramsay, *Functional data analysis*: Wiley Online Library, 2006.

[106] Y. Nesterov, "Gradient methods for minimizing composite functions," *Mathematical Programming,* vol. 140, no. 1, pp. 125-161, 2013.
[107] N. Parikh, and S. Boyd, "Proximal algorithms," *Foundations and Trends in Optimization,* vol. 1, no. 3, pp. 123-231, 2013.
[108] A. Beck, and M. Teboulle, "A fast iterative shrinkage-thresholding algorithm for linear inverse problems," *SIAM Journal on Imaging Sciences,* vol. 2, no. 1, pp. 183-202, 2009.
[109] J. Scott, N. Gupta, C. Weber, S. Newsome, T. Wohlers, and T. Caffrey, "Additive manufacturing: status and opportunities," *Science and Technology Policy Institute,* pp. 1-29, 2012.
[110] G. Tapia, and A. Elwany, "A review on process monitoring and control in metal-based additive manufacturing," *Journal of Manufacturing Science and Engineering,* vol. 136, no. 6, pp. 060801, 2014.
[111] W. E. Frazier, "Metal additive manufacturing: a review," *Journal of Materials Engineering and Performance,* vol. 23, no. 6, pp. 1917-1928, 2014.
[112] J. Winder, and R. Bibb, "Medical rapid prototyping technologies: state of the art and current limitations for application in oral and maxillofacial surgery," *Journal of Oral and Maxillofacial Surgery,* vol. 63, no. 7, pp. 1006-1015, 2005.
[113] B. Lyons, "Additive manufacturing in aerospace: Examples and research outlook," *The Bridge,* vol. 44, no. 3, 2014.
[114] B. N. Johnson, K. Z. Lancaster, I. B. Hogue, F. Meng, Y. L. Kong, L. W. Enquist, and M. C. McAlpine, "3D printed nervous system on a chip," *Lab on a Chip,* vol. 16, no. 8, pp. 1393-1400, 2016.
[115] T. Campbell, C. Williams, O. Ivanova, and B. Garrett, "Could 3D printing change the world," *Technologies, Potential, and Implications of Additive Manufacturing, Atlantic Council, Washington, DC,* 2011.
[116] A. Garg, K. Tai, and M. Savalani, "State-of-the-art in empirical modelling of rapid prototyping processes," *Rapid Prototyping Journal,* vol. 20, no. 2, pp. 164-178, 2014.
[117] A. K. Sood, R. Ohdar, and S. Mahapatra, "Improving dimensional accuracy of fused deposition modelling processed part using grey Taguchi method," *Materials & Design,* vol. 30, no. 10, pp. 4243-4252, 2009.
[118] I. Gajdoš, and J. Slota, "Influence of printing conditions on structure in FDM prototypes," *Tehnički Vjesnik,* vol. 20, no. 2, pp. 231-236, 2013.
[119] A. Boschetto, and L. Bottini, "Accuracy prediction in fused deposition modeling," *The International Journal of Advanced Manufacturing Technology,* vol. 73. no. 5, pp. 913-928, 2014.
[120] D. Ahn, H. Kim, and S. Lee, "Surface roughness prediction using measured data and interpolation in layered manufacturing," *Journal of Materials Processing Technology,* vol. 209, no. 2, pp. 664-671, 2009.
[121] C. J. Luis Pérez, J. Vivancos Calvet, and M. A. Sebastián Pérez, "Geometric roughness analysis in solid free-form manufacturing processes," *Journal of Materials Processing Technology,* vol. 119, no. 1–3, pp. 52-57, 2001.
[122] A. Boschetto, V. Giordano, and F. Veniali, "Modelling micro geometrical profiles in fused deposition process," *The International Journal of Advanced Manufacturing Technology,* vol. 61, no. 9-12, pp. 945-956, 2012.

[123] M. K. Agarwala, V. R. Jamalabad, N. A. Langrana, A. Safari, P. J. Whalen, and S. C. Danforth, "Structural quality of parts processed by fused deposition," *Rapid Prototyping Journal*, vol. 2, no. 4, pp. 4-19, 1996.
[124] J. F. Rodriguez, J. P. Thomas, and J. E. Renaud, "Characterization of the mesostructure of fused-deposition acrylonitrile-butadiene-styrene materials," *Rapid Prototyping Journal*, vol. 6, no. 3, pp. 175-186, 2000.
[125] R. K. Chen, T. T. Lo, L. Chen, and A. J. Shih, "Nano-CT characterization of structural voids and air bubbles in fused deposition modeling for additive manufacturing," *ASME 2015 International Manufacturing Science and Engineering Conference*, pp. V001T02A071: American Society of Mechanical Engineers, 2015.
[126] W. Cheng, J. Fuh, A. Nee, Y. Wong, H. Loh, and T. Miyazawa, "Multi-objective optimization of part-building orientation in stereolithography," *Rapid Prototyping Journal*, vol. 1, no. 4, pp. 12-23, 1995.
[127] F. Xu, Y. Wong, H. Loh, J. Fuh, and T. Miyazawa, "Optimal orientation with variable slicing in stereolithography," *Rapid Prototyping Journal*, vol. 3, no. 3, pp. 76-88, 1997.
[128] K. Bastani, P. K. Rao, and Z. Kong, "An online sparse estimation-based classification approach for real-time monitoring in advanced manufacturing processes from heterogeneous sensor data," *IIE Transactions*, vol. 48, no. 7, pp. 579-598, 2016.
[129] E. Fodran, M. Koch, and U. Menon, "Mechanical and dimensional characteristics of fused deposition modeling build styles," *Solid Freeform Fabrication Proceeding*, pp. 419-442, 1996.
[130] J. F. R. Matas, "Modeling the mechanical behavior of fused deposition acrylonitrile-butadiene-styrene polymer components," University of Notre Dame, 1999.
[131] D. Ahn, J.-H. Kweon, S. Kwon, J. Song, and S. Lee, "Representation of surface roughness in fused deposition modeling," *Journal of Materials Processing Technology*, vol. 209, no. 15, pp. 5593-5600, 2009.
[132] B. Lee, J. Abdullah, and Z. Khan, "Optimization of rapid prototyping parameters for production of flexible ABS object," *Journal of Materials Processing Technology*, vol. 169, no. 1, pp. 54-61, 2005.
[133] A. Sood, R. K. Ohdar, and S. S. Mahapatra, "A hybrid ANN-BFOA approach for optimization of FDM process parameters," *Swarm, Evolutionary, and Memetic Computing, Lecture Notes in Computer Science*, B. Panigrahi, S. Das, P. Suganthan and S. Dash, eds., pp. 396-403: Springer Berlin Heidelberg, 2010.
[134] A. Boschetto, V. Giordano, and F. Veniali, "Surface roughness prediction in fused deposition modelling by neural networks," *The International Journal of Advanced Manufacturing Technology*, vol. 67, no. 9-12, pp. 2727-2742, 2013.
[135] R. Anitha, S. Arunachalam, and P. Radhakrishnan, "Critical parameters influencing the quality of prototypes in fused deposition modelling," *Journal of Materials Processing Technology*, vol. 118, no. 1–3, pp. 385-388, 2001.
[136] M. Mani, B. Lane, A. Donmez, S. Feng, S. Moylan, and R. Fesperman, "Measurement science needs for real-time control of additive manufacturing powder bed fusion processes," *National Institute of Standards and Technology, Gaithersburg, MD, NIST Interagency/Internal Report (NISTIR)*, vol. 8036, 2015.
[137] N. Shamsaei, A. Yadollahi, L. Bian, and S. M. Thompson, "An overview of direct laser deposition for additive manufacturing; Part II: Mechanical behavior, process parameter optimization and control," *Additive Manufacturing*, vol. 8, pp. 12-35, 2015.

[138] R. B. Dinwiddie, L. J. Love, and J. C. Rowe, "Real-time process monitoring and temperature mapping of a 3D polymer printing process," *SPIE Defense, Security, and Sensing, International Society for Optics and Photonics*, pp. 87050L, 2013.
[139] C. Kousiatza, and D. Karalekas, "*In-situ* monitoring of strain and temperature distributions during fused deposition modeling process," *Materials & Design,* vol. 97, pp. 400-406, 2016.
[140] K. Tong, S. Joshi, and E. A. Lehtihet, "Error compensation for fused deposition modeling (FDM) machine by correcting slice files," *Rapid Prototyping Journal,* vol. 14, no. 1, pp. 4-14, 2008
[141] Q. Huang, H. Nouri, K. Xu, Y. Chen, S. Sosina, and T. Dasgupta, "Statistical predictive modeling and compensation of geometric deviations of three-dimensional printed products," *Journal of Manufacturing Science and Engineering,* vol. 136, no. 6, pp. 061008, 2014.
[142] A. Wang, S. Song, Q. Huang, and F. Tsung, "In-plane shape-deviation modeling and compensation for fused deposition modeling processes," *IEEE Transactions on Automation Science and Engineering,* vol. 14, no. 2, pp. 1-9, 2016.
[143] I. Olkin, and R. F. Tate, "Multivariate correlation models with mixed discrete and continuous variables," *The Annals of Mathematical Statistics,* vol. 32, no. 2, pp. 448-465, 1961.
[144] D. R. Cox, and N. Wermuth, "Response models for mixed binary and quantitative variables," *Biometrika,* vol. 79, no. 3, pp. 441-461, 1992.
[145] G. M. Fitzmaurice, and N. M. Laird, "Regression models for mixed discrete and continuous responses with potentially missing values," *Biometrics,* vol. 53, no. 1, pp. 110-122, 1997.
[146] K. Wang, and F. Tsung, "Run-to-run process adjustment using categorical observations," *Journal of Quality Technology,* vol. 39, no. 4, pp. 312-325, 2007.
[147] S. Zhou, N. Jin, and J. Jin, "Cycle-based signal monitoring using a directionally variant multivariate control chart system," *IIE transactions,* vol. 37, no. 11, pp. 971-982, 2005.
[148] C. Cheng, A. Sa-Ngasoongsong, O. Beyca, T. Le, H. Yang, Z. Kong, and S. T. Bukkapatnam, "Time series forecasting for nonlinear and non-stationary processes: a review and comparative study," *IIE Transactions,* vol. 47, no. 10, pp. 1053-1071, 2015.
[149] R. F. Tate, "Correlation between a discrete and a continuous variable. Point-biserial correlation," *The Annals of Mathematical Statistics,* vol. 25, no. 3, pp. 603-607, 1954.
[150] P. J. Catalano, and L. M. Ryan, "Bivariate latent variable models for clustered discrete and continuous outcomes," *Journal of the American Statistical Association,* vol. 87, no. 419, pp. 651-658, 1992.
[151] G. M. Fitzmaurice, and N. M. Laird, "Regression models for a bivariate discrete and continuous outcome with clustering," *Journal of the American Statistical Association,* vol. 90, no. 431, pp. 845-852, 1995.
[152] J. O. Ramsay, and B. W. Silverman, *Functional data analysis*, New York: Springer, 2005.
[153] T. Hastie, R. Tibshirani, and M. Wainwright, *Statistical learning with sparsity: the lasso and generalizations*, Boca Raton: CRC Press, Taylor & Francis Group, 2015.
[154] P. Breheny, and J. Huang, "Penalized methods for bi-level variable selection," *Statistics and its Interface,* vol. 2, no. 3, pp. 369, 2009.

[155] J. Friedman, T. Hastie, and R. Tibshirani, "Regularization paths for generalized linear models via coordinate descent," *Journal of Statistical Software,* vol. 33, no. 1, pp. 1-22, 2010.
[156] N. Tandon, and A. Choudhury, "A review of vibration and acoustic measurement methods for the detection of defects in rolling element bearings," *Tribology International,* vol. 32, no. 8, pp. 469-480, 1999.
[157] Y. Sun, A. K. Wong, and M. S. Kamel, "Classification of imbalanced data: A review," *International Journal of Pattern Recognition and Artificial Intelligence,* vol. 23, no. 04, pp. 687-719, 2009.
[158] N. Malfait, and J. O. Ramsay, "The historical functional linear model," *Canadian Journal of Statistics,* vol. 31, no. 2, pp. 115-128, 2003.
[159] N. Parikh, and S. Boyd, "Proximal algorithms," *Foundations and Trends® in Optimization,* vol. 1, no. 3, pp. 127-239, 2014.
[160] S. Boyd, N. Parikh, E. Chu, B. Peleato, and J. Eckstein, "Distributed optimization and statistical learning via the alternating direction method of multipliers," *Foundations and Trends® in Machine Learning,* vol. 3, no. 1, pp. 1-122, 2011.
[161] S. L. Lauritzen, and T. S. Richardson, "Chain graph models and their causal interpretations," *Journal of the Royal Statistical Society: Series B (Statistical Methodology),* vol. 64, no. 3, pp. 321-348, 2002.

Appendices

Appendix A

The approximation of Eq. (2.2) by quadratic programming with second-order Taylor expansion is briefly summarized here, see [64] for details. The log-likelihood function

$$\mathrm{L}(\boldsymbol{\beta}) = \sum_{i=1}^{n}\Big(y_i \log p(\boldsymbol{x}_i) + (1-y_i)\log\big(1-p(\boldsymbol{x}_i)\big)\Big)$$

$$= \sum_{i=1}^{n}\left(y_i \log\frac{p(\boldsymbol{x}_i)}{1-p(\boldsymbol{x}_i)} + \log\big(1-p(\boldsymbol{x}_i)\big)\right)$$

$$= \sum_{i=1}^{n}\Big(y_i \boldsymbol{x}_i{}^T\boldsymbol{\beta} + \log\big(1-p(\boldsymbol{x}_i)\big)\Big)$$

$$= \sum_{i=1}^{n}\Big(y_i \boldsymbol{x}_i{}^T\boldsymbol{\beta} - \log\big(1+e^{\boldsymbol{x}_i{}^T\boldsymbol{\beta}}\big)\Big).$$

The first and second order derivatives of the log-likelihood function are

$$\frac{\partial \mathrm{L}(\boldsymbol{\beta})}{\partial \boldsymbol{\beta}} = \sum_{i=1}^{n}\left(y_i\boldsymbol{x}_i - \frac{e^{\boldsymbol{x}_i{}^T\boldsymbol{\beta}}}{1+e^{\boldsymbol{x}_i{}^T\boldsymbol{\beta}}}\boldsymbol{x}_i\right) = \sum_{i=1}^{n}\big(y_i - p(\boldsymbol{x}_i;\boldsymbol{\beta})\big)\boldsymbol{x}_i = \boldsymbol{X}^T(\boldsymbol{y}-\boldsymbol{p}),$$

$$\frac{\partial^2 L(\boldsymbol{\beta})}{\partial \boldsymbol{\beta}\partial \boldsymbol{\beta}^T} = -\sum_{i=1}^{n}\Big(\boldsymbol{x}_i\boldsymbol{x}_i{}^T p(\boldsymbol{x}_i;\boldsymbol{\beta})\big(1-p(\boldsymbol{x}_i;\boldsymbol{\beta})\big)\Big) = -\boldsymbol{X}^T\boldsymbol{W}\boldsymbol{X},$$

where $\boldsymbol{X}$ is an $n \times p$ matrix, $\boldsymbol{y}$ and $\boldsymbol{p}$ are $n \times 1$ vector, and $\boldsymbol{W} = diag\Big(p(\boldsymbol{x}_1;\boldsymbol{\beta})\big(1-p(\boldsymbol{x}_1;\boldsymbol{\beta})\big), \dots, p(\boldsymbol{x}_n;\boldsymbol{\beta})\big(1-p(\boldsymbol{x}_n;\boldsymbol{\beta})\big)\Big)$ is an $n \times n$ diagonal matrix.

The second order Taylor expansion at the initial estimator $\widetilde{\boldsymbol{\beta}}$ is

$$\mathrm{L}(\boldsymbol{\beta}) = \mathrm{L}\big(\widetilde{\boldsymbol{\beta}}\big) + \big(\boldsymbol{\beta} - \widetilde{\boldsymbol{\beta}}\big)^T\boldsymbol{X}^T(\boldsymbol{y}-\boldsymbol{p}) - \frac{1}{2}\big(\boldsymbol{\beta} - \widetilde{\boldsymbol{\beta}}\big)^T\boldsymbol{X}^T\boldsymbol{W}\boldsymbol{X}\big(\boldsymbol{\beta} - \widetilde{\boldsymbol{\beta}}\big)$$

$$= C_1 - \frac{1}{2}\boldsymbol{\beta}^T\boldsymbol{X}^T\boldsymbol{W}\boldsymbol{X}\boldsymbol{\beta} + \boldsymbol{\beta}^T\boldsymbol{X}^T\boldsymbol{W}(\boldsymbol{X}\widetilde{\boldsymbol{\beta}} + \boldsymbol{W}^{-1}(\boldsymbol{y}-\boldsymbol{p}))$$

$$= C_2 - \frac{1}{2}(\widetilde{\boldsymbol{y}} - \boldsymbol{X}\boldsymbol{\beta})^T\boldsymbol{W}(\widetilde{\boldsymbol{y}} - \boldsymbol{X}\boldsymbol{\beta}),$$

where $\widetilde{\boldsymbol{y}} = \boldsymbol{X}\widetilde{\boldsymbol{\beta}} + \boldsymbol{W}^{-1}(\boldsymbol{y}-\boldsymbol{p})$ is a constant.

Appendix B

The detailed simulation results are summarized in Tables B1-B3. The values in the tables are calculated as the averages and the standard errors (in the parenthesis) based on 50 simulation replicates under each simulation scenarios. In the tables, n_{tr} shows training sample size for the models. The validation sample size is the same as training sample size, and testing sample size is the twice of training sample size. The training, validation and testing samples are generated from the same model. Testing error is the error for the testing data. Overall variable selection error is calculated as the percentage of total incorrectly selected variables in the final estimated model among all predictors. Type I variable selection error is the percentage of significant variables not being selected in the final estimated model, and Type II variable selection error is the percentage of insignificant variables being selected in the final estimated model. The result is highlighted in bold if its performance is the best among all methods under that simulation setting. If multiple results are comparable (fall into 1 standard deviation of the minimum error), then all these comparable results are treated as the best.

Table B1. Testing Errors for 50 Replications in Functional Variable Selection

Sample Size	Methods	ρ=0, τ=0		ρ=0, τ=0.3		ρ=0.6, τ=0		ρ=0.6, τ=0.3	
		$den.$=0.1	$den.$=0.4	$den.$=0.1	$den.$=0.4	$den.$=0.1	$den.$=0.4	$den.$=0.1	$den.$=0.4
n_{tr}=20	LR	0.475 (0.016)	0.446 (0.014)	0.470 (0.013)	0.449 (0.015)	0.484 (0.014)	0.452 (0.018)	0.472 (0.017)	0.424 (0.018)
	Lasso	**0.418 (0.018)**	0.418 (0.018)	0.388 (0.020)	0.342 (0.017)	0.429 (0.018)	0.259 (0.014)	0.402 (0.018)	0.240 (0.015)
	Ridge	0.438 (0.014)	0.370 (0.017)	0.404 (0.019)	0.292 (0.014)	0.439 (0.017)	0.211 (0.014)	0.396 (0.015)	0.202 (0.013)
	NNG	0.423 (0.018)	0.399 (0.017)	**0.353 (0.016)**	0.324 (0.015)	0.399 (0.015)	0.264 (0.018)	0.384 (0.016)	0.215 (0.013)
	GrpLasso	**0.417 (0.015)**	**0.324 (0.017)**	**0.350 (0.016)**	**0.266 (0.014)**	**0.377 (0.016)**	**0.192 (0.012)**	**0.345 (0.015)**	**0.172 (0.012)**
	HLasso	**0.408 (0.017)**	0.375 (0.020)	0.403 (0.020)	0.321 (0.016)	0.403 (0.015)	0.231 (0.012)	0.448 (0.017)	0.246 (0.016)
	HNNG	**0.400 (0.019)**	0.369 (0.018)	**0.350 (0.015)**	0.289 (0.012)	**0.378 (0.016)**	0.212 (0.013)	0.366 (0.016)	0.196 (0.012)
n_{tr}=100	LR	0.305 (0.003)	0.219 (0.003)	0.300 (0.003)	0.199 (0.002)	0.309 (0.002)	0.176 (0.003)	0.309 (0.003)	0.177 (0.003)
	Lasso	0.278 (0.003)	0.202 (0.002)	0.278 (0.003)	0.173 (0.002)	0.274 (0.003)	0.153 (0.002)	**0.275 (0.002)**	0.135 (0.002)
	Ridge	0.311	0.210	0.302	0.173	0.297	0.154	0.297	0.135

		(0.003)	(0.002)	(0.002)	(0.002)	(0.003)	(0.003)	(0.002)	(0.002)
	NNG	0.275 (0.003)	0.219 (0.003)	0.276 (0.003)	0.181 (0.002)	0.277 (0.003)	0.155 (0.002)	0.280 (0.003)	0.140 (0.002)
	GrpLasso	0.293 (0.003)	**0.192 (0.002)**	0.287 (0.003)	**0.160 (0.002)**	0.285 (0.002)	0.141 (0.002)	0.282 (0.002)	**0.121 (0.002)**
	HLasso	0.353 (0.005)	**0.192 (0.003)**	0.283 (0.003)	0.163 (0.003)	0.286 (0.003)	0.145 (0.002)	0.286 (0.003)	0.126 (0.002)
	HNNG	**0.266 (0.003)**	0.200 (0.002)	**0.265 (0.003)**	0.165 (0.002)	**0.263 (0.002)**	**0.137 (0.002)**	**0.274 (0.003)**	0.125 (0.002)
n_{tr}=200	LR	0.286 (0.001)	0.181 (0.001)	0.285 (0.001)	0.163 (0.001)	0.285 (0.002)	0.138 (0.001)	0.283 (0.001)	0.133 (0.001)
	Lasso	0.265 (0.001)	0.176 (0.001)	0.270 (0.001)	0.154 (0.001)	0.270 (0.002)	0.130 (0.001)	**0.263 (0.001)**	0.122 (0.001)
	Ridge	0.286 (0.001)	0.181 (0.001)	0.285 (0.001)	0.158 (0.001)	0.285 (0.002)	0.130 (0.001)	0.278 (0.001)	0.123 (0.001)
	NNG	0.262 (0.001)	0.181 (0.001)	0.264 (0.001)	0.158 (0.001)	0.266 (0.001)	0.131 (0.001)	**0.262 (0.001)**	0.123 (0.001)
	GrpLasso	0.275 (0.001)	0.176 (0.001)	0.276 (0.001)	0.151 (0.001)	0.275 (0.002)	0.125 (0.001)	0.271 (0.001)	**0.117 (0.001)**
	HLasso	0.264 (0.001)	0.172 (0.001)	0.267 (0.002)	**0.150 (0.001)**	0.275 (0.002)	0.133 (0.001)	0.285 (0.003)	0.121 (0.001)
	HNNG	**0.257 (0.001)**	**0.169 (0.001)**	**0.260 (0.001)**	**0.149 (0.001)**	**0.264 (0.001)**	**0.122 (0.001)**	**0.263 (0.001)**	**0.117 (0.001)**

Table B2. Type I and Type II Variable Selection Errors for 50 Replications in Functional Variable Selection

Sample Size	Methods	ρ=0, τ=0				ρ=0, τ=0.3			
		$den.$=0.1		$den.$=0.4		$den.$=0.1		$den.$=0.4	
		Type I	Type II	Type I	Type II	Type I	Type II	Type I	Type II
n_{tr}=20	LR	0.690 (0.333)	0.509 (0.125)	0.605 (0.160)	0.490 (0.151)	0.620 (0.372)	0.500 (0.091)	0.612 (0.184)	0.505 (0.118)
	Lasso	0.460 (0.376)	**0.180 (0.142)**	0.627 (0.218)	**0.180 (0.151)**	0.360 (0.365)	**0.161 (0.120)**	0.587 (0.230)	**0.222 (0.146)**
	Ridge	**0.090 (0.261)**	0.821 (0.305)	**0.050 (0.134)**	0.930 (0.183)	**0.090 (0.241)**	0.801 (0.326)	**0.015 (0.041)**	0.970 (0.047)
	NNG	0.570 (0.391)	**0.136 (0.186)**	0.650 (0.297)	**0.198 (0.297)**	0.440 (0.345)	**0.127 (0.197)**	0.563 (0.336)	**0.298 (0.351)**
	GrpLasso	0.370 (0.438)	0.558 (0.393)	**0.140 (0.248)**	0.610 (0.337)	**0.230 (0.307)**	0.603 (0.298)	0.120 (0.238)	0.730 (0.287)
	HLasso	0.520 (0.349)	0.363 (0.141)	0.420 (0.234)	**0.163 (0.144)**	0.640 (0.268)	**0.177 (0.115)**	0.540 (0.222)	**0.243 (0.205)**
	HNNG	0.510 (0.357)	**0.146 (0.199)**	0.557 (0.324)	**0.273 (0.289)**	0.420 (0.341)	**0.127 (0.181)**	0.415 (0.276)	**0.365 (0.272)**
		ρ=0.6, τ=0				ρ=0.6, τ=0.3			
		$den.$=0.1		$den.$=0.4		$den.$=0.1		$den.$=0.4	
		Type I	Type II	Type I	Type II	Type I	Type II	Type I	Type II
	LR	0.610 (0.339)	0.520 (0.088)	0.545 (0.131)	0.527 (0.107)	0.640 (0.336)	0.500 (0.095)	0.550 (0.158)	0.495 (0.111)
	Lasso	0.450 (0.381)	**0.179 (0.143)**	0.487 (0.191)	**0.225 (0.113)**	0.470 (0.397)	**0.182 (0.126)**	0.455 (0.169)	0.222 (0.132)
	Ridge	**0.090 (0.241)**	0.841 (0.267)	**0.005 (0.025)**	0.980 (0.043)	**0.060 (0.218)**	0.896 (0.197)	**0.005 (0.025)**	0.983 (0.037)
	NNG	0.610 (0.368)	**0.113 (0.157)**	0.465 (0.313)	0.343 (0.353)	0.560 (0.424)	**0.124 (0.147)**	0.320 (0.259)	0.425 (0.366)
	GrpLasso	**0.300**	0.572	**0.020**	0.755	**0.220**	0.591	**0.020**	0.672

		(0.378)	(0.336)	**(0.099)**	(0.283)	**(0.306)**	(0.307)	**(0.099)**	(0.301)
	HLasso	0.380 (0.312)	0.448 (0.151)	0.130 (0.222)	**0.203 (0.135)**	0.800 (0.247)	**0.106 (0.116)**	0.270 (0.252)	**0.138 (0.085)**
	HNNG	0.510 (0.385)	**0.138 (0.202)**	0.325 (0.276)	**0.333 (0.247)**	0.540 (0.389)	**0.147 (0.159)**	0.277 (0.231)	0.360 (0.253)
n_{tr}=100		ρ=0, τ=0				ρ=0, τ=0.3			
		$den.$=0.1		$den.$=0.4		$den.$=0.1		$den.$=0.4	
		Type I	Type II	Type I	Type II	Type I	Type II	Type I	Type II
	LR	1.000 (0.000)	0.499 (0.110)	0.995 (0.025)	0.488 (0.115)	1.000 (0.000)	0.487 (0.072)	0.980 (0.053)	0.498 (0.123)
	Lasso	0.010 (0.071)	0.344 (0.164)	0.012 (0.046)	0.552 (0.194)	0.020 (0.099)	0.358 (0.178)	0.022 (0.055)	0.530 (0.194)
	Ridge	**0.000 (0.000)**	0.973 (0.041)	**0.000 (0.000)**	0.988 (0.029)	**0.000 (0.000)**	0.988 (0.028)	**0.000 (0.000)**	0.997 (0.017)
	NNG	0.040 (0.137)	**0.090 (0.085)**	0.085 (0.142)	0.348 (0.316)	0.060 (0.164)	**0.124 (0.148)**	0.080 (0.131)	0.350 (0.302)
	GrpLasso	**0.000 (0.000)**	0.872 (0.170)	**0.000 (0.000)**	0.933 (0.176)	**0.000 (0.000)**	0.933 (0.120)	**0.000 (0.000)**	0.892 (0.203)
	HLasso	0.540 (0.222)	0.204 (0.099)	0.020 (0.099)	**0.172 (0.062)**	0.050 (0.152)	0.550 (0.154)	0.010 (0.071)	**0.207 (0.122)**
	HNNG	0.020 (0.099)	**0.089 (0.104)**	0.052 (0.076)	0.303 (0.217)	0.030 (0.120)	**0.136 (0.155)**	0.052 (0.095)	**0.278 (0.211)**
		ρ=0.6, τ=0				ρ=0.6, τ=0.3			
		$den.$=0.1		$den.$=0.4		$den.$=0.1		$den.$=0.4	
		Type I	Type II	Type I	Type II	Type I	Type II	Type I	Type II
	LR	1.000 (0.000)	0.503 (0.084)	0.942 (0.077)	0.502 (0.114)	0.990 (0.071)	0.493 (0.068)	0.907 (0.094)	0.483 (0.097)
	Lasso	**0.000 (0.000)**	0.269 (0.163)	0.035 (0.057)	0.465 (0.146)	**0.000 (0.000)**	0.344 (0.220)	0.070 (0.076)	0.433 (0.149)
	Ridge	**0.000 (0.000)**	0.970 (0.056)	**0.000 (0.000)**	0.990 (0.027)	**0.000 (0.000)**	0.970 (0.045)	**0.000 (0.000)**	0.990 (0.027)
	NNG	0.050 (0.152)	**0.129 (0.178)**	0.063 (0.095)	0.495 (0.313)	0.020 (0.099)	**0.192 (0.204)**	0.058 (0.092)	0.535 (0.316)
	GrpLasso	**0.000 (0.000)**	0.856 (0.188)	**0.000 (0.000)**	0.908 (0.174)	**0.000 (0.000)**	0.911 (0.153)	**0.000 (0.000)**	0.875 (0.227)
	HLasso	**0.000 (0.000)**	0.656 (0.214)	**0.000 (0.000)**	**0.308 (0.216)**	0.200 (0.247)	0.356 (0.110)	**0.000 (0.000)**	**0.175 (0.059)**
	HNNG	0.020 (0.099)	**0.086 (0.105)**	0.037 (0.073)	**0.242 (0.155)**	0.010 (0.071)	**0.147 (0.183)**	0.027 (0.058)	0.305 (0.178)
n_{tr}=200		ρ=0, τ=0				ρ=0, τ=0.3			
		$den.$=0.1		$den.$=0.4		$den.$=0.1		$den.$=0.4	
		Type I	Type II	Type I	Type II	Type I	Type II	Type I	Type II
	LR	1.000 (0.000)	0.507 (0.104)	1.000 (0.000)	0.493 (0.144)	1.000 (0.000)	0.493 (0.087)	1.000 (0.000)	0.513 (0.137)
	Lasso	**0.000 (0.000)**	0.371 (0.186)	**0.000 (0.000)**	0.627 (0.203)	**0.000 (0.000)**	0.328 (0.215)	**0.000 (0.000)**	0.595 (0.187)
	Ridge	**0.000 (0.000)**	0.986 (0.025)	**0.000 (0.000)**	0.997 (0.017)	**0.000 (0.000)**	0.979 (0.032)	**0.000 (0.000)**	0.993 (0.023)
	NNG	**0.000 (0.000)**	**0.140 (0.224)**	0.003 (0.018)	0.505 (0.384)	**0.000 (0.000)**	**0.103 (0.109)**	0.005 (0.025)	0.533 (0.331)
	GrpLasso	**0.000 (0.000)**	0.944 (0.138)	**0.000 (0.000)**	0.933 (0.154)	**0.000 (0.000)**	0.917 (0.140)	**0.000 (0.000)**	0.950 (0.161)
	HLasso	**0.000 (0.000)**	0.478 (0.091)	**0.000 (0.000)**	0.425 (0.237)	**0.000 (0.000)**	0.456 (0.055)	**0.000 (0.000)**	**0.233 (0.176)**
	HNNG	**0.000 (0.000)**	**0.082 (0.076)**	0.012 (0.038)	**0.145 (0.132)**	**0.000 (0.000)**	**0.090 (0.137)**	0.002 (0.018)	**0.285 (0.208)**
		ρ=0.6, τ=0				ρ=0.6, τ=0.3			

		$den.$=0.1		$den.$=0.4		$den.$=0.1		$den.$=0.4	
		Type I	Type II	Type I	Type II	Type I	Type II	Type I	Type II
	LR	1.000 (0.000)	0.509 (0.092)	0.997 (0.018)	0.498 (0.090)	1.000 (0.000)	0.513 (0.086)	0.975 (0.057)	0.520 (0.106)
	Lasso	**0.000 (0.000)**	0.377 (0.174)	0.002 (0.018)	0.530 (0.203)	**0.000 (0.000)**	0.349 (0.203)	0.015 (0.041)	0.442 (0.177)
	Ridge	**0.000 (0.000)**	0.990 (0.024)	**0.000 (0.000)**	0.992 (0.030)	**0.000 (0.000)**	0.980 (0.046)	**0.000 (0.000)**	1.000 (0.000)
	NNG	0.010 (0.071)	**0.131 (0.186)**	0.010 (0.043)	0.467 (0.296)	**0.000 (0.000)**	**0.170 (0.246)**	0.018 (0.044)	0.480 (0.301)
	GrpLasso	**0.000 (0.000)**	0.956 (0.117)	**0.000 (0.000)**	0.933 (0.176)	**0.000 (0.000)**	0.933 (0.154)	**0.000 (0.000)**	0.883 (0.207)
	HLasso	**0.000 (0.000)**	0.706 (0.181)	**0.000 (0.000)**	0.813 (0.229)	0.200 (0.267)	0.356 (0.119)	**0.000 (0.000)**	**0.167 (0.000)**
	HNNG	**0.000 (0.000)**	**0.091 (0.079)**	0.007 (0.030)	**0.207 (0.150)**	**0.000 (0.000)**	**0.164 (0.165)**	0.005 (0.025)	**0.285 (0.157)**

Table B3. Overall Variable Selection Errors for 50 Replications in Functional Variable Selection

Sample Size	Methods	ρ=0, τ=0		ρ=0, τ=0.3		ρ=0.6, τ=0		ρ=0.6, τ=0.3	
		$den.$=0.1	$den.$=0.4	$den.$=0.1	$den.$=0.4	$den.$=0.1	$den.$=0.4	$den.$=0.1	$den.$=0.4
n_{tr}=20	LR	0.527 (0.114)	0.536 (0.118)	0.512 (0.098)	0.548 (0.121)	0.529 (0.090)	0.534 (0.084)	0.514 (0.101)	0.517 (0.103)
	Lasso	**0.208 (0.118)**	**0.359 (0.076)**	**0.182 (0.107)**	**0.368 (0.091)**	**0.206 (0.120)**	0.330 (0.069)	**0.211 (0.114)**	0.315 (0.095)
	Ridge	0.748 (0.254)	0.578 (0.066)	0.730 (0.275)	0.588 (0.034)	0.766 (0.221)	0.590 (0.027)	0.812 (0.159)	0.592 (0.026)
	NNG	**0.179 (0.149)**	**0.379 (0.089)**	**0.158 (0.166)**	**0.404 (0.105)**	**0.163 (0.129)**	0.392 (0.129)	**0.168 (0.120)**	0.383 (0.149)
	GrpLasso	0.539 (0.315)	0.422 (0.155)	0.566 (0.247)	**0.486 (0.174)**	0.545 (0.272)	0.461 (0.167)	0.554 (0.255)	0.411 (0.169)
	HLasso	0.379 (0.117)	**0.266 (0.136)**	**0.223 (0.082)**	**0.362 (0.179)**	0.441 (0.126)	**0.174 (0.130)**	**0.175 (0.085)**	**0.191 (0.098)**
	HNNG	**0.182 (0.168)**	**0.387 (0.098)**	**0.156 (0.156)**	**0.385 (0.111)**	**0.175 (0.164)**	0.330 (0.107)	**0.186 (0.139)**	0.327 (0.121)
n_{tr}=100	LR	0.549 (0.099)	0.691 (0.069)	0.538 (0.065)	0.691 (0.081)	0.553 (0.076)	0.678 (0.074)	0.543 (0.061)	0.653 (0.078)
	Lasso	0.311 (0.147)	0.336 (0.112)	0.324 (0.158)	0.327 (0.118)	0.242 (0.147)	0.293 (0.091)	0.310 (0.198)	0.288 (0.087)
	Ridge	0.876 (0.037)	0.593 (0.018)	0.889 (0.025)	0.598 (0.010)	0.873 (0.058)	0.594 (0.016)	0.873 (0.041)	0.594 (0.016)
	NNG	**0.085 (0.075)**	0.2420 (0.171)	**0.118 (0.132)**	0.242 (0.171)	**0.121 (0.159)**	0.322 (0.171)	**0.175 (0.183)**	0.344 (0.181)
	GrpLasso	0.785 (0.153)	0.560 (0.106)	0.840 (0.108)	0.535 (0.122)	0.770 (0.169)	0.545 (0.105)	0.820 (0.138)	0.525 (0.136)
	HLasso	0.238 (0.067)	**0.111 (0.046)**	0.500 (0.137)	**0.128 (0.087)**	0.590 (0.193)	**0.185 (0.130)**	0.340 (0.074)	**0.105 (0.035)**
	HNNG	**0.082 (0.092)**	0.203 (0.121)	**0.125 (0.138)**	**0.188 (0.124)**	**0.079 (0.094)**	**0.160 (0.091)**	**0.133 (0.164)**	0.194 (0.102)
n_{tr}=200	LR	0.556 (0.094)	0.696 (0.086)	0.544 (0.079)	0.708 (0.082)	0.558 (0.083)	0.698 (0.054)	0.562 (0.077)	0.702 (0.073)
	Lasso	0.334 (0.168)	0.376 (0.122)	0.295 (0.194)	0.357 (0.112)	0.339 (0.156)	0.319 (0.122)	0.314 (0.183)	0.271 (0.110)
	Ridge	0.887 (0.022)	0.598 (0.010)	0.881 (0.028)	0.596 (0.014)	0.891 (0.022)	0.595 (0.018)	0.882 (0.041)	0.600 (0.000)
	NNG	**0.126 (0.202)**	0.304 (0.229)	**0.093 (0.098)**	0.322 (0.196)	**0.119 (0.167)**	0.284 (0.175)	**0.153 (0.221)**	0.295 (0.177)
	GrpLasso	0.850 (0.124)	0.560 (0.093)	0.825 (0.126)	0.570 (0.096)	0.860 (0.106)	0.560 (0.106)	0.840 (0.139)	0.530 (0.124)

	HLasso	0.430 (0.082)	0.255 (0.142)	0.410 (0.050)	**0.140 (0.106)**	0.635 (0.163)	0.488 (0.137)	0.340 (0.080)	**0.100 (0.000)**
	HNNG	**0.074 (0.069)**	**0.092 (0.078)**	**0.081 (0.123)**	**0.172 (0.124)**	**0.082 (0.071)**	**0.127 (0.090)**	**0.148 (0.148)**	0.173 (0.094)

Appendix C

The predictors selected in the models are visualized in Figures C1-C4. Recall that the four groups of variables are heater power, SP value, pull speed and furnace pressure. We use the two detail levels wavelet coefficients and the coarse level wavelet coefficients during the modeling. The number of wavelet coefficients for two detail levels and coarse level are 11, 9 and 7. In the figures, the vertical axis represents the index of features, and the horizontal axis represents the model used. A feature is marked if it is selected larger or equal to 7 times over 14 CV folds in leave-one-out CV. From these figures, we can conclude that the proposed model selects features from the coarse levels of heater power and SP value, which implies that the changes in thermal field are responsible for polycrystalline defects in the production.

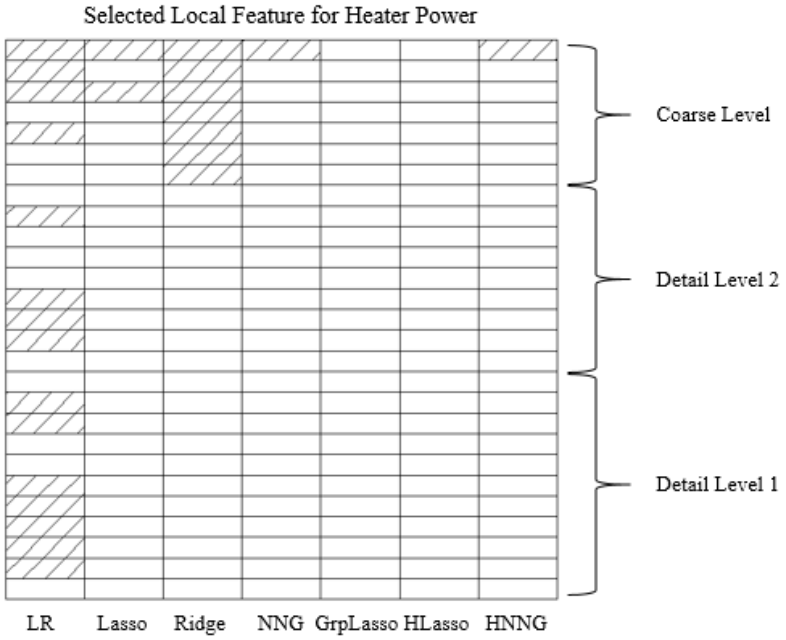

Figure C1. Selected Local Features for Heater Power

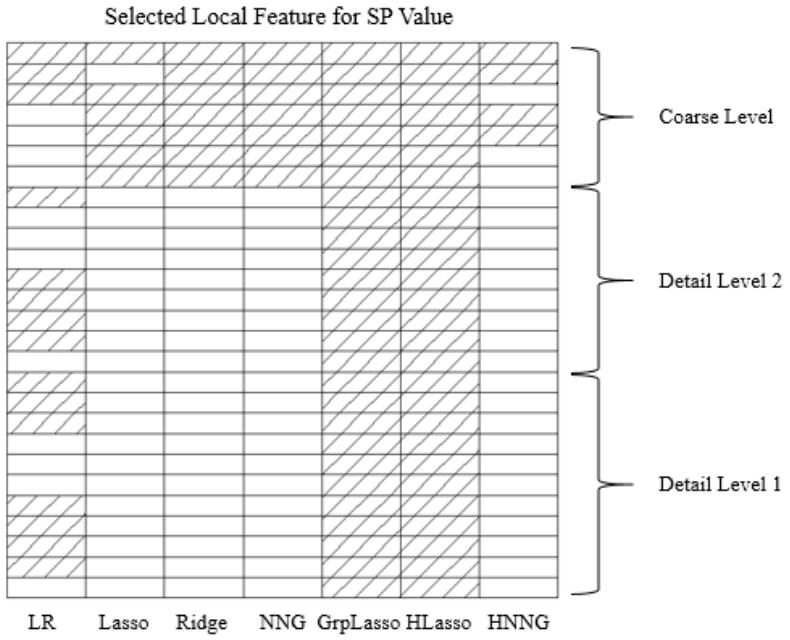

Figure C2. Selected Local Features for SP Value

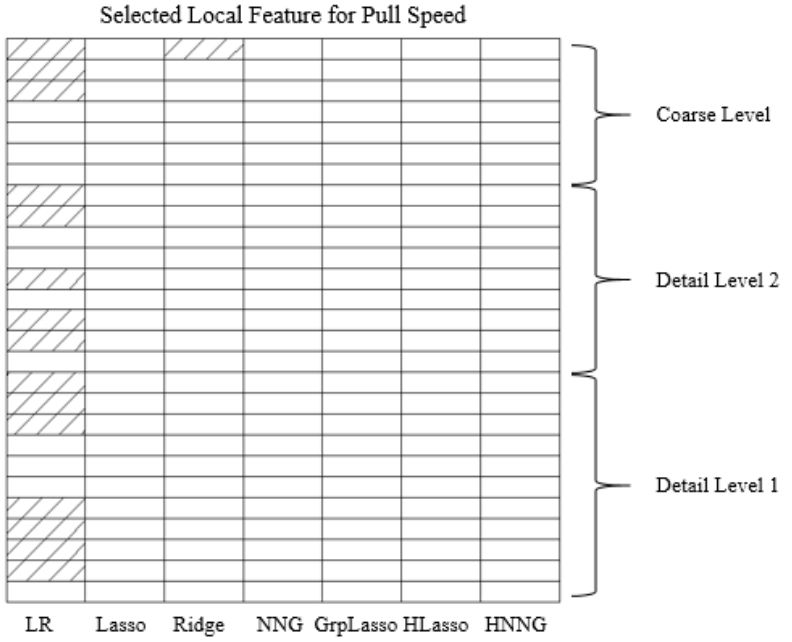

Figure C3. Selected Local Features for Pull Speed

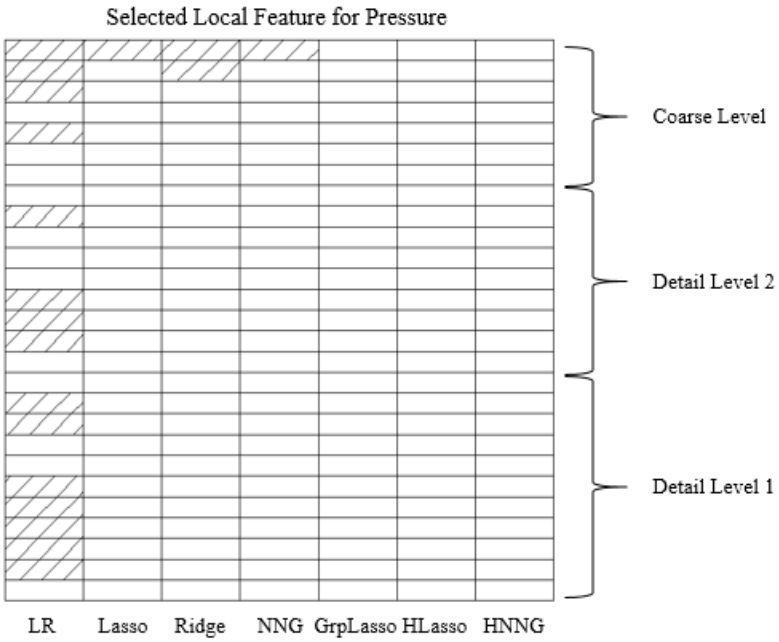

Figure C4. Selected Local Features for Pressure

Appendix D

The average RMSEs of testing data over 100 replications in all 144 scenarios in the simulation studies of functional graphical modeling are summarized in Table D1.

Table D1. Average RMSEs of Testing Data for Simulation Studies (Grp Diff: Group Difference; N: Node)

Density	Sample size	Overlap	Correlation	SNR	SNR Grp Diff	Proposed					Benchmark Separate Node					Benchmark Summary Statistics				
						N1	N2	N3	N4	N5	N1	N2	N3	N4	N5	N1	N2	N3	N4	N5
1	1	1	1	1	1	0.35	0.40	0.41	0.43	0.43	0.88	2.05	2.25	2.45	2.64	1.31	2.72	2.95	3.19	3.42
1	1	2	1	1	1	0.30	0.31	0.31	0.31	0.31	0.89	2.05	2.24	2.45	2.66	1.30	2.72	2.95	3.19	3.43
1	1	3	1	1	1	1.14	2.84	3.13	3.41	3.68	1.16	2.88	3.16	3.44	3.72	1.16	2.89	3.15	3.44	3.70
1	2	1	1	1	1	0.33	0.33	0.33	0.33	0.33	0.34	0.37	0.38	0.39	0.39	1.31	2.72	2.95	3.19	3.42
1	2	2	1	1	1	0.33	0.33	0.33	0.33	0.33	0.35	0.38	0.38	0.39	0.40	1.32	2.72	2.95	3.19	3.43
1	2	3	1	1	1	0.32	0.32	0.32	0.33	0.33	0.34	0.39	0.40	0.41	0.42	0.36	0.36	0.36	0.36	0.36
2	1	1	1	1	1	0.30	0.33	0.33	0.33	0.33	1.71	5.63	5.95	6.23	6.53	2.10	6.68	7.06	7.38	7.73
2	1	2	1	1	1	0.28	0.31	0.31	0.32	0.32	1.71	5.65	5.95	6.23	6.54	2.09	6.68	7.03	7.36	7.73
2	1	3	1	1	1	2.47	8.13	8.57	9.01	9.49	2.50	8.17	8.62	9.06	9.50	2.53	8.24	8.69	9.13	9.56
2	2	1	1	1	1	0.29	0.30	0.30	0.30	0.30	0.35	0.63	0.66	0.68	0.70	2.10	6.68	7.02	7.38	7.73
2	2	2	1	1	1	0.29	0.30	0.30	0.30	0.30	0.35	0.63	0.65	0.68	0.70	2.09	6.66	7.03	7.38	7.74
2	2	3	1	1	1	0.30	0.33	0.33	0.34	0.34	0.36	0.70	0.73	0.77	0.79	0.39	0.40	0.40	0.41	0.41
1	1	1	2	1	1	0.25	0.25	0.25	0.26	0.26	0.82	1.93	2.11	2.31	2.48	1.32	2.85	3.09	3.34	3.59
1	1	2	2	1	1	0.24	0.25	0.25	0.25	0.25	0.81	1.92	2.11	2.30	2.48	1.32	2.84	3.10	3.34	3.57
1	1	3	2	1	1	1.03	2.49	2.76	2.99	3.25	1.05	2.58	2.84	3.10	3.36	1.09	2.55	2.81	3.08	3.34
1	2	1	2	1	1	0.28	0.28	0.28	0.28	0.28	0.30	0.33	0.34	0.35	0.36	1.33	2.84	3.09	3.33	3.58
1	2	2	2	1	1	0.23	0.23	0.23	0.23	0.23	0.25	0.29	0.30	0.31	0.32	1.31	2.83	3.08	3.33	3.58
1	2	3	2	1	1	0.23	0.23	0.24	0.24	0.24	0.26	0.31	0.32	0.33	0.35	0.35	0.35	0.35	0.35	0.35
2	1	1	2	1	1	0.31	0.35	0.35	0.36	0.36	1.63	5.52	5.81	6.10	6.40	2.21	7.64	8.02	8.42	8.85
2	1	2	2	1	1	0.31	0.35	0.35	0.36	0.36	1.63	5.46	5.82	6.12	6.36	2.22	7.57	8.01	8.48	8.82
2	1	3	2	1	1	2.19	7.55	7.94	8.35	8.73	2.21	7.59	8.01	8.42	8.83	2.22	7.66	8.05	8.46	8.87
2	2	1	2	1	1	0.30	0.30	0.31	0.31	0.31	0.35	0.67	0.70	0.73	0.75	2.20	7.60	8.00	8.39	8.82
2	2	2	2	1	1	0.28	0.29	0.29	0.29	0.29	0.34	0.66	0.69	0.72	0.75	2.19	7.58	7.99	8.42	8.80
2	2	3	2	1	1	0.29	0.35	0.36	0.36	0.37	0.37	0.76	0.79	0.83	0.86	0.38	0.40	0.40	0.40	0.40
1	1	1	3	1	1	0.26	0.27	0.27	0.27	0.27	0.68	1.55	1.71	1.87	2.02	1.40	3.14	3.40	3.69	3.96
1	1	2	3	1	1	0.27	0.27	0.27	0.27	0.28	0.68	1.56	1.72	1.86	2.00	1.40	3.14	3.42	3.69	3.97
1	1	3	3	1	1	0.80	2.02	2.22	2.43	2.65	0.86	2.10	2.32	2.53	2.75	0.89	2.08	2.29	2.51	2.72
1	2	1	3	1	1	0.26	0.26	0.26	0.26	0.27	0.28	0.33	0.33	0.34	0.35	1.39	3.12	3.40	3.67	3.94

Density	Sample size	Overlap	Correlation	SNR	SNR Grp Diff	Proposed					Benchmark Separate Node					Benchmark Summary Statistics				
						N1	N2	N3	N4	N5	N1	N2	N3	N4	N5	N1	N2	N3	N4	N5
1	2	2	3	1	1	0.27	0.27	0.27	0.27	0.27	0.29	0.33	0.34	0.35	0.36	1.39	3.12	3.39	3.67	3.94
1	2	3	3	1	1	0.29	0.30	0.30	0.30	0.30	0.31	0.36	0.37	0.38	0.40	0.42	0.43	0.43	0.43	0.43
2	1	1	3	1	1	0.29	0.35	0.36	0.37	0.37	1.33	4.46	4.65	4.92	5.16	2.56	9.77	10.28	10.84	11.41
2	1	2	3	1	1	0.31	0.38	0.38	0.38	0.40	1.34	4.43	4.67	4.92	5.16	2.57	9.78	10.32	10.82	11.33
2	1	3	3	1	1	1.75	5.98	6.31	6.66	6.99	1.79	6.12	6.45	6.78	7.09	1.81	6.17	6.48	6.79	7.18
2	2	1	3	1	1	0.26	0.28	0.28	0.29	0.29	0.34	0.78	0.82	0.86	0.89	2.55	9.75	10.28	10.79	11.34
2	2	2	3	1	1	0.26	0.28	0.28	0.28	0.28	0.34	0.78	0.82	0.85	0.89	2.55	9.75	10.28	10.81	11.35
2	2	3	3	1	1	0.46	1.02	1.07	1.11	1.16	0.37	0.90	0.94	0.98	1.03	0.40	0.42	0.42	0.42	0.42
1	1	1	1	1	2	0.28	0.29	0.29	0.29	0.29	0.90	2.07	2.27	2.47	2.67	1.31	2.73	2.97	3.19	3.43
1	1	2	1	1	2	0.29	0.30	0.30	0.30	0.30	0.91	2.09	2.26	2.47	2.66	1.32	2.73	2.96	3.19	3.44
1	1	3	1	1	2	1.07	2.80	3.07	3.32	3.62	1.14	2.86	3.16	3.42	3.73	1.11	2.85	3.11	3.37	3.71
1	2	1	1	1	2	0.26	0.26	0.26	0.26	0.26	0.30	0.33	0.36	0.38	0.41	1.30	2.72	2.95	3.18	3.42
1	2	2	1	1	2	0.29	0.29	0.29	0.29	0.29	0.33	0.37	0.39	0.41	0.43	1.31	2.72	2.96	3.19	3.42
1	2	3	1	1	2	0.28	0.28	0.28	0.29	0.29	0.33	0.38	0.41	0.44	0.47	0.38	0.38	0.39	0.39	0.39
2	1	1	1	1	2	0.31	0.34	0.35	0.36	0.36	1.73	5.61	5.95	6.25	6.59	2.11	6.66	7.04	7.39	7.77
2	1	2	1	1	2	0.32	0.35	0.36	0.37	0.37	1.74	5.64	5.92	6.26	6.58	2.11	6.68	6.98	7.37	7.75
2	1	3	1	1	2	2.35	7.82	8.23	8.62	9.05	2.40	7.84	8.24	8.68	9.07	2.41	7.85	8.29	8.71	9.14
2	2	1	1	1	2	0.30	0.30	0.31	0.31	0.31	0.42	0.72	0.83	0.91	0.94	2.10	6.67	7.02	7.37	7.73
2	2	2	1	1	2	0.31	0.32	0.32	0.32	0.32	0.43	0.72	0.84	0.91	0.95	2.10	6.66	7.02	7.39	7.74
2	2	3	1	1	2	0.30	0.33	0.34	0.35	0.35	0.45	0.81	0.96	1.05	1.09	0.38	0.39	0.39	0.39	0.39
1	1	1	2	1	2	0.29	0.29	0.29	0.29	0.29	0.86	1.95	2.14	2.34	2.53	1.33	2.85	3.09	3.36	3.59
1	1	2	2	1	2	0.26	0.26	0.26	0.27	0.27	0.84	1.94	2.14	2.33	2.53	1.31	2.85	3.09	3.33	3.58
1	1	3	2	1	2	0.93	2.62	2.88	3.14	3.42	1.02	2.68	2.94	3.22	3.50	0.97	2.66	2.92	3.19	3.46
1	2	1	2	1	2	0.31	0.31	0.31	0.31	0.31	0.34	0.38	0.40	0.42	0.44	1.34	2.85	3.09	3.34	3.58
1	2	2	2	1	2	0.26	0.26	0.27	0.27	0.27	0.30	0.34	0.37	0.39	0.42	1.32	2.83	3.08	3.33	3.58
1	2	3	2	1	2	0.27	0.27	0.27	0.27	0.28	0.32	0.37	0.40	0.43	0.46	0.37	0.37	0.37	0.37	0.37
2	1	1	2	1	2	0.32	0.36	0.37	0.38	0.39	1.64	5.55	5.82	6.12	6.42	2.21	7.63	8.02	8.41	8.83
2	1	2	2	1	2	0.31	0.35	0.37	0.37	0.38	1.65	5.51	5.84	6.15	6.41	2.22	7.60	8.01	8.45	8.79
2	1	3	2	1	2	2.21	7.57	7.89	8.29	8.69	2.26	7.53	7.95	8.35	8.76	2.26	7.53	7.96	8.35	8.70
2	2	1	2	1	2	0.28	0.29	0.30	0.30	0.30	0.41	0.76	0.88	0.98	1.01	2.19	7.59	7.99	8.40	8.81
2	2	2	2	1	2	0.30	0.31	0.32	0.32	0.32	0.43	0.76	0.90	0.98	1.02	2.19	7.59	8.01	8.40	8.81
2	2	3	2	1	2	0.34	0.38	0.40	0.41	0.41	0.48	0.86	1.01	1.11	1.16	0.44	0.45	0.45	0.45	0.45
1	1	1	3	1	2	0.30	0.30	0.31	0.31	0.31	0.73	1.59	1.75	1.92	2.08	1.40	3.14	3.41	3.68	3.97
1	1	2	3	1	2	0.28	0.29	0.29	0.29	0.29	0.73	1.60	1.75	1.92	2.08	1.40	3.14	3.41	3.68	3.98
1	1	3	3	1	2	0.75	1.94	2.13	2.32	2.54	0.84	2.09	2.27	2.50	2.70	0.81	2.04	2.24	2.43	2.63
1	2	1	3	1	2	0.32	0.32	0.32	0.32	0.32	0.35	0.39	0.42	0.44	0.47	1.40	3.12	3.40	3.67	3.94
1	2	2	3	1	2	0.29	0.29	0.29	0.29	0.30	0.33	0.37	0.40	0.42	0.45	1.39	3.12	3.40	3.66	3.95

Density	Sample size	Overlap	Correlation	SNR	SNR Grp Diff	Proposed					Benchmark Separate Node					Benchmark Summary Statistics				
						N1	N2	N3	N4	N5	N1	N2	N3	N4	N5	N1	N2	N3	N4	N5
1	2	3	3	1	2	0.30	0.30	0.30	0.31	0.31	0.35	0.40	0.43	0.46	0.49	0.39	0.40	0.40	0.40	0.40
2	1	1	3	1	2	0.31	0.37	0.39	0.41	0.41	1.37	4.52	4.77	5.04	5.28	2.56	9.78	10.32	10.85	11.40
2	1	2	3	1	2	0.35	0.41	0.43	0.44	0.45	1.39	4.50	4.76	5.01	5.30	2.57	9.80	10.31	10.88	11.39
2	1	3	3	1	2	1.73	5.91	6.24	6.56	6.86	1.78	6.05	6.37	6.74	7.04	1.79	5.98	6.30	6.61	6.91
2	2	1	3	1	2	0.41	0.72	0.75	0.78	0.81	0.44	0.91	1.06	1.17	1.23	2.55	9.74	10.26	10.82	11.32
2	2	2	3	1	2	0.30	0.32	0.33	0.34	0.34	0.45	0.91	1.06	1.18	1.23	2.55	9.74	10.27	10.79	11.35
2	2	3	3	1	2	0.30	0.44	0.47	0.49	0.50	0.47	1.05	1.24	1.36	1.44	0.37	0.38	0.38	0.38	0.39
1	1	1	1	2	1	0.33	0.43	0.43	0.46	0.47	1.32	2.80	3.04	3.29	3.53	1.32	2.73	2.95	3.20	3.42
1	1	2	1	2	1	0.32	0.42	0.45	0.46	0.48	1.33	2.79	3.06	3.30	3.53	1.32	2.73	2.97	3.19	3.41
1	1	3	1	2	1	1.23	2.75	3.02	3.33	3.58	1.63	3.53	3.85	4.17	4.48	1.20	2.68	2.95	3.21	3.49
1	2	1	1	2	1	0.30	0.33	0.34	0.34	0.35	0.90	1.90	2.07	2.24	2.40	1.31	2.72	2.95	3.19	3.42
1	2	2	1	2	1	0.29	0.33	0.33	0.34	0.35	0.90	1.91	2.07	2.23	2.41	1.31	2.72	2.95	3.19	3.43
1	2	3	1	2	1	0.31	0.38	0.39	0.40	0.42	0.94	2.01	2.19	2.38	2.55	0.37	0.37	0.37	0.37	0.37
2	1	1	1	2	1	0.42	1.01	1.07	1.14	1.18	2.17	6.90	7.26	7.61	8.00	2.10	6.68	7.02	7.38	7.77
2	1	2	1	2	1	0.44	1.01	1.13	1.13	1.20	2.17	6.90	7.24	7.61	7.97	2.11	6.67	7.02	7.36	7.77
2	1	3	1	2	1	2.35	7.89	8.29	8.73	9.15	2.74	8.79	9.26	9.72	10.18	2.40	7.86	8.31	8.72	9.16
2	2	1	1	2	1	0.33	0.52	0.57	0.57	0.59	1.53	5.04	5.33	5.58	5.85	2.10	6.66	7.02	7.37	7.73
2	2	2	1	2	1	0.34	0.54	0.56	0.58	0.61	1.53	5.05	5.31	5.59	5.87	2.10	6.66	7.02	7.36	7.72
2	2	3	1	2	1	0.39	0.87	0.91	0.95	0.99	1.64	5.53	5.83	6.15	6.45	0.37	0.39	0.39	0.39	0.39
1	1	1	2	2	1	0.34	0.45	0.46	0.49	0.51	1.33	2.89	3.15	3.39	3.64	1.33	2.84	3.11	3.34	3.59
1	1	2	2	2	1	0.36	0.46	0.49	0.51	0.53	1.33	2.89	3.16	3.38	3.65	1.34	2.86	3.10	3.33	3.58
1	1	3	2	2	1	1.18	2.65	2.94	3.21	3.49	1.61	3.62	3.95	4.28	4.62	1.17	2.56	2.86	3.11	3.37
1	2	1	2	2	1	0.31	0.34	0.34	0.35	0.36	0.83	1.79	1.94	2.11	2.26	1.32	2.84	3.09	3.33	3.58
1	2	2	2	2	1	0.30	0.33	0.34	0.35	0.35	0.84	1.78	1.95	2.11	2.26	1.33	2.84	3.09	3.34	3.58
1	2	3	2	2	1	0.32	0.39	0.40	0.41	0.42	0.88	1.91	2.07	2.25	2.42	0.38	0.38	0.38	0.38	0.38
2	1	1	2	2	1	0.43	1.18	1.22	1.28	1.34	2.24	7.53	7.96	8.35	8.75	2.20	7.64	8.02	8.44	8.85
2	1	2	2	2	1	0.45	1.18	1.25	1.32	1.37	2.24	7.54	7.94	8.34	8.77	2.20	7.61	8.03	8.47	8.85
2	1	3	2	2	1	2.19	7.53	7.94	8.36	8.90	2.75	9.17	9.63	10.19	10.69	2.22	7.75	8.16	8.56	8.97
2	2	1	2	2	1	0.32	0.58	0.61	0.63	0.65	1.43	4.95	5.25	5.50	5.77	2.20	7.58	7.99	8.40	8.81
2	2	2	2	2	1	0.33	0.58	0.60	0.62	0.66	1.43	4.96	5.25	5.52	5.77	2.19	7.58	7.99	8.40	8.80
2	2	3	2	2	1	0.40	0.95	0.98	1.05	1.10	1.58	5.53	5.83	6.14	6.44	0.37	0.39	0.39	0.39	0.39
1	1	1	3	2	1	0.33	0.48	0.49	0.53	0.56	1.31	2.97	3.23	3.49	3.76	1.39	3.13	3.40	3.68	3.94
1	1	2	3	2	1	0.34	0.48	0.51	0.52	0.57	1.30	2.96	3.22	3.49	3.75	1.39	3.13	3.42	3.69	3.98
1	1	3	3	2	1	0.97	2.31	2.51	2.74	3.00	1.54	3.50	3.79	4.12	4.41	0.92	2.27	2.49	2.70	2.93
1	2	1	3	2	1	0.30	0.34	0.35	0.36	0.37	0.71	1.54	1.68	1.81	1.96	1.39	3.12	3.39	3.66	3.93
1	2	2	3	2	1	0.30	0.34	0.35	0.36	0.37	0.71	1.54	1.68	1.82	1.95	1.39	3.12	3.39	3.67	3.95
1	2	3	3	2	1	0.33	0.42	0.43	0.46	0.49	0.79	1.73	1.89	2.04	2.21	0.38	0.39	0.39	0.39	0.39

Density	Sample size	Overlap	Correlation	SNR	SNR Grp Diff	Proposed					Benchmark Separate Node					Benchmark Summary Statistics				
						N1	N2	N3	N4	N5	N1	N2	N3	N4	N5	N1	N2	N3	N4	N5
2	1	1	3	2	1	0.47	1.43	1.56	1.61	1.68	2.38	8.72	9.13	9.67	10.07	2.56	9.81	10.34	10.89	11.40
2	1	2	3	2	1	0.49	1.49	1.55	1.64	1.72	2.37	8.69	9.18	9.72	10.17	2.55	9.84	10.35	10.85	11.39
2	1	3	3	2	1	1.88	6.35	6.55	7.01	7.19	2.75	9.80	10.24	10.80	11.33	1.91	6.19	6.52	6.84	7.21
2	2	1	3	2	1	0.36	0.72	0.76	0.79	0.84	1.30	4.75	5.00	5.25	5.54	2.56	9.75	10.26	10.80	11.33
2	2	2	3	2	1	0.46	1.11	1.17	1.22	1.28	1.29	4.75	5.01	5.26	5.54	2.55	9.74	10.28	10.81	11.35
2	2	3	3	2	1	0.46	1.28	1.35	1.41	1.45	1.49	5.39	5.68	5.96	6.25	0.43	0.45	0.45	0.45	0.45
1	1	1	1	2	2	0.39	0.48	0.56	0.61	0.65	1.69	3.02	3.44	3.81	4.19	1.31	2.72	2.96	3.18	3.41
1	1	2	1	2	2	0.41	0.49	0.57	0.61	0.69	1.69	3.03	3.47	3.82	4.18	1.32	2.72	2.97	3.19	3.44
1	1	3	1	2	2	1.27	2.89	3.14	3.47	3.66	1.99	3.83	4.19	4.71	5.03	1.20	2.80	3.09	3.38	3.66
1	2	1	1	2	2	0.30	0.33	0.35	0.37	0.38	1.59	2.26	2.80	3.16	3.51	1.30	2.71	2.94	3.18	3.42
1	2	2	1	2	2	0.33	0.35	0.38	0.39	0.41	1.59	2.26	2.81	3.16	3.52	1.31	2.71	2.95	3.18	3.43
1	2	3	1	2	2	0.38	0.44	0.50	0.52	0.55	1.63	2.35	2.89	3.26	3.62	0.42	0.42	0.42	0.42	0.42
2	1	1	1	2	2	0.58	1.19	1.42	1.60	1.69	2.78	7.44	8.27	8.99	9.44	2.10	6.68	7.05	7.40	7.74
2	1	2	1	2	2	0.58	1.22	1.50	1.61	1.72	2.77	7.49	8.29	8.96	9.45	2.10	6.69	7.04	7.38	7.72
2	1	3	1	2	2	2.35	8.05	8.45	8.87	9.30	3.33	9.49	10.23	11.00	11.63	2.36	8.05	8.48	8.88	9.30
2	2	1	1	2	2	0.38	0.61	0.71	0.77	0.78	2.67	5.75	6.93	7.71	7.94	2.10	6.67	7.02	7.37	7.74
2	2	2	1	2	2	0.36	0.59	0.69	0.76	0.80	2.66	5.77	6.90	7.74	7.92	2.09	6.67	7.01	7.38	7.72
2	2	3	1	2	2	0.54	1.01	1.21	1.36	1.35	2.79	6.21	7.33	8.21	8.31	0.40	0.41	0.42	0.42	0.42
1	1	1	2	2	2	0.42	0.53	0.60	0.65	0.69	1.81	3.20	3.67	4.12	4.48	1.34	2.86	3.09	3.35	3.60
1	1	2	2	2	2	0.40	0.51	0.57	0.64	0.69	1.79	3.18	3.67	4.11	4.52	1.33	2.84	3.10	3.34	3.60
1	1	3	2	2	2	1.20	2.71	2.94	3.23	3.53	2.05	3.89	4.27	4.86	5.23	1.04	2.58	2.83	3.09	3.34
1	2	1	2	2	2	0.31	0.34	0.36	0.38	0.40	1.45	2.15	2.63	3.01	3.35	1.32	2.84	3.08	3.33	3.57
1	2	2	2	2	2	0.31	0.34	0.37	0.39	0.40	1.45	2.15	2.64	3.02	3.34	1.32	2.83	3.09	3.34	3.58
1	2	3	2	2	2	0.37	0.42	0.47	0.52	0.56	1.50	2.28	2.78	3.17	3.52	0.38	0.38	0.38	0.38	0.38
2	1	1	2	2	2	0.73	1.59	1.92	2.12	2.19	3.06	8.28	9.42	10.33	10.73	2.21	7.63	8.01	8.45	8.82
2	1	2	2	2	2	0.72	1.61	1.97	2.11	2.21	3.05	8.36	9.34	10.24	10.84	2.21	7.60	7.99	8.44	8.83
2	1	3	2	2	2	2.35	7.92	8.30	8.82	9.22	3.50	9.97	11.26	12.06	12.92	2.27	7.85	8.26	8.69	9.09
2	2	1	2	2	2	0.39	0.65	0.77	0.82	0.87	2.50	5.74	6.88	7.71	7.93	2.19	7.59	8.00	8.40	8.81
2	2	2	2	2	2	0.38	0.66	0.75	0.83	0.88	2.48	5.71	6.89	7.71	7.95	2.19	7.61	8.00	8.42	8.81
2	2	3	2	2	2	0.52	1.08	1.31	1.45	1.49	2.58	6.11	7.31	8.08	8.27	0.37	0.38	0.38	0.39	0.39
1	1	1	3	2	2	0.43	0.54	0.63	0.70	0.74	1.95	3.41	4.00	4.53	4.99	1.39	3.15	3.41	3.68	3.95
1	1	2	3	2	2	0.40	0.52	0.62	0.70	0.75	1.95	3.39	3.98	4.54	5.02	1.38	3.13	3.41	3.68	3.95
1	1	3	3	2	2	1.01	2.18	2.42	2.63	2.93	2.12	3.80	4.38	4.96	5.47	0.86	2.10	2.32	2.57	2.77
1	2	1	3	2	2	0.37	0.41	0.43	0.46	0.48	1.19	1.86	2.23	2.55	2.81	1.41	3.13	3.40	3.67	3.95
1	2	2	3	2	2	0.35	0.39	0.42	0.45	0.47	1.19	1.86	2.22	2.55	2.82	1.40	3.13	3.40	3.67	3.95
1	2	3	3	2	2	0.39	0.47	0.53	0.58	0.62	1.23	2.00	2.40	2.73	2.98	0.41	0.41	0.41	0.41	0.42
2	1	1	3	2	2	0.80	1.93	2.33	2.54	2.58	3.63	10.03	11.67	13.05	13.42	2.57	9.78	10.30	10.84	11.36

Density	Sample size	Overlap	Correlation	SNR	SNR Grp Diff	Proposed					Benchmark Separate Node					Benchmark Summary Statistics				
						N1	N2	N3	N4	N5	N1	N2	N3	N4	N5	N1	N2	N3	N4	N5
2	1	2	3	2	2	0.78	1.93	2.36	2.53	2.55	3.66	10.02	11.70	13.00	13.57	2.56	9.77	10.39	10.81	11.38
2	1	3	3	2	2	2.00	6.40	6.70	7.00	7.51	3.81	10.78	12.42	13.61	14.24	1.84	6.01	6.33	6.64	7.00
2	2	1	3	2	2	0.53	1.19	1.38	1.47	1.56	2.07	5.39	6.30	7.04	7.31	2.55	9.75	10.27	10.82	11.34
2	2	2	3	2	2	0.51	1.20	1.38	1.48	1.54	2.05	5.40	6.34	7.06	7.28	2.55	9.74	10.29	10.80	11.33
2	2	3	3	2	2	0.76	1.90	2.18	2.40	2.53	2.19	5.85	6.79	7.51	7.60	0.43	0.44	0.44	0.44	0.45

The average overall variable selection accuracy values over 100 replications in all 144 scenarios in the simulation studies of functional graphical modeling are summarized in Table D2.

Table D2. Average Overall Variable Selection Accuracy for Simulation Studies (Grp Diff: Group Difference; N: Node)

Density	Sample size	Overlap	Correlation	SNR	SNR Grp Diff	Proposed					Benchmark Separate Node					Benchmark Summary Statistics				
						N1	N2	N3	N4	N5	N1	N2	N3	N4	N5	N1	N2	N3	N4	N5
1	1	1	1	1	1	0.99	1.00	1.00	1.00	1.00	0.86	0.74	0.72	0.71	0.70	0.81	0.72	0.71	0.69	0.68
1	1	2	1	1	1	0.99	1.00	1.00	1.00	1.00	0.86	0.74	0.72	0.71	0.69	0.81	0.71	0.70	0.69	0.68
1	1	3	1	1	1	0.87	0.73	0.72	0.72	0.70	0.87	0.71	0.70	0.68	0.67	0.88	0.80	0.79	0.78	0.78
1	2	1	1	1	1	0.99	1.00	1.00	1.00	1.00	0.99	1.00	0.99	0.99	0.99	0.77	0.69	0.68	0.67	0.66
1	2	2	1	1	1	0.99	1.00	1.00	1.00	1.00	0.99	1.00	0.99	0.99	0.99	0.77	0.69	0.68	0.67	0.66
1	2	3	1	1	1	0.99	1.00	1.00	1.00	1.00	0.99	1.00	0.99	0.99	0.99	0.93	0.93	0.93	0.93	0.93
2	1	1	1	1	1	0.97	1.00	1.00	1.00	1.00	0.68	0.47	0.47	0.46	0.46	0.69	0.57	0.57	0.56	0.55
2	1	2	1	1	1	0.97	1.00	1.00	1.00	1.00	0.68	0.47	0.47	0.46	0.46	0.69	0.57	0.57	0.56	0.56
2	1	3	1	1	1	0.67	0.54	0.54	0.54	0.54	0.65	0.50	0.50	0.50	0.50	0.72	0.65	0.65	0.64	0.64
2	2	1	1	1	1	0.97	1.00	1.00	1.00	1.00	0.97	0.89	0.89	0.88	0.88	0.66	0.55	0.54	0.54	0.54
2	2	2	1	1	1	0.98	1.00	1.00	1.00	1.00	0.96	0.90	0.89	0.88	0.88	0.66	0.55	0.54	0.54	0.54
2	2	3	1	1	1	0.97	1.00	1.00	1.00	1.00	0.96	0.90	0.89	0.89	0.88	0.87	0.88	0.88	0.88	0.88
1	1	1	2	1	1	0.99	1.00	1.00	1.00	1.00	0.86	0.75	0.74	0.73	0.72	0.81	0.72	0.71	0.70	0.69
1	1	2	2	1	1	0.99	1.00	1.00	1.00	1.00	0.86	0.75	0.74	0.73	0.72	0.81	0.72	0.71	0.70	0.70
1	1	3	2	1	1	0.86	0.79	0.77	0.76	0.76	0.85	0.77	0.76	0.75	0.74	0.86	0.83	0.81	0.81	0.81
1	2	1	2	1	1	0.99	1.00	1.00	1.00	1.00	0.99	0.99	0.99	0.99	0.98	0.77	0.69	0.68	0.67	0.66

Density	Sample size	Overlap	Correlation	SNR	SNR Grp Diff	Proposed					Benchmark Separate Node					Benchmark Summary Statistics				
						N1	N2	N3	N4	N5	N1	N2	N3	N4	N5	N1	N2	N3	N4	N5
1	2	2	2	1	1	0.99	1.00	1.00	1.00	1.00	0.99	0.99	0.99	0.99	0.98	0.77	0.69	0.68	0.67	0.66
1	2	3	2	1	1	0.99	1.00	1.00	1.00	1.00	0.99	0.99	0.99	0.99	0.98	0.93	0.93	0.93	0.93	0.93
2	1	1	2	1	1	0.97	0.99	0.99	0.99	0.98	0.67	0.45	0.45	0.44	0.44	0.69	0.57	0.57	0.57	0.56
2	1	2	2	1	1	0.97	0.99	0.98	0.98	0.97	0.67	0.45	0.45	0.45	0.44	0.69	0.58	0.57	0.57	0.57
2	1	3	2	1	1	0.67	0.50	0.50	0.49	0.49	0.66	0.46	0.46	0.45	0.45	0.72	0.62	0.62	0.61	0.61
2	2	1	2	1	1	0.98	1.00	1.00	1.00	1.00	0.96	0.88	0.88	0.87	0.87	0.67	0.55	0.55	0.54	0.54
2	2	2	2	1	1	0.98	1.00	1.00	1.00	1.00	0.96	0.88	0.88	0.87	0.87	0.67	0.55	0.55	0.55	0.54
2	2	3	2	1	1	0.97	1.00	1.00	0.99	1.00	0.96	0.88	0.88	0.87	0.87	0.87	0.89	0.89	0.89	0.89
1	1	1	3	1	1	0.99	1.00	1.00	1.00	1.00	0.86	0.75	0.73	0.72	0.71	0.81	0.75	0.74	0.73	0.73
1	1	2	3	1	1	0.99	1.00	1.00	1.00	1.00	0.86	0.75	0.73	0.72	0.71	0.81	0.75	0.74	0.73	0.73
1	1	3	3	1	1	0.87	0.77	0.76	0.74	0.73	0.86	0.74	0.73	0.71	0.70	0.86	0.81	0.79	0.80	0.79
1	2	1	3	1	1	0.99	1.00	1.00	1.00	1.00	0.98	0.97	0.97	0.97	0.96	0.78	0.71	0.70	0.69	0.68
1	2	2	3	1	1	0.99	1.00	1.00	1.00	1.00	0.98	0.97	0.97	0.96	0.96	0.78	0.71	0.70	0.69	0.68
1	2	3	3	1	1	0.99	1.00	1.00	1.00	1.00	0.98	0.98	0.97	0.97	0.96	0.91	0.92	0.92	0.92	0.92
2	1	1	3	1	1	0.97	0.95	0.95	0.95	0.96	0.62	0.39	0.38	0.38	0.38	0.70	0.62	0.62	0.61	0.61
2	1	2	3	1	1	0.97	0.94	0.96	0.96	0.95	0.62	0.39	0.38	0.38	0.38	0.70	0.62	0.62	0.62	0.61
2	1	3	3	1	1	0.64	0.44	0.44	0.44	0.44	0.61	0.39	0.39	0.38	0.38	0.69	0.59	0.58	0.58	0.58
2	2	1	3	1	1	0.98	0.99	0.99	0.98	0.97	0.93	0.87	0.87	0.87	0.87	0.67	0.58	0.58	0.57	0.57
2	2	2	3	1	1	0.97	0.99	0.98	0.98	0.98	0.93	0.87	0.87	0.87	0.86	0.67	0.58	0.58	0.57	0.57
2	2	3	3	1	1	0.98	0.85	0.83	0.81	0.81	0.93	0.87	0.87	0.87	0.87	0.86	0.88	0.88	0.88	0.88
1	1	1	1	1	2	0.99	1.00	1.00	1.00	1.00	0.86	0.73	0.71	0.70	0.69	0.81	0.72	0.70	0.69	0.69
1	1	2	1	1	2	0.99	1.00	1.00	1.00	1.00	0.85	0.73	0.71	0.70	0.69	0.81	0.72	0.70	0.70	0.69
1	1	3	1	1	2	0.88	0.77	0.75	0.74	0.73	0.86	0.74	0.71	0.70	0.68	0.88	0.82	0.81	0.80	0.79
1	2	1	1	1	2	0.99	1.00	1.00	1.00	1.00	0.98	0.99	0.98	0.97	0.96	0.77	0.69	0.68	0.67	0.66
1	2	2	1	1	2	0.99	1.00	1.00	1.00	1.00	0.98	0.99	0.98	0.97	0.96	0.77	0.69	0.68	0.67	0.66
1	2	3	1	1	2	0.99	1.00	1.00	1.00	1.00	0.98	0.99	0.98	0.97	0.96	0.92	0.93	0.93	0.93	0.93
2	1	1	1	1	2	0.97	1.00	1.00	0.99	0.99	0.66	0.47	0.47	0.46	0.46	0.69	0.57	0.56	0.56	0.56

Density	Sample size	Overlap	Correlation	SNR	SNR Grp Diff	Proposed					Benchmark Separate Node					Benchmark Summary Statistics				
						N1	N2	N3	N4	N5	N1	N2	N3	N4	N5	N1	N2	N3	N4	N5
2	1	2	1	1	2	0.97	0.99	0.99	0.99	0.99	0.66	0.47	0.47	0.46	0.46	0.69	0.58	0.57	0.57	0.56
2	1	3	1	1	2	0.69	0.55	0.54	0.54	0.54	0.66	0.49	0.48	0.49	0.47	0.72	0.63	0.63	0.63	0.63
2	2	1	1	1	2	0.97	1.00	1.00	1.00	1.00	0.94	0.89	0.87	0.86	0.86	0.66	0.55	0.54	0.54	0.53
2	2	2	1	1	2	0.97	1.00	1.00	1.00	1.00	0.94	0.89	0.87	0.86	0.86	0.66	0.55	0.54	0.54	0.54
2	2	3	1	1	2	0.97	1.00	1.00	1.00	1.00	0.94	0.89	0.87	0.86	0.86	0.87	0.89	0.89	0.89	0.89
1	1	1	2	1	2	0.99	1.00	1.00	1.00	1.00	0.85	0.75	0.73	0.72	0.70	0.81	0.72	0.71	0.70	0.69
1	1	2	2	1	2	0.99	1.00	1.00	1.00	1.00	0.85	0.75	0.73	0.72	0.70	0.81	0.72	0.71	0.70	0.69
1	1	3	2	1	2	0.88	0.76	0.75	0.75	0.74	0.86	0.74	0.73	0.71	0.70	0.88	0.81	0.81	0.80	0.79
1	2	1	2	1	2	0.99	1.00	1.00	1.00	1.00	0.98	0.98	0.97	0.97	0.96	0.77	0.69	0.68	0.67	0.66
1	2	2	2	1	2	0.99	1.00	1.00	1.00	1.00	0.98	0.98	0.97	0.97	0.96	0.77	0.69	0.68	0.67	0.66
1	2	3	2	1	2	0.99	1.00	1.00	1.00	1.00	0.98	0.98	0.97	0.97	0.96	0.92	0.93	0.93	0.93	0.93
2	1	1	2	1	2	0.97	0.99	0.98	0.98	0.98	0.66	0.45	0.45	0.44	0.44	0.69	0.58	0.57	0.57	0.56
2	1	2	2	1	2	0.97	0.99	0.98	0.98	0.98	0.66	0.45	0.45	0.45	0.44	0.69	0.58	0.58	0.57	0.56
2	1	3	2	1	2	0.68	0.53	0.52	0.53	0.50	0.66	0.45	0.45	0.44	0.44	0.73	0.62	0.62	0.61	0.62
2	2	1	2	1	2	0.97	1.00	1.00	1.00	1.00	0.92	0.89	0.86	0.86	0.86	0.66	0.55	0.55	0.54	0.54
2	2	2	2	1	2	0.97	1.00	1.00	1.00	1.00	0.92	0.89	0.87	0.86	0.86	0.66	0.55	0.55	0.55	0.54
2	2	3	2	1	2	0.97	1.00	1.00	1.00	1.00	0.92	0.89	0.87	0.86	0.87	0.86	0.88	0.88	0.88	0.88
1	1	1	3	1	2	0.99	1.00	1.00	1.00	1.00	0.85	0.74	0.72	0.71	0.70	0.81	0.74	0.74	0.73	0.73
1	1	2	3	1	2	0.99	1.00	1.00	1.00	1.00	0.85	0.74	0.72	0.71	0.70	0.81	0.75	0.74	0.73	0.73
1	1	3	3	1	2	0.87	0.78	0.76	0.75	0.73	0.85	0.72	0.70	0.68	0.68	0.87	0.80	0.78	0.78	0.77
1	2	1	3	1	2	0.99	1.00	1.00	1.00	1.00	0.97	0.97	0.95	0.94	0.94	0.78	0.71	0.70	0.69	0.68
1	2	2	3	1	2	0.99	1.00	1.00	1.00	1.00	0.97	0.97	0.95	0.94	0.94	0.78	0.71	0.70	0.69	0.68
1	2	3	3	1	2	0.98	1.00	1.00	1.00	1.00	0.96	0.97	0.96	0.95	0.94	0.92	0.92	0.92	0.92	0.93
2	1	1	3	1	2	0.97	0.95	0.96	0.95	0.96	0.62	0.39	0.39	0.39	0.39	0.69	0.62	0.61	0.61	0.61
2	1	2	3	1	2	0.97	0.96	0.95	0.95	0.95	0.62	0.39	0.39	0.39	0.38	0.69	0.62	0.62	0.61	0.61
2	1	3	3	1	2	0.65	0.46	0.45	0.43	0.44	0.62	0.38	0.37	0.37	0.36	0.69	0.57	0.56	0.56	0.55
2	2	1	3	1	2	0.97	0.96	0.93	0.91	0.89	0.87	0.87	0.86	0.85	0.85	0.67	0.58	0.58	0.57	0.57

Density	Sample size	Overlap	Correlation	SNR	SNR Grp Diff	Proposed					Benchmark Separate Node					Benchmark Summary Statistics				
						N1	N2	N3	N4	N5	N1	N2	N3	N4	N5	N1	N2	N3	N4	N5
2	2	2	3	1	2	0.98	0.95	0.93	0.91	0.90	0.87	0.87	0.86	0.85	0.85	0.67	0.58	0.58	0.57	0.57
2	2	3	3	1	2	0.97	0.89	0.89	0.89	0.92	0.87	0.86	0.86	0.85	0.85	0.87	0.89	0.89	0.89	0.89
1	1	1	1	2	1	0.98	0.97	0.97	0.97	0.96	0.67	0.51	0.49	0.48	0.47	0.81	0.71	0.71	0.69	0.69
1	1	2	1	2	1	0.98	0.97	0.97	0.96	0.96	0.67	0.50	0.49	0.48	0.48	0.81	0.72	0.71	0.70	0.69
1	1	3	1	2	1	0.87	0.75	0.74	0.73	0.73	0.67	0.51	0.50	0.48	0.47	0.87	0.82	0.81	0.81	0.80
1	2	1	1	2	1	0.99	1.00	1.00	0.99	0.99	0.72	0.63	0.63	0.62	0.62	0.77	0.69	0.68	0.67	0.66
1	2	2	1	2	1	0.99	1.00	1.00	0.99	0.99	0.72	0.63	0.63	0.62	0.62	0.77	0.69	0.68	0.67	0.66
1	2	3	1	2	1	0.99	0.99	0.99	0.99	0.99	0.72	0.63	0.63	0.62	0.62	0.93	0.93	0.93	0.93	0.93
2	1	1	1	2	1	0.93	0.85	0.86	0.84	0.84	0.53	0.42	0.42	0.41	0.41	0.69	0.57	0.57	0.56	0.56
2	1	2	1	2	1	0.93	0.86	0.85	0.84	0.83	0.53	0.42	0.41	0.41	0.41	0.69	0.57	0.57	0.56	0.56
2	1	3	1	2	1	0.68	0.58	0.57	0.56	0.58	0.53	0.43	0.43	0.42	0.43	0.73	0.65	0.65	0.65	0.65
2	2	1	1	2	1	0.97	0.93	0.91	0.91	0.89	0.65	0.62	0.62	0.62	0.62	0.66	0.55	0.54	0.54	0.54
2	2	2	1	2	1	0.97	0.92	0.91	0.90	0.89	0.65	0.62	0.62	0.62	0.62	0.66	0.55	0.55	0.54	0.54
2	2	3	1	2	1	0.96	0.89	0.88	0.88	0.87	0.65	0.62	0.62	0.62	0.62	0.87	0.88	0.88	0.88	0.88
1	1	1	2	2	1	0.98	0.96	0.95	0.95	0.94	0.67	0.53	0.52	0.52	0.50	0.81	0.72	0.71	0.70	0.69
1	1	2	2	2	1	0.98	0.96	0.95	0.95	0.94	0.67	0.53	0.52	0.51	0.50	0.81	0.72	0.71	0.70	0.69
1	1	3	2	2	1	0.86	0.77	0.76	0.75	0.74	0.67	0.53	0.52	0.51	0.51	0.87	0.83	0.82	0.82	0.81
1	2	1	2	2	1	0.98	1.00	0.99	0.99	0.99	0.75	0.69	0.68	0.68	0.68	0.77	0.69	0.68	0.67	0.66
1	2	2	2	2	1	0.98	0.99	0.99	0.99	0.99	0.75	0.69	0.68	0.68	0.67	0.77	0.69	0.68	0.67	0.66
1	2	3	2	2	1	0.98	0.99	0.99	0.99	0.98	0.75	0.68	0.68	0.68	0.68	0.92	0.92	0.92	0.92	0.92
2	1	1	2	2	1	0.92	0.83	0.83	0.82	0.82	0.54	0.45	0.44	0.43	0.44	0.69	0.58	0.57	0.57	0.57
2	1	2	2	2	1	0.91	0.81	0.81	0.81	0.81	0.54	0.44	0.44	0.44	0.43	0.69	0.58	0.58	0.57	0.56
2	1	3	2	2	1	0.67	0.52	0.50	0.51	0.49	0.53	0.43	0.43	0.43	0.43	0.72	0.63	0.62	0.62	0.62
2	2	1	2	2	1	0.97	0.88	0.88	0.87	0.86	0.69	0.67	0.67	0.67	0.67	0.67	0.55	0.55	0.54	0.54
2	2	2	2	2	1	0.97	0.88	0.88	0.87	0.84	0.68	0.67	0.67	0.67	0.67	0.66	0.55	0.55	0.55	0.54
2	2	3	2	2	1	0.95	0.86	0.85	0.85	0.84	0.68	0.67	0.67	0.67	0.67	0.87	0.88	0.88	0.88	0.88
1	1	1	3	2	1	0.95	0.92	0.92	0.91	0.91	0.72	0.63	0.62	0.62	0.62	0.81	0.75	0.74	0.74	0.73

Density	Sample size	Overlap	Correlation	SNR	SNR Grp Diff	Proposed					Benchmark Separate Node					Benchmark Summary Statistics				
						N1	N2	N3	N4	N5	N1	N2	N3	N4	N5	N1	N2	N3	N4	N5
1	1	2	3	2	1	0.96	0.93	0.91	0.92	0.90	0.72	0.63	0.63	0.62	0.62	0.81	0.75	0.74	0.73	0.73
1	1	3	3	2	1	0.85	0.75	0.75	0.74	0.72	0.72	0.62	0.62	0.61	0.60	0.86	0.80	0.80	0.79	0.78
1	2	1	3	2	1	0.98	0.97	0.96	0.96	0.95	0.82	0.78	0.78	0.78	0.77	0.78	0.71	0.70	0.69	0.68
1	2	2	3	2	1	0.98	0.97	0.97	0.96	0.95	0.82	0.78	0.78	0.78	0.78	0.78	0.71	0.70	0.69	0.69
1	2	3	3	2	1	0.98	0.96	0.96	0.95	0.95	0.81	0.78	0.78	0.78	0.78	0.91	0.92	0.92	0.92	0.92
2	1	1	3	2	1	0.86	0.79	0.78	0.78	0.77	0.61	0.56	0.55	0.56	0.55	0.70	0.62	0.62	0.61	0.61
2	1	2	3	2	1	0.86	0.78	0.77	0.78	0.78	0.61	0.55	0.55	0.55	0.56	0.70	0.62	0.62	0.61	0.61
2	1	3	3	2	1	0.64	0.45	0.47	0.45	0.44	0.60	0.55	0.55	0.55	0.54	0.69	0.57	0.56	0.57	0.57
2	2	1	3	2	1	0.93	0.79	0.77	0.76	0.77	0.74	0.73	0.72	0.72	0.72	0.67	0.58	0.58	0.57	0.57
2	2	2	3	2	1	0.94	0.79	0.78	0.76	0.76	0.74	0.73	0.72	0.72	0.72	0.67	0.58	0.58	0.57	0.57
2	2	3	3	2	1	0.92	0.81	0.80	0.78	0.78	0.73	0.72	0.72	0.72	0.72	0.86	0.88	0.88	0.88	0.88
1	1	1	1	2	2	0.96	0.96	0.94	0.93	0.92	0.56	0.51	0.49	0.46	0.47	0.81	0.72	0.71	0.70	0.69
1	1	2	1	2	2	0.96	0.96	0.94	0.93	0.92	0.56	0.51	0.48	0.46	0.47	0.81	0.72	0.70	0.70	0.69
1	1	3	1	2	2	0.86	0.77	0.75	0.73	0.72	0.55	0.52	0.49	0.46	0.48	0.87	0.82	0.81	0.81	0.80
1	2	1	1	2	2	0.98	0.99	0.98	0.98	0.97	0.59	0.65	0.61	0.59	0.61	0.77	0.69	0.68	0.67	0.66
1	2	2	1	2	2	0.98	0.99	0.98	0.98	0.97	0.59	0.65	0.61	0.59	0.61	0.77	0.69	0.68	0.67	0.66
1	2	3	1	2	2	0.98	0.98	0.97	0.97	0.96	0.59	0.65	0.61	0.59	0.61	0.92	0.92	0.92	0.92	0.92
2	1	1	1	2	2	0.87	0.85	0.83	0.80	0.82	0.47	0.42	0.41	0.41	0.41	0.69	0.57	0.57	0.56	0.56
2	1	2	1	2	2	0.87	0.85	0.81	0.79	0.80	0.47	0.42	0.42	0.41	0.41	0.69	0.58	0.56	0.57	0.56
2	1	3	1	2	2	0.67	0.53	0.52	0.51	0.50	0.46	0.42	0.41	0.41	0.41	0.73	0.62	0.61	0.62	0.61
2	2	1	1	2	2	0.95	0.89	0.87	0.84	0.86	0.55	0.62	0.59	0.58	0.58	0.66	0.55	0.54	0.54	0.53
2	2	2	1	2	2	0.95	0.90	0.87	0.85	0.84	0.54	0.62	0.59	0.58	0.58	0.66	0.55	0.54	0.54	0.54
2	2	3	1	2	2	0.93	0.88	0.84	0.84	0.84	0.54	0.62	0.59	0.58	0.59	0.87	0.89	0.89	0.88	0.88
1	1	1	2	2	2	0.95	0.95	0.94	0.92	0.92	0.58	0.54	0.53	0.49	0.51	0.81	0.72	0.71	0.70	0.69
1	1	2	2	2	2	0.95	0.94	0.93	0.92	0.92	0.58	0.54	0.53	0.50	0.51	0.81	0.72	0.71	0.70	0.69
1	1	3	2	2	2	0.86	0.77	0.77	0.74	0.72	0.58	0.54	0.53	0.50	0.50	0.87	0.81	0.80	0.81	0.80
1	2	1	2	2	2	0.98	0.98	0.98	0.97	0.96	0.63	0.69	0.65	0.64	0.65	0.77	0.69	0.68	0.67	0.66

Density	Sample size	Overlap	Correlation	SNR	SNR Grp Diff	Proposed					Benchmark Separate Node					Benchmark Summary Statistics				
						N1	N2	N3	N4	N5	N1	N2	N3	N4	N5	N1	N2	N3	N4	N5
1	2	2	2	2	2	0.98	0.99	0.98	0.97	0.96	0.62	0.69	0.65	0.64	0.65	0.77	0.69	0.68	0.67	0.66
1	2	3	2	2	2	0.98	0.98	0.97	0.96	0.95	0.62	0.69	0.65	0.64	0.65	0.92	0.93	0.93	0.93	0.93
2	1	1	2	2	2	0.86	0.83	0.80	0.79	0.80	0.49	0.44	0.44	0.44	0.44	0.69	0.58	0.57	0.57	0.56
2	1	2	2	2	2	0.85	0.84	0.79	0.79	0.80	0.50	0.44	0.44	0.44	0.44	0.69	0.58	0.58	0.57	0.57
2	1	3	2	2	2	0.69	0.51	0.48	0.49	0.50	0.49	0.44	0.44	0.43	0.43	0.73	0.62	0.62	0.62	0.62
2	2	1	2	2	2	0.94	0.88	0.83	0.81	0.81	0.58	0.66	0.63	0.62	0.62	0.66	0.55	0.55	0.54	0.54
2	2	2	2	2	2	0.94	0.87	0.84	0.83	0.82	0.58	0.66	0.63	0.62	0.62	0.66	0.55	0.55	0.55	0.54
2	2	3	2	2	2	0.92	0.86	0.82	0.81	0.81	0.58	0.66	0.63	0.61	0.62	0.87	0.88	0.88	0.89	0.89
1	1	1	3	2	2	0.92	0.92	0.90	0.88	0.89	0.67	0.63	0.64	0.61	0.61	0.81	0.75	0.74	0.73	0.73
1	1	2	3	2	2	0.92	0.92	0.90	0.89	0.88	0.66	0.63	0.63	0.61	0.61	0.81	0.75	0.74	0.73	0.73
1	1	3	3	2	2	0.84	0.75	0.72	0.72	0.69	0.67	0.62	0.62	0.61	0.61	0.87	0.81	0.81	0.80	0.79
1	2	1	3	2	2	0.97	0.96	0.94	0.93	0.91	0.72	0.77	0.75	0.73	0.73	0.78	0.71	0.70	0.69	0.69
1	2	2	3	2	2	0.96	0.95	0.94	0.92	0.91	0.72	0.77	0.75	0.73	0.73	0.78	0.71	0.70	0.69	0.68
1	2	3	3	2	2	0.96	0.95	0.94	0.92	0.90	0.72	0.77	0.75	0.73	0.73	0.91	0.92	0.92	0.92	0.92
2	1	1	3	2	2	0.80	0.80	0.77	0.77	0.77	0.59	0.53	0.55	0.55	0.53	0.70	0.61	0.62	0.61	0.61
2	1	2	3	2	2	0.80	0.80	0.76	0.77	0.77	0.59	0.53	0.55	0.54	0.53	0.70	0.62	0.62	0.61	0.61
2	1	3	3	2	2	0.64	0.46	0.46	0.45	0.46	0.59	0.54	0.55	0.55	0.53	0.70	0.59	0.59	0.59	0.59
2	2	1	3	2	2	0.87	0.78	0.72	0.72	0.72	0.67	0.71	0.70	0.69	0.69	0.67	0.58	0.58	0.57	0.57
2	2	2	3	2	2	0.88	0.77	0.74	0.70	0.72	0.67	0.71	0.70	0.69	0.69	0.67	0.58	0.58	0.57	0.57
2	2	3	3	2	2	0.86	0.79	0.76	0.75	0.75	0.67	0.71	0.70	0.69	0.69	0.86	0.88	0.88	0.88	0.88

The average true positive rate (proportion of significant variables being selected) values over 100 replications in all 144 scenarios in the simulation studies of functional graphical modeling are summarized in Table D3.

Table D3. Average True Positive Rate for Simulation Studies (Grp Diff: Group Difference; N: Node)

Density	Sample size	Overlap	Correlation	SNR	SNR Grp Diff	Proposed					Benchmark Separate Node					Benchmark Summary Statistics				
						N1	N2	N3	N4	N5	N1	N2	N3	N4	N5	N1	N2	N3	N4	N5
1	1	1	1	1	1	0.85	1.00	1.00	1.00	1.00	0.48	0.67	0.68	0.69	0.70	0.11	0.23	0.25	0.26	0.27
1	1	2	1	1	1	0.86	1.00	1.00	1.00	1.00	0.49	0.67	0.69	0.69	0.70	0.11	0.23	0.25	0.26	0.27
1	1	3	1	1	1	0.46	0.70	0.71	0.70	0.72	0.45	0.67	0.69	0.70	0.71	0.24	0.35	0.37	0.38	0.37
1	2	1	1	1	1	0.87	1.00	1.00	1.00	1.00	0.87	1.00	1.00	1.00	1.00	0.17	0.27	0.28	0.29	0.31
1	2	2	1	1	1	0.87	1.00	1.00	1.00	1.00	0.87	1.00	1.00	1.00	1.00	0.17	0.27	0.28	0.29	0.31
1	2	3	1	1	1	0.87	1.00	1.00	1.00	1.00	0.87	1.00	1.00	1.00	1.00	0.45	0.52	0.52	0.52	0.52
2	1	1	1	1	1	0.85	1.00	1.00	1.00	1.00	0.49	0.74	0.74	0.74	0.75	0.19	0.39	0.39	0.39	0.41
2	1	2	1	1	1	0.86	1.00	1.00	1.00	1.00	0.48	0.74	0.74	0.75	0.75	0.19	0.38	0.39	0.39	0.39
2	1	3	1	1	1	0.50	0.69	0.68	0.68	0.68	0.51	0.70	0.70	0.70	0.71	0.27	0.37	0.37	0.37	0.37
2	2	1	1	1	1	0.87	1.00	1.00	1.00	1.00	0.85	1.00	1.00	1.00	1.00	0.23	0.43	0.43	0.44	0.45
2	2	2	1	1	1	0.88	1.00	1.00	1.00	1.00	0.85	1.00	1.00	1.00	1.00	0.23	0.42	0.43	0.44	0.45
2	2	3	1	1	1	0.86	1.00	1.00	1.00	1.00	0.85	1.00	1.00	1.00	1.00	0.46	0.53	0.53	0.53	0.53
1	1	1	2	1	1	0.87	1.00	1.00	1.00	1.00	0.49	0.67	0.69	0.69	0.70	0.11	0.23	0.24	0.25	0.26
1	1	2	2	1	1	0.85	1.00	1.00	1.00	1.00	0.49	0.68	0.69	0.70	0.70	0.11	0.23	0.24	0.25	0.26
1	1	3	2	1	1	0.51	0.70	0.72	0.73	0.74	0.50	0.66	0.68	0.69	0.70	0.28	0.36	0.37	0.37	0.37
1	2	1	2	1	1	0.86	1.00	1.00	1.00	1.00	0.86	1.00	1.00	1.00	1.00	0.16	0.26	0.28	0.29	0.30
1	2	2	2	1	1	0.87	1.00	1.00	1.00	1.00	0.86	1.00	1.00	1.00	1.00	0.16	0.27	0.28	0.29	0.30
1	2	3	2	1	1	0.86	1.00	1.00	1.00	1.00	0.86	1.00	1.00	1.00	1.00	0.46	0.53	0.53	0.53	0.53
2	1	1	2	1	1	0.85	1.00	1.00	1.00	1.00	0.49	0.78	0.78	0.78	0.79	0.19	0.38	0.38	0.38	0.39
2	1	2	2	1	1	0.86	1.00	1.00	1.00	1.00	0.49	0.78	0.78	0.78	0.79	0.19	0.37	0.38	0.38	0.39
2	1	3	2	1	1	0.52	0.77	0.78	0.79	0.78	0.52	0.78	0.79	0.79	0.79	0.28	0.41	0.41	0.42	0.42
2	2	1	2	1	1	0.88	1.00	1.00	1.00	1.00	0.85	1.00	1.00	1.00	1.00	0.23	0.42	0.42	0.43	0.44
2	2	2	2	1	1	0.88	1.00	1.00	1.00	1.00	0.85	1.00	1.00	1.00	1.00	0.23	0.42	0.42	0.43	0.43
2	2	3	2	1	1	0.86	1.00	1.00	1.00	1.00	0.84	1.00	1.00	1.00	1.00	0.46	0.53	0.54	0.54	0.54
1	1	1	3	1	1	0.87	1.00	1.00	1.00	1.00	0.49	0.70	0.71	0.72	0.73	0.11	0.19	0.20	0.21	0.22
1	1	2	3	1	1	0.86	1.00	1.00	1.00	1.00	0.49	0.70	0.71	0.72	0.73	0.11	0.20	0.20	0.21	0.21
1	1	3	3	1	1	0.5	0.7	0.7	0.7	0.7	0.5	0.7	0.7	0.7	0.7	0.3	0.3	0.3	0.3	0.3

Density	Sample size	Overlap	Correlation	SNR	SNR Grp Diff	Proposed					Benchmark Separate Node					Benchmark Summary Statistics				
						N1	N2	N3	N4	N5	N1	N2	N3	N4	N5	N1	N2	N3	N4	N5
						2	4	5	7	8	0	1	2	2	3	0	8	8	9	9
1	2	1	3	1	1	0.88	1.00	1.00	1.00	1.00	0.85	1.00	1.00	1.00	1.00	0.15	0.24	0.25	0.26	0.27
1	2	2	3	1	1	0.88	1.00	1.00	1.00	1.00	0.85	1.00	1.00	1.00	1.00	0.15	0.24	0.25	0.26	0.27
1	2	3	3	1	1	0.86	1.00	1.00	1.00	1.00	0.84	1.00	1.00	1.00	1.00	0.48	0.54	0.54	0.54	0.54
2	1	1	3	1	1	0.86	1.00	1.00	1.00	1.00	0.56	0.88	0.88	0.88	0.88	0.17	0.30	0.31	0.31	0.32
2	1	2	3	1	1	0.86	1.00	1.00	1.00	1.00	0.56	0.88	0.88	0.88	0.88	0.17	0.30	0.30	0.30	0.31
2	1	3	3	1	1	0.54	0.91	0.91	0.90	0.91	0.55	0.89	0.89	0.90	0.90	0.30	0.47	0.47	0.48	0.48
2	2	1	3	1	1	0.88	1.00	1.00	1.00	1.00	0.82	1.00	1.00	1.00	1.00	0.21	0.37	0.37	0.38	0.38
2	2	2	3	1	1	0.87	1.00	1.00	1.00	1.00	0.82	1.00	1.00	1.00	1.00	0.21	0.37	0.37	0.38	0.38
2	2	3	3	1	1	0.88	1.00	1.00	1.00	1.00	0.82	1.00	1.00	1.00	1.00	0.47	0.52	0.53	0.52	0.52
1	1	1	1	1	2	0.86	1.00	1.00	1.00	1.00	0.47	0.67	0.68	0.69	0.70	0.11	0.23	0.25	0.26	0.27
1	1	2	1	1	2	0.86	1.00	1.00	1.00	1.00	0.48	0.67	0.68	0.69	0.70	0.11	0.23	0.25	0.26	0.27
1	1	3	1	1	2	0.48	0.66	0.68	0.69	0.70	0.46	0.66	0.67	0.68	0.69	0.25	0.34	0.35	0.36	0.36
1	2	1	1	1	2	0.87	1.00	1.00	1.00	1.00	0.85	1.00	1.00	1.00	1.00	0.16	0.27	0.28	0.29	0.31
1	2	2	1	1	2	0.88	1.00	1.00	1.00	1.00	0.85	1.00	1.00	1.00	1.00	0.17	0.27	0.28	0.29	0.31
1	2	3	1	1	2	0.86	1.00	1.00	1.00	1.00	0.85	1.00	1.00	1.00	1.00	0.47	0.53	0.53	0.53	0.53
2	1	1	1	1	2	0.86	1.00	1.00	1.00	1.00	0.49	0.74	0.74	0.75	0.74	0.19	0.38	0.39	0.39	0.41
2	1	2	1	1	2	0.86	1.00	1.00	1.00	1.00	0.49	0.73	0.74	0.75	0.74	0.18	0.37	0.39	0.39	0.40
2	1	3	1	1	2	0.50	0.68	0.70	0.71	0.71	0.50	0.72	0.73	0.72	0.74	0.27	0.38	0.38	0.38	0.38
2	2	1	1	1	2	0.86	1.00	1.00	1.00	1.00	0.83	1.00	1.00	1.00	1.00	0.23	0.42	0.43	0.44	0.45
2	2	2	1	1	2	0.86	1.00	1.00	1.00	1.00	0.83	1.00	1.00	1.00	1.00	0.23	0.42	0.43	0.44	0.44
2	2	3	1	1	2	0.85	1.00	1.00	1.00	1.00	0.83	1.00	1.00	1.00	1.00	0.46	0.52	0.52	0.52	0.53
1	1	1	2	1	2	0.86	1.00	1.00	1.00	1.00	0.48	0.67	0.68	0.69	0.70	0.11	0.23	0.24	0.25	0.26
1	1	2	2	1	2	0.86	1.00	1.00	1.00	1.00	0.48	0.68	0.68	0.69	0.71	0.11	0.23	0.24	0.25	0.26
1	1	3	2	1	2	0.52	0.67	0.69	0.71	0.72	0.50	0.66	0.66	0.69	0.69	0.29	0.35	0.36	0.37	0.37
1	2	1	2	1	2	0.86	1.00	1.00	1.00	1.00	0.84	1.00	1.00	1.00	1.00	0.16	0.26	0.27	0.29	0.30
1	2	2	2	1	2	0.87	1.00	1.00	1.00	1.00	0.84	1.00	1.00	1.00	1.00	0.16	0.26	0.27	0.29	0.30

Density	Sample size	Overlap	Correlation	SNR	SNR Grp Diff	Proposed					Benchmark Separate Node					Benchmark Summary Statistics				
						N1	N2	N3	N4	N5	N1	N2	N3	N4	N5	N1	N2	N3	N4	N5
1	2	3	2	1	2	0.86	1.00	1.00	1.00	1.00	0.84	1.00	1.00	1.00	1.00	0.45	0.52	0.52	0.53	0.53
2	1	1	2	1	2	0.85	1.00	1.00	1.00	1.00	0.49	0.78	0.78	0.79	0.79	0.19	0.37	0.38	0.38	0.40
2	1	2	2	1	2	0.85	1.00	1.00	1.00	1.00	0.49	0.78	0.78	0.78	0.79	0.19	0.37	0.37	0.38	0.39
2	1	3	2	1	2	0.48	0.76	0.77	0.77	0.78	0.49	0.79	0.78	0.80	0.79	0.26	0.41	0.41	0.42	0.42
2	2	1	2	1	2	0.86	1.00	1.00	1.00	1.00	0.83	1.00	1.00	1.00	1.00	0.22	0.42	0.42	0.43	0.44
2	2	2	2	1	2	0.86	1.00	1.00	1.00	1.00	0.83	1.00	1.00	1.00	1.00	0.23	0.41	0.42	0.43	0.43
2	2	3	2	1	2	0.85	1.00	1.00	1.00	1.00	0.83	1.00	1.00	1.00	1.00	0.48	0.55	0.55	0.55	0.55
1	1	1	3	1	2	0.85	1.00	1.00	1.00	1.00	0.47	0.69	0.70	0.71	0.71	0.11	0.19	0.20	0.21	0.22
1	1	2	3	1	2	0.86	1.00	1.00	1.00	1.00	0.47	0.69	0.70	0.71	0.71	0.11	0.19	0.20	0.21	0.21
1	1	3	3	1	2	0.50	0.76	0.77	0.79	0.81	0.47	0.71	0.73	0.73	0.74	0.27	0.39	0.40	0.40	0.41
1	2	1	3	1	2	0.87	1.00	1.00	1.00	1.00	0.82	0.99	1.00	1.00	1.00	0.15	0.24	0.25	0.26	0.27
1	2	2	3	1	2	0.86	1.00	1.00	1.00	1.00	0.82	0.99	1.00	1.00	1.00	0.15	0.24	0.25	0.26	0.27
1	2	3	3	1	2	0.85	1.00	1.00	1.00	1.00	0.82	0.99	1.00	1.00	1.00	0.46	0.53	0.53	0.54	0.54
2	1	1	3	1	2	0.84	1.00	1.00	1.00	1.00	0.55	0.87	0.87	0.87	0.86	0.17	0.30	0.31	0.31	0.31
2	1	2	3	1	2	0.85	1.00	1.00	1.00	1.00	0.55	0.87	0.87	0.87	0.87	0.17	0.30	0.31	0.31	0.31
2	1	3	3	1	2	0.57	0.88	0.89	0.90	0.90	0.56	0.87	0.88	0.87	0.88	0.31	0.47	0.48	0.48	0.48
2	2	1	3	1	2	0.87	1.00	1.00	1.00	1.00	0.79	1.00	1.00	1.00	0.99	0.21	0.37	0.37	0.38	0.38
2	2	2	3	1	2	0.88	1.00	1.00	1.00	1.00	0.80	1.00	1.00	1.00	1.00	0.22	0.37	0.37	0.37	0.38
2	2	3	3	1	2	0.86	1.00	1.00	1.00	1.00	0.80	1.00	1.00	1.00	1.00	0.48	0.54	0.54	0.54	0.54
1	1	1	1	2	1	0.83	1.00	1.00	1.00	1.00	0.47	0.65	0.66	0.68	0.68	0.11	0.23	0.24	0.26	0.27
1	1	2	1	2	1	0.83	1.00	1.00	1.00	1.00	0.47	0.65	0.67	0.67	0.68	0.11	0.23	0.24	0.26	0.27
1	1	3	1	2	1	0.46	0.69	0.70	0.70	0.72	0.47	0.65	0.66	0.68	0.68	0.25	0.35	0.36	0.36	0.36
1	2	1	1	2	1	0.86	1.00	1.00	1.00	1.00	0.74	0.90	0.91	0.92	0.93	0.16	0.27	0.28	0.30	0.31
1	2	2	1	2	1	0.85	1.00	1.00	1.00	1.00	0.74	0.90	0.91	0.92	0.93	0.16	0.27	0.28	0.30	0.30
1	2	3	1	2	1	0.86	1.00	1.00	1.00	1.00	0.74	0.91	0.92	0.92	0.93	0.46	0.52	0.52	0.52	0.52
2	1	1	1	2	1	0.81	1.00	1.00	1.00	1.00	0.55	0.71	0.70	0.72	0.72	0.19	0.38	0.39	0.40	0.40
2	1	2	1	2	1	0.8	1.0	1.0	1.0	1.0	0.5	0.7	0.7	0.7	0.7	0.1	0.3	0.3	0.4	0.4

Density	Sample size	Overlap	Correlation	SNR	SNR Grp Diff	Proposed					Benchmark Separate Node					Benchmark Summary Statistics				
						N1	N2	N3	N4	N5	N1	N2	N3	N4	N5	N1	N2	N3	N4	N5
						1	0	0	0	0	5	1	2	1	2	9	8	9	0	1
2	1	3	1	2	1	0.51	0.66	0.67	0.68	0.67	0.55	0.69	0.69	0.70	0.70	0.26	0.37	0.37	0.37	0.36
2	2	1	1	2	1	0.85	1.00	1.00	1.00	1.00	0.70	0.84	0.84	0.84	0.84	0.23	0.42	0.43	0.44	0.45
2	2	2	1	2	1	0.85	1.00	1.00	1.00	1.00	0.70	0.84	0.84	0.84	0.84	0.23	0.42	0.43	0.44	0.44
2	2	3	1	2	1	0.84	1.00	1.00	1.00	1.00	0.70	0.84	0.84	0.84	0.84	0.46	0.53	0.53	0.53	0.53
1	1	1	2	2	1	0.83	1.00	1.00	1.00	1.00	0.46	0.62	0.63	0.63	0.64	0.11	0.23	0.24	0.25	0.26
1	1	2	2	2	1	0.81	1.00	1.00	1.00	1.00	0.45	0.62	0.63	0.64	0.65	0.11	0.23	0.24	0.25	0.26
1	1	3	2	2	1	0.45	0.67	0.69	0.70	0.72	0.45	0.63	0.64	0.65	0.65	0.25	0.34	0.35	0.35	0.36
1	2	1	2	2	1	0.84	1.00	1.00	1.00	1.00	0.70	0.86	0.87	0.88	0.88	0.16	0.26	0.28	0.29	0.30
1	2	2	2	2	1	0.85	1.00	1.00	1.00	1.00	0.69	0.86	0.87	0.88	0.89	0.16	0.26	0.27	0.29	0.30
1	2	3	2	2	1	0.85	1.00	1.00	1.00	1.00	0.69	0.85	0.86	0.87	0.88	0.46	0.54	0.54	0.54	0.54
2	1	1	2	2	1	0.81	1.00	1.00	1.00	1.00	0.52	0.66	0.67	0.68	0.67	0.19	0.37	0.38	0.38	0.39
2	1	2	2	2	1	0.80	1.00	1.00	1.00	1.00	0.52	0.67	0.67	0.67	0.68	0.19	0.36	0.37	0.38	0.40
2	1	3	2	2	1	0.53	0.76	0.77	0.76	0.77	0.54	0.69	0.69	0.69	0.69	0.28	0.40	0.40	0.40	0.40
2	2	1	2	2	1	0.84	1.00	1.00	1.00	1.00	0.63	0.75	0.75	0.75	0.75	0.23	0.42	0.42	0.43	0.44
2	2	2	2	2	1	0.85	1.00	1.00	1.00	1.00	0.63	0.75	0.75	0.75	0.75	0.23	0.42	0.42	0.43	0.43
2	2	3	2	2	1	0.84	1.00	1.00	1.00	1.00	0.63	0.75	0.75	0.75	0.75	0.47	0.53	0.53	0.53	0.53
1	1	1	3	2	1	0.79	0.99	0.99	1.00	1.00	0.35	0.48	0.49	0.48	0.49	0.11	0.19	0.20	0.21	0.22
1	1	2	3	2	1	0.79	0.98	1.00	1.00	1.00	0.36	0.48	0.48	0.48	0.48	0.11	0.19	0.20	0.20	0.22
1	1	3	3	2	1	0.48	0.72	0.73	0.74	0.74	0.35	0.48	0.48	0.48	0.49	0.29	0.38	0.38	0.39	0.39
1	2	1	3	2	1	0.84	1.00	1.00	1.00	1.00	0.56	0.70	0.71	0.72	0.72	0.15	0.24	0.25	0.26	0.27
1	2	2	3	2	1	0.84	1.00	1.00	1.00	1.00	0.56	0.70	0.71	0.71	0.72	0.15	0.24	0.25	0.26	0.27
1	2	3	3	2	1	0.82	1.00	1.00	1.00	1.00	0.55	0.70	0.71	0.71	0.72	0.47	0.54	0.54	0.54	0.54
2	1	1	3	2	1	0.78	0.99	1.00	0.99	1.00	0.39	0.47	0.48	0.47	0.48	0.17	0.30	0.30	0.31	0.31
2	1	2	3	2	1	0.77	0.99	0.99	0.99	0.99	0.39	0.48	0.49	0.48	0.48	0.17	0.29	0.31	0.31	0.32
2	1	3	3	2	1	0.56	0.89	0.87	0.88	0.88	0.40	0.49	0.49	0.49	0.50	0.31	0.46	0.47	0.47	0.47
2	2	1	3	2	1	0.83	1.00	1.00	1.00	1.00	0.45	0.53	0.53	0.53	0.53	0.21	0.37	0.37	0.38	0.38

Density	Sample size	Overlap	Correlation	SNR	SNR Grp Diff	Proposed					Benchmark Separate Node					Benchmark Summary Statistics				
						N1	N2	N3	N4	N5	N1	N2	N3	N4	N5	N1	N2	N3	N4	N5
2	2	2	3	2	1	0.83	1.00	1.00	1.00	1.00	0.45	0.53	0.53	0.53	0.53	0.21	0.37	0.37	0.38	0.38
2	2	3	3	2	1	0.81	1.00	1.00	1.00	1.00	0.44	0.52	0.52	0.53	0.52	0.48	0.53	0.54	0.53	0.53
1	1	1	1	2	2	0.78	0.98	1.00	0.99	1.00	0.51	0.66	0.65	0.67	0.67	0.11	0.23	0.24	0.26	0.27
1	1	2	1	2	2	0.77	0.98	1.00	0.99	1.00	0.51	0.66	0.66	0.68	0.68	0.11	0.23	0.25	0.26	0.26
1	1	3	1	2	2	0.46	0.64	0.66	0.68	0.68	0.53	0.64	0.65	0.66	0.68	0.27	0.34	0.35	0.35	0.36
1	2	1	1	2	2	0.85	1.00	1.00	1.00	1.00	0.69	0.89	0.85	0.85	0.85	0.16	0.27	0.28	0.29	0.31
1	2	2	1	2	2	0.85	1.00	1.00	1.00	1.00	0.69	0.89	0.86	0.85	0.85	0.16	0.27	0.29	0.29	0.31
1	2	3	1	2	2	0.84	1.00	1.00	1.00	1.00	0.69	0.89	0.86	0.85	0.85	0.47	0.53	0.53	0.54	0.54
2	1	1	1	2	2	0.79	1.00	1.00	1.00	1.00	0.59	0.71	0.71	0.70	0.71	0.19	0.38	0.38	0.40	0.41
2	1	2	1	2	2	0.78	1.00	1.00	1.00	1.00	0.60	0.71	0.70	0.71	0.71	0.18	0.37	0.40	0.39	0.40
2	1	3	1	2	2	0.52	0.72	0.70	0.73	0.73	0.61	0.71	0.72	0.70	0.71	0.29	0.40	0.40	0.40	0.41
2	2	1	1	2	2	0.84	1.00	1.00	1.00	1.00	0.65	0.83	0.79	0.78	0.78	0.23	0.42	0.43	0.44	0.45
2	2	2	1	2	2	0.84	1.00	1.00	1.00	1.00	0.65	0.83	0.79	0.78	0.78	0.23	0.42	0.43	0.44	0.44
2	2	3	1	2	2	0.82	1.00	1.00	1.00	1.00	0.64	0.83	0.79	0.78	0.78	0.46	0.54	0.54	0.54	0.54
1	1	1	2	2	2	0.76	0.98	1.00	0.99	1.00	0.47	0.62	0.61	0.64	0.63	0.11	0.23	0.23	0.25	0.26
1	1	2	2	2	2	0.75	0.98	1.00	1.00	1.00	0.47	0.63	0.61	0.63	0.63	0.11	0.23	0.24	0.25	0.26
1	1	3	2	2	2	0.46	0.69	0.70	0.70	0.73	0.48	0.64	0.62	0.64	0.65	0.28	0.37	0.37	0.37	0.38
1	2	1	2	2	2	0.84	1.00	1.00	1.00	1.00	0.64	0.84	0.80	0.80	0.80	0.16	0.26	0.27	0.29	0.30
1	2	2	2	2	2	0.83	1.00	1.00	1.00	1.00	0.63	0.85	0.81	0.80	0.80	0.16	0.26	0.27	0.29	0.30
1	2	3	2	2	2	0.82	1.00	1.00	1.00	1.00	0.63	0.84	0.80	0.80	0.80	0.47	0.54	0.54	0.54	0.54
2	1	1	2	2	2	0.77	1.00	1.00	1.00	1.00	0.55	0.68	0.67	0.66	0.67	0.19	0.37	0.38	0.39	0.40
2	1	2	2	2	2	0.78	1.00	1.00	1.00	1.00	0.54	0.67	0.67	0.66	0.67	0.19	0.37	0.38	0.38	0.39
2	1	3	2	2	2	0.44	0.77	0.79	0.80	0.78	0.54	0.68	0.67	0.67	0.68	0.26	0.40	0.40	0.40	0.40
2	2	1	2	2	2	0.83	1.00	1.00	1.00	1.00	0.57	0.75	0.71	0.70	0.71	0.22	0.41	0.42	0.43	0.43
2	2	2	2	2	2	0.84	1.00	1.00	1.00	1.00	0.58	0.76	0.71	0.70	0.71	0.23	0.41	0.42	0.43	0.44
2	2	3	2	2	2	0.82	1.00	1.00	1.00	1.00	0.58	0.76	0.71	0.70	0.71	0.46	0.53	0.53	0.53	0.53
1	1	1	3	2	2	0.7	0.9	1.0	0.9	0.9	0.3	0.4	0.4	0.4	0.5	0.1	0.1	0.2	0.2	0.2

Density	Sample size	Overlap	Correlation	SNR	SNR Grp Diff	Proposed					Benchmark Separate Node					Benchmark Summary Statistics				
						N1	N2	N3	N4	N5	N1	N2	N3	N4	N5	N1	N2	N3	N4	N5
						0	7	0	9	9	5	9	6	8	0	1	9	0	1	2
1	1	2	3	2	2	0.70	0.96	0.99	0.98	0.97	0.35	0.50	0.47	0.48	0.49	0.11	0.19	0.20	0.21	0.21
1	1	3	3	2	2	0.46	0.73	0.74	0.75	0.77	0.35	0.51	0.46	0.48	0.49	0.28	0.37	0.38	0.38	0.40
1	2	1	3	2	2	0.81	0.99	1.00	1.00	1.00	0.47	0.71	0.65	0.65	0.66	0.15	0.24	0.25	0.26	0.27
1	2	2	3	2	2	0.82	1.00	1.00	1.00	1.00	0.47	0.71	0.65	0.65	0.66	0.15	0.24	0.25	0.26	0.27
1	2	3	3	2	2	0.81	0.99	1.00	1.00	1.00	0.47	0.71	0.66	0.65	0.65	0.47	0.54	0.54	0.54	0.54
2	1	1	3	2	2	0.72	0.98	0.97	0.96	0.95	0.38	0.52	0.48	0.47	0.52	0.17	0.31	0.30	0.31	0.32
2	1	2	3	2	2	0.69	0.97	0.96	0.96	0.95	0.37	0.52	0.48	0.48	0.51	0.17	0.29	0.30	0.31	0.31
2	1	3	3	2	2	0.56	0.89	0.88	0.89	0.88	0.38	0.52	0.48	0.48	0.52	0.31	0.46	0.45	0.46	0.46
2	2	1	3	2	2	0.82	1.00	1.00	1.00	1.00	0.38	0.57	0.52	0.51	0.54	0.21	0.37	0.37	0.38	0.38
2	2	2	3	2	2	0.82	1.00	1.00	1.00	1.00	0.38	0.57	0.51	0.51	0.54	0.21	0.37	0.37	0.37	0.38
2	2	3	3	2	2	0.79	1.00	1.00	1.00	0.99	0.38	0.57	0.52	0.51	0.54	0.48	0.54	0.54	0.54	0.54

The average true negative rate (proportion of insignificant variables being eliminated) values over 100 replications in all 144 scenarios in the simulation studies of functional graphical modeling are summarized in Table D4.

Table D4. Average True Negative Rate for Simulation Studies (Grp Diff: Group Difference; N: Node)

Density	Sample size	Overlap	Correlation	SNR	SNR Grp Diff	Proposed					Benchmark Separate Node					Benchmark Summary Statistics				
						N1	N2	N3	N4	N5	N1	N2	N3	N4	N5	N1	N2	N3	N4	N5
1	1	1	1	1	1	1.00	1.00	1.00	1.00	1.00	0.91	0.75	0.73	0.71	0.70	0.89	0.77	0.76	0.74	0.73
1	1	2	1	1	1	1.00	1.00	1.00	1.00	1.00	0.91	0.75	0.73	0.71	0.69	0.89	0.77	0.75	0.74	0.73
1	1	3	1	1	1	0.92	0.74	0.73	0.72	0.70	0.91	0.72	0.70	0.68	0.67	0.95	0.84	0.83	0.82	0.82
1	2	1	1	1	1	1.00	1.00	1.00	1.00	1.00	1.00	0.99	0.99	0.99	0.99	0.84	0.73	0.72	0.71	0.70
1	2	2	1	1	1	1.00	1.00	1.00	1.00	1.00	1.00	1.00	0.99	0.99	0.99	0.83	0.73	0.72	0.71	0.70
1	2	3	1	1	1	1.00	1.00	1.00	1.00	1.00	1.00	0.99	0.99	0.99	0.99	0.98	0.98	0.98	0.98	0.98
2	1	1	1	1	1	1.0	1.0	1.0	1.0	1.0	0.7	0.4	0.4	0.3	0.3	0.8	0.6	0.6	0.6	0.5

Density	Sample size	Overlap	Correlation	SNR	SNR Grp Diff	Proposed					Benchmark Separate Node					Benchmark Summary Statistics				
						N1	N2	N3	N4	N5	N1	N2	N3	N4	N5	N1	N2	N3	N4	N5
						0	0	0	0	0	2	1	0	9	9	1	2	2	1	9
2	1	2	1	1	1	1.00	1.00	1.00	1.00	1.00	0.72	0.40	0.40	0.39	0.39	0.81	0.62	0.61	0.61	0.61
2	1	3	1	1	1	0.71	0.50	0.51	0.51	0.51	0.68	0.45	0.45	0.45	0.44	0.83	0.72	0.72	0.71	0.71
2	2	1	1	1	1	1.00	1.00	1.00	1.00	1.00	0.99	0.87	0.86	0.85	0.85	0.77	0.58	0.57	0.57	0.56
2	2	2	1	1	1	1.00	1.00	1.00	1.00	1.00	0.99	0.87	0.86	0.85	0.85	0.77	0.58	0.57	0.57	0.56
2	2	3	1	1	1	1.00	1.00	1.00	1.00	1.00	0.99	0.87	0.87	0.86	0.85	0.97	0.97	0.97	0.97	0.97
1	1	1	2	1	1	1.00	1.00	1.00	1.00	1.00	0.91	0.76	0.75	0.73	0.72	0.89	0.77	0.76	0.75	0.74
1	1	2	2	1	1	1.00	1.00	1.00	1.00	1.00	0.90	0.76	0.75	0.73	0.72	0.89	0.78	0.76	0.75	0.74
1	1	3	2	1	1	0.90	0.80	0.78	0.77	0.76	0.89	0.78	0.77	0.75	0.74	0.93	0.88	0.86	0.86	0.86
1	2	1	2	1	1	1.00	1.00	1.00	1.00	1.00	1.00	0.99	0.99	0.98	0.98	0.84	0.74	0.73	0.72	0.70
1	2	2	2	1	1	1.00	1.00	1.00	1.00	1.00	1.00	0.99	0.99	0.98	0.98	0.84	0.74	0.72	0.72	0.70
1	2	3	2	1	1	1.00	1.00	1.00	1.00	1.00	1.00	0.99	0.99	0.98	0.98	0.98	0.98	0.98	0.98	0.98
2	1	1	2	1	1	1.00	0.99	0.98	0.98	0.98	0.71	0.37	0.37	0.36	0.35	0.81	0.62	0.62	0.62	0.61
2	1	2	2	1	1	1.00	0.98	0.98	0.97	0.97	0.71	0.37	0.36	0.37	0.36	0.81	0.63	0.62	0.62	0.61
2	1	3	2	1	1	0.71	0.43	0.43	0.41	0.42	0.70	0.38	0.37	0.37	0.36	0.83	0.68	0.67	0.66	0.66
2	2	1	2	1	1	1.00	1.00	1.00	1.00	1.00	0.99	0.85	0.84	0.84	0.83	0.78	0.59	0.58	0.57	0.57
2	2	2	2	1	1	1.00	1.00	1.00	1.00	1.00	0.99	0.85	0.85	0.84	0.83	0.77	0.59	0.58	0.58	0.57
2	2	3	2	1	1	1.00	1.00	1.00	0.99	0.99	0.99	0.85	0.85	0.84	0.83	0.97	0.97	0.97	0.97	0.97
1	1	1	3	1	1	1.00	1.00	1.00	1.00	1.00	0.90	0.75	0.73	0.72	0.71	0.89	0.81	0.80	0.79	0.79
1	1	2	3	1	1	1.00	1.00	1.00	1.00	1.00	0.90	0.76	0.73	0.72	0.71	0.89	0.81	0.80	0.79	0.79
1	1	3	3	1	1	0.91	0.77	0.76	0.74	0.72	0.90	0.75	0.73	0.71	0.70	0.93	0.86	0.84	0.84	0.83
1	2	1	3	1	1	1.00	1.00	1.00	1.00	1.00	1.00	0.97	0.97	0.96	0.96	0.85	0.76	0.75	0.74	0.73
1	2	2	3	1	1	1.00	1.00	1.00	1.00	1.00	1.00	0.97	0.97	0.96	0.96	0.85	0.76	0.75	0.74	0.73
1	2	3	3	1	1	1.00	1.00	1.00	1.00	1.00	1.00	0.97	0.97	0.96	0.96	0.96	0.96	0.96	0.96	0.96
2	1	1	3	1	1	1.00	0.94	0.93	0.93	0.95	0.64	0.26	0.26	0.26	0.25	0.83	0.70	0.69	0.69	0.68
2	1	2	3	1	1	1.00	0.93	0.95	0.95	0.94	0.64	0.27	0.26	0.26	0.26	0.83	0.70	0.70	0.70	0.69
2	1	3	3	1	1	0.66	0.32	0.32	0.32	0.32	0.63	0.27	0.26	0.25	0.25	0.79	0.61	0.60	0.60	0.60

Density	Sample size	Overlap	Correlation	SNR	SNR Grp Diff	Proposed					Benchmark Separate Node					Benchmark Summary Statistics				
						N1	N2	N3	N4	N5	N1	N2	N3	N4	N5	N1	N2	N3	N4	N5
2	2	1	3	1	1	1.00	0.99	0.99	0.98	0.97	0.95	0.84	0.84	0.83	0.83	0.79	0.63	0.63	0.62	0.62
2	2	2	3	1	1	1.00	0.99	0.98	0.97	0.97	0.95	0.84	0.84	0.83	0.83	0.79	0.63	0.63	0.62	0.62
2	2	3	3	1	1	1.00	0.81	0.79	0.77	0.76	0.95	0.84	0.84	0.83	0.83	0.96	0.97	0.97	0.97	0.97
1	1	1	1	1	2	1.00	1.00	1.00	1.00	1.00	0.90	0.74	0.72	0.70	0.69	0.89	0.77	0.75	0.74	0.73
1	1	2	1	1	2	1.00	1.00	1.00	1.00	1.00	0.90	0.74	0.72	0.70	0.69	0.89	0.77	0.75	0.74	0.73
1	1	3	1	1	2	0.92	0.78	0.76	0.75	0.74	0.90	0.74	0.72	0.70	0.68	0.95	0.87	0.86	0.85	0.83
1	2	1	1	1	2	1.00	1.00	1.00	1.00	1.00	1.00	0.98	0.98	0.97	0.96	0.84	0.74	0.72	0.71	0.70
1	2	2	1	1	2	1.00	1.00	1.00	1.00	1.00	1.00	0.98	0.98	0.97	0.96	0.83	0.74	0.72	0.71	0.70
1	2	3	1	1	2	1.00	1.00	1.00	1.00	1.00	1.00	0.98	0.98	0.97	0.96	0.97	0.97	0.97	0.97	0.97
2	1	1	1	1	2	1.00	1.00	1.00	0.99	0.99	0.71	0.40	0.40	0.39	0.39	0.81	0.62	0.61	0.60	0.60
2	1	2	1	1	2	1.00	0.99	0.99	0.99	0.98	0.71	0.41	0.40	0.39	0.39	0.81	0.63	0.61	0.61	0.60
2	1	3	1	1	2	0.73	0.52	0.50	0.50	0.50	0.70	0.43	0.42	0.43	0.41	0.84	0.69	0.70	0.70	0.70
2	2	1	1	1	2	1.00	1.00	1.00	1.00	1.00	0.96	0.87	0.84	0.82	0.83	0.77	0.58	0.57	0.56	0.56
2	2	2	1	1	2	1.00	1.00	1.00	1.00	1.00	0.96	0.87	0.84	0.82	0.83	0.77	0.58	0.57	0.57	0.56
2	2	3	1	1	2	1.00	1.00	1.00	1.00	1.00	0.96	0.87	0.84	0.82	0.83	0.98	0.98	0.98	0.98	0.98
1	1	1	2	1	2	1.00	1.00	1.00	1.00	1.00	0.89	0.76	0.74	0.72	0.70	0.89	0.77	0.76	0.75	0.74
1	1	2	2	1	2	1.00	1.00	1.00	1.00	1.00	0.90	0.76	0.74	0.72	0.70	0.89	0.77	0.76	0.75	0.74
1	1	3	2	1	2	0.92	0.77	0.76	0.75	0.74	0.90	0.75	0.74	0.71	0.70	0.94	0.87	0.86	0.85	0.84
1	2	1	2	1	2	1.00	1.00	1.00	1.00	1.00	0.99	0.98	0.97	0.96	0.95	0.84	0.74	0.73	0.71	0.70
1	2	2	2	1	2	1.00	1.00	1.00	1.00	1.00	0.99	0.98	0.97	0.96	0.95	0.84	0.74	0.73	0.71	0.70
1	2	3	2	1	2	1.00	1.00	1.00	1.00	1.00	0.99	0.98	0.97	0.96	0.95	0.97	0.97	0.97	0.97	0.97
2	1	1	2	1	2	1.00	0.99	0.97	0.97	0.97	0.71	0.37	0.37	0.35	0.35	0.81	0.63	0.62	0.62	0.61
2	1	2	2	1	2	1.00	0.99	0.97	0.97	0.97	0.70	0.37	0.36	0.36	0.35	0.81	0.63	0.63	0.62	0.61
2	1	3	2	1	2	0.74	0.47	0.46	0.47	0.43	0.71	0.37	0.37	0.35	0.35	0.84	0.67	0.67	0.66	0.67
2	2	1	2	1	2	1.00	1.00	1.00	1.00	1.00	0.94	0.86	0.83	0.82	0.83	0.77	0.59	0.58	0.57	0.57
2	2	2	2	1	2	1.00	1.00	1.00	1.00	1.00	0.94	0.86	0.83	0.82	0.83	0.77	0.59	0.58	0.57	0.57
2	2	3	2	1	2	1.00	1.00	1.00	1.00	0.99	0.94	0.86	0.84	0.83	0.83	0.96	0.96	0.96	0.96	0.96

Density	Sample size	Overlap	Correlation	SNR	SNR Grp Diff	Proposed					Benchmark Separate Node					Benchmark Summary Statistics				
						N1	N2	N3	N4	N5	N1	N2	N3	N4	N5	N1	N2	N3	N4	N5
1	1	1	3	1	2	1.00	1.00	1.00	1.00	1.00	0.89	0.75	0.73	0.71	0.70	0.89	0.81	0.80	0.79	0.79
1	1	2	3	1	2	1.00	1.00	1.00	1.00	1.00	0.89	0.75	0.73	0.71	0.70	0.89	0.81	0.80	0.79	0.79
1	1	3	3	1	2	0.91	0.78	0.75	0.75	0.72	0.89	0.72	0.70	0.68	0.68	0.93	0.84	0.82	0.82	0.81
1	2	1	3	1	2	1.00	1.00	1.00	1.00	1.00	0.98	0.96	0.95	0.94	0.93	0.85	0.76	0.75	0.74	0.73
1	2	2	3	1	2	1.00	1.00	1.00	1.00	1.00	0.98	0.96	0.95	0.94	0.93	0.85	0.76	0.75	0.74	0.73
1	2	3	3	1	2	1.00	1.00	1.00	1.00	1.00	0.98	0.96	0.95	0.94	0.93	0.97	0.97	0.97	0.97	0.97
2	1	1	3	1	2	1.00	0.94	0.95	0.93	0.94	0.63	0.27	0.27	0.27	0.27	0.83	0.69	0.69	0.69	0.68
2	1	2	3	1	2	1.00	0.95	0.94	0.93	0.94	0.63	0.28	0.27	0.27	0.26	0.82	0.70	0.69	0.69	0.69
2	1	3	3	1	2	0.67	0.35	0.34	0.32	0.32	0.63	0.26	0.25	0.25	0.23	0.79	0.59	0.58	0.58	0.57
2	2	1	3	1	2	1.00	0.95	0.91	0.89	0.87	0.89	0.84	0.82	0.81	0.82	0.79	0.63	0.63	0.62	0.62
2	2	2	3	1	2	1.00	0.94	0.91	0.88	0.88	0.89	0.84	0.82	0.81	0.82	0.78	0.63	0.63	0.62	0.62
2	2	3	3	1	2	1.00	0.86	0.87	0.86	0.90	0.89	0.83	0.82	0.81	0.81	0.97	0.97	0.97	0.97	0.97
1	1	1	1	2	1	0.99	0.97	0.97	0.96	0.95	0.69	0.49	0.47	0.45	0.45	0.89	0.77	0.76	0.74	0.73
1	1	2	1	2	1	1.00	0.97	0.96	0.96	0.95	0.69	0.49	0.47	0.46	0.45	0.89	0.77	0.76	0.74	0.73
1	1	3	1	2	1	0.91	0.76	0.75	0.73	0.74	0.70	0.50	0.48	0.46	0.45	0.94	0.87	0.87	0.86	0.85
1	2	1	1	2	1	1.00	1.00	1.00	0.99	0.99	0.72	0.60	0.59	0.59	0.58	0.83	0.73	0.72	0.71	0.70
1	2	2	1	2	1	1.00	1.00	1.00	0.99	0.99	0.72	0.60	0.60	0.59	0.58	0.84	0.74	0.72	0.71	0.70
1	2	3	1	2	1	1.00	0.99	0.99	0.99	0.99	0.72	0.60	0.60	0.59	0.58	0.98	0.98	0.98	0.98	0.98
2	1	1	1	2	1	0.96	0.82	0.82	0.80	0.80	0.52	0.35	0.35	0.33	0.33	0.81	0.62	0.62	0.61	0.60
2	1	2	1	2	1	0.96	0.83	0.81	0.80	0.79	0.52	0.35	0.34	0.34	0.33	0.81	0.62	0.61	0.60	0.60
2	1	3	1	2	1	0.72	0.56	0.54	0.54	0.55	0.52	0.37	0.36	0.35	0.36	0.84	0.72	0.72	0.72	0.72
2	2	1	1	2	1	1.00	0.91	0.89	0.89	0.86	0.64	0.57	0.57	0.57	0.57	0.77	0.58	0.57	0.57	0.56
2	2	2	1	2	1	1.00	0.89	0.89	0.87	0.86	0.64	0.57	0.57	0.57	0.57	0.77	0.58	0.57	0.57	0.56
2	2	3	1	2	1	0.99	0.86	0.85	0.85	0.84	0.63	0.57	0.57	0.57	0.57	0.97	0.97	0.97	0.97	0.97
1	1	1	2	2	1	0.99	0.96	0.95	0.95	0.93	0.70	0.52	0.51	0.50	0.49	0.89	0.77	0.76	0.75	0.74
1	1	2	2	2	1	0.99	0.96	0.95	0.94	0.93	0.70	0.52	0.51	0.50	0.48	0.89	0.77	0.76	0.75	0.74
1	1	3	2	2	1	0.91	0.79	0.77	0.75	0.74	0.70	0.52	0.51	0.49	0.49	0.94	0.88	0.88	0.87	0.87

Density	Sample size	Overlap	Correlation	SNR	SNR Grp Diff	Proposed					Benchmark Separate Node					Benchmark Summary Statistics				
						N1	N2	N3	N4	N5	N1	N2	N3	N4	N5	N1	N2	N3	N4	N5
1	2	1	2	2	1	1.00	1.00	0.99	0.99	0.99	0.76	0.67	0.66	0.66	0.65	0.84	0.74	0.73	0.72	0.70
1	2	2	2	2	1	1.00	0.99	0.99	0.99	0.98	0.76	0.67	0.66	0.66	0.65	0.84	0.74	0.73	0.72	0.70
1	2	3	2	2	1	1.00	0.99	0.99	0.98	0.98	0.76	0.67	0.66	0.66	0.65	0.97	0.97	0.97	0.97	0.97
2	1	1	2	2	1	0.94	0.78	0.79	0.77	0.77	0.55	0.39	0.39	0.37	0.38	0.81	0.63	0.62	0.62	0.61
2	1	2	2	2	1	0.94	0.77	0.77	0.76	0.76	0.55	0.38	0.38	0.38	0.37	0.81	0.63	0.63	0.62	0.60
2	1	3	2	2	1	0.71	0.46	0.43	0.44	0.41	0.53	0.37	0.37	0.37	0.37	0.83	0.69	0.68	0.68	0.68
2	2	1	2	2	1	1.00	0.85	0.85	0.84	0.83	0.70	0.65	0.65	0.65	0.65	0.78	0.59	0.58	0.57	0.57
2	2	2	2	2	1	0.99	0.86	0.85	0.83	0.80	0.70	0.65	0.65	0.65	0.65	0.77	0.59	0.58	0.58	0.57
2	2	3	2	2	1	0.98	0.82	0.82	0.81	0.80	0.70	0.65	0.65	0.65	0.65	0.97	0.97	0.97	0.97	0.97
1	1	1	3	2	1	0.97	0.91	0.91	0.90	0.90	0.76	0.65	0.63	0.64	0.63	0.89	0.81	0.80	0.79	0.79
1	1	2	3	2	1	0.98	0.93	0.90	0.91	0.88	0.75	0.65	0.64	0.64	0.64	0.89	0.81	0.80	0.79	0.78
1	1	3	3	2	1	0.89	0.76	0.75	0.74	0.72	0.76	0.64	0.63	0.63	0.62	0.93	0.85	0.84	0.83	0.82
1	2	1	3	2	1	1.00	0.97	0.96	0.96	0.95	0.84	0.79	0.79	0.79	0.78	0.85	0.76	0.75	0.74	0.73
1	2	2	3	2	1	1.00	0.97	0.96	0.96	0.95	0.85	0.79	0.79	0.79	0.78	0.85	0.76	0.75	0.74	0.73
1	2	3	3	2	1	0.99	0.96	0.96	0.95	0.94	0.84	0.79	0.79	0.78	0.78	0.96	0.96	0.96	0.96	0.96
2	1	1	3	2	1	0.88	0.73	0.73	0.73	0.71	0.66	0.58	0.57	0.58	0.57	0.83	0.70	0.69	0.69	0.68
2	1	2	3	2	1	0.88	0.72	0.72	0.73	0.73	0.66	0.57	0.56	0.57	0.58	0.83	0.70	0.69	0.69	0.68
2	1	3	3	2	1	0.66	0.34	0.37	0.34	0.33	0.65	0.56	0.56	0.56	0.56	0.78	0.60	0.59	0.59	0.59
2	2	1	3	2	1	0.96	0.74	0.71	0.70	0.72	0.81	0.78	0.77	0.77	0.77	0.79	0.63	0.63	0.62	0.62
2	2	2	3	2	1	0.96	0.73	0.73	0.70	0.69	0.81	0.78	0.77	0.77	0.77	0.79	0.63	0.63	0.62	0.62
2	2	3	3	2	1	0.94	0.76	0.75	0.73	0.73	0.81	0.77	0.77	0.77	0.77	0.96	0.97	0.97	0.97	0.97
1	1	1	1	2	2	0.98	0.96	0.93	0.92	0.92	0.56	0.49	0.47	0.44	0.45	0.89	0.77	0.76	0.75	0.73
1	1	2	1	2	2	0.98	0.96	0.93	0.92	0.91	0.56	0.49	0.47	0.43	0.45	0.89	0.77	0.76	0.74	0.73
1	1	3	1	2	2	0.90	0.78	0.76	0.74	0.73	0.55	0.50	0.47	0.44	0.46	0.94	0.87	0.86	0.86	0.85
1	2	1	1	2	2	1.00	0.99	0.98	0.98	0.97	0.58	0.62	0.58	0.56	0.59	0.83	0.74	0.72	0.71	0.70
1	2	2	1	2	2	1.00	0.99	0.98	0.97	0.96	0.57	0.62	0.58	0.56	0.59	0.83	0.73	0.72	0.71	0.70
1	2	3	1	2	2	1.00	0.98	0.97	0.96	0.96	0.57	0.62	0.58	0.56	0.58	0.97	0.97	0.97	0.97	0.97

Density	Sample size	Overlap	Correlation	SNR	SNR Grp Diff	Proposed					Benchmark Separate Node					Benchmark Summary Statistics				
						N1	N2	N3	N4	N5	N1	N2	N3	N4	N5	N1	N2	N3	N4	N5
2	1	1	1	2	2	0.90	0.81	0.79	0.75	0.77	0.44	0.35	0.34	0.34	0.33	0.81	0.62	0.62	0.60	0.59
2	1	2	1	2	2	0.89	0.81	0.77	0.74	0.75	0.43	0.35	0.34	0.33	0.34	0.82	0.63	0.60	0.61	0.60
2	1	3	1	2	2	0.71	0.48	0.47	0.45	0.44	0.42	0.34	0.33	0.34	0.33	0.84	0.68	0.67	0.67	0.66
2	2	1	1	2	2	0.98	0.87	0.84	0.80	0.82	0.52	0.57	0.54	0.53	0.54	0.77	0.58	0.57	0.56	0.56
2	2	2	1	2	2	0.97	0.88	0.84	0.82	0.80	0.52	0.57	0.54	0.53	0.53	0.77	0.58	0.57	0.57	0.56
2	2	3	1	2	2	0.96	0.85	0.80	0.80	0.80	0.52	0.57	0.54	0.52	0.54	0.97	0.97	0.97	0.97	0.97
1	1	1	2	2	2	0.97	0.95	0.93	0.91	0.91	0.59	0.53	0.52	0.48	0.50	0.89	0.77	0.77	0.75	0.74
1	1	2	2	2	2	0.97	0.94	0.93	0.92	0.91	0.60	0.53	0.52	0.48	0.50	0.89	0.77	0.77	0.75	0.74
1	1	3	2	2	2	0.91	0.78	0.78	0.75	0.72	0.59	0.52	0.52	0.48	0.49	0.94	0.86	0.85	0.85	0.84
1	2	1	2	2	2	1.00	0.98	0.97	0.97	0.95	0.62	0.68	0.64	0.62	0.63	0.84	0.74	0.73	0.71	0.70
1	2	2	2	2	2	1.00	0.98	0.97	0.97	0.95	0.62	0.67	0.64	0.62	0.63	0.84	0.74	0.73	0.71	0.70
1	2	3	2	2	2	0.99	0.98	0.97	0.96	0.94	0.62	0.68	0.64	0.62	0.63	0.97	0.97	0.97	0.97	0.97
2	1	1	2	2	2	0.88	0.79	0.75	0.74	0.74	0.48	0.37	0.38	0.38	0.38	0.81	0.63	0.62	0.61	0.60
2	1	2	2	2	2	0.86	0.80	0.73	0.73	0.75	0.49	0.38	0.38	0.38	0.38	0.81	0.63	0.63	0.62	0.61
2	1	3	2	2	2	0.76	0.45	0.41	0.41	0.43	0.48	0.38	0.39	0.37	0.37	0.85	0.68	0.68	0.68	0.68
2	2	1	2	2	2	0.96	0.84	0.79	0.77	0.76	0.58	0.63	0.61	0.59	0.60	0.77	0.59	0.58	0.57	0.57
2	2	2	2	2	2	0.96	0.83	0.80	0.79	0.78	0.58	0.63	0.61	0.60	0.59	0.77	0.59	0.58	0.58	0.56
2	2	3	2	2	2	0.94	0.83	0.78	0.77	0.77	0.58	0.63	0.61	0.59	0.60	0.97	0.97	0.97	0.97	0.97
1	1	1	3	2	2	0.95	0.91	0.89	0.87	0.88	0.70	0.65	0.66	0.62	0.63	0.89	0.81	0.80	0.79	0.79
1	1	2	3	2	2	0.95	0.92	0.89	0.88	0.87	0.70	0.65	0.65	0.62	0.63	0.89	0.81	0.80	0.79	0.79
1	1	3	3	2	2	0.88	0.75	0.72	0.71	0.68	0.71	0.63	0.64	0.62	0.63	0.93	0.86	0.85	0.84	0.83
1	2	1	3	2	2	0.99	0.95	0.93	0.92	0.90	0.75	0.77	0.76	0.74	0.74	0.85	0.76	0.75	0.74	0.73
1	2	2	3	2	2	0.98	0.95	0.94	0.91	0.90	0.74	0.78	0.76	0.74	0.74	0.85	0.76	0.75	0.74	0.73
1	2	3	3	2	2	0.98	0.95	0.93	0.91	0.89	0.75	0.78	0.76	0.74	0.74	0.96	0.96	0.96	0.96	0.96
2	1	1	3	2	2	0.82	0.76	0.72	0.73	0.72	0.64	0.54	0.56	0.57	0.53	0.83	0.69	0.69	0.69	0.68
2	1	2	3	2	2	0.83	0.76	0.70	0.72	0.73	0.65	0.54	0.56	0.56	0.53	0.83	0.70	0.69	0.69	0.69
2	1	3	3	2	2	0.66	0.36	0.35	0.34	0.35	0.64	0.54	0.57	0.56	0.53	0.80	0.62	0.63	0.62	0.62

Density	Sample size	Overlap	Correlation	SNR	SNR Grp Diff	Proposed					Benchmark Separate Node					Benchmark Summary Statistics				
						N1	N2	N3	N4	N5	N1	N2	N3	N4	N5	N1	N2	N3	N4	N5
2	2	1	3	2	2	0.89	0.72	0.65	0.65	0.64	0.74	0.75	0.74	0.73	0.73	0.79	0.63	0.63	0.62	0.62
2	2	2	3	2	2	0.90	0.71	0.67	0.63	0.65	0.74	0.75	0.74	0.73	0.73	0.79	0.63	0.63	0.62	0.62
2	2	3	3	2	2	0.88	0.74	0.70	0.69	0.69	0.74	0.74	0.74	0.73	0.73	0.96	0.96	0.96	0.96	0.96

Appendix E

A list of average RMSPE and CE over 50 replications in all simulation settings in functional QQ modeling is provided in Table E1.

Table E1. A Summary of Average Simulation RMSPE and CE over 50 Replications

Scenario	Number of Variables	Correlation Structure	Density	Proposed RMSPE	Proposed CE	Benchmark RMSPE	Benchmark CE
1	1	1	1	1.0865	0.1129	1.0769	0.1188
1	1	1	2	1.1663	0.1032	1.1268	0.1107
1	1	2	1	1.1127	0.1214	1.0775	0.1284
1	1	2	2	1.1492	0.0852	1.1041	0.0892
1	1	3	1	1.1203	0.1034	1.0773	0.1102
1	1	3	2	1.1229	0.1079	1.0993	0.1136
1	1	4	1	1.1054	0.1135	1.0738	0.1141
1	1	4	2	1.1426	0.1072	1.1026	0.1055
1	2	1	1	1.3804	0.1127	1.1786	0.1204
1	2	1	2	1.6142	0.1571	1.2821	0.1570
1	2	2	1	1.2222	0.1243	1.1546	0.1262
1	2	2	2	1.4317	0.1483	1.2512	0.1372
1	2	3	1	1.2474	0.1235	1.1584	0.1329
1	2	3	2	1.5340	0.1518	1.2771	0.1472
1	2	4	1	1.2670	0.1134	1.1389	0.1180
1	2	4	2	1.4369	0.1431	1.2664	0.1378
2	1	1	1	1.2994	0.1936	1.8130	0.1885
2	1	1	2	1.5604	0.0805	3.6152	0.0920
2	1	2	1	1.4727	0.1043	2.6651	0.1062
2	1	2	2	1.7602	0.1073	4.1287	0.1164
2	1	3	1	1.4994	0.1358	2.6161	0.1525
2	1	3	2	1.6809	0.0861	3.8548	0.0983
2	1	4	1	1.4490	0.1139	2.4669	0.1126
2	1	4	2	1.8118	0.0964	3.9760	0.1009
2	2	1	1	2.0460	0.1125	4.1137	0.1285
2	2	1	2	2.8974	0.1548	6.1735	0.1610
2	2	2	1	2.1353	0.1111	4.0156	0.1172
2	2	2	2	2.7716	0.1457	5.8007	0.1392
2	2	3	1	1.7733	0.1221	2.9406	0.1306
2	2	3	2	2.5897	0.1188	5.5870	0.1252
2	2	4	1	2.2009	0.1323	4.1539	0.1366
2	2	4	2	2.4345	0.1276	4.6330	0.1233
3	1	1	1	1.3892	0.1602	2.8617	0.1683
3	1	1	2	1.4558	0.0971	3.6046	0.1032
3	1	2	1	1.6121	0.1183	3.4845	0.1236
3	1	2	2	1.8246	0.1042	5.1936	0.1051
3	1	3	1	1.3055	0.1034	3.1276	0.1123
3	1	3	2	1.5440	0.1002	4.3513	0.1095
3	1	4	1	1.3827	0.1025	3.3366	0.1067
3	1	4	2	2.2698	0.1200	5.6937	0.1223
3	2	1	1	2.6219	0.1203	5.5551	0.1313
3	2	1	2	3.9184	0.1459	7.1633	0.1512
3	2	2	1	2.1192	0.1430	4.3016	0.1441
3	2	2	2	3.6031	0.1494	8.4271	0.1400
3	2	3	1	2.5813	0.1204	5.3761	0.1234
3	2	3	2	3.8382	0.1591	8.7265	0.1588
3	2	4	1	2.9252	0.1238	6.1438	0.1252

3	2	4	2	3.6898	0.1204	10.5126	0.1223
4	1	1	1	1.9742	0.1058	4.7032	0.1068
4	1	1	2	2.6997	0.0959	7.3108	0.1052
4	1	2	1	2.1945	0.1087	5.2952	0.1171
4	1	2	2	3.2626	0.0895	9.2346	0.0927
4	1	3	1	2.1128	0.1409	4.4398	0.1503
4	1	3	2	2.8520	0.1014	6.9199	0.1069
4	1	4	1	2.2132	0.0915	5.2201	0.0980
4	1	4	2	3.1816	0.1103	8.5026	0.1109
4	2	1	1	4.1162	0.1157	9.0381	0.1202
4	2	1	2	5.1031	0.1485	10.9618	0.1571
4	2	2	1	3.7915	0.1268	8.4084	0.1226
4	2	2	2	4.2843	0.1262	10.3731	0.1276
4	2	3	1	3.8820	0.1499	8.0561	0.1506
4	2	3	2	5.5660	0.1322	12.7692	0.1452
4	2	4	1	3.4839	0.1060	8.5761	0.1000
4	2	4	2	5.2754	0.1277	12.2301	0.1234

A list of average variable selection accuracy over 50 replications in all simulation settings in functional QQ modeling is provided in Table E2.

Table E2. A Summary of Average Simulation Variable Selection Accuracy over 50 Replications

Scenario	Number of Variables	Correlation Structure	Density	Proposed Linear $m = 1$	Proposed Linear $m = 0$	Proposed Logistic	Benchmark Linear $m = 1$	Benchmark Linear $m = 0$	Benchmark Logistic
1	1	1	1	1.0000	1.0000	0.9583	1.0000	1.0000	1.0000
1	1	1	2	1.0000	1.0000	1.0000	1.0000	1.0000	1.0000
1	1	2	1	1.0000	1.0000	1.0000	1.0000	1.0000	1.0000
1	1	2	2	1.0000	1.0000	0.9583	1.0000	1.0000	0.9583
1	1	3	1	1.0000	1.0000	1.0000	1.0000	1.0000	1.0000
1	1	3	2	1.0000	1.0000	0.9583	1.0000	1.0000	1.0000
1	1	4	1	1.0000	1.0000	1.0000	0.9583	0.9583	1.0000
1	1	4	2	1.0000	1.0000	1.0000	0.9167	0.9167	1.0000
1	2	1	1	1.0000	1.0000	0.9375	1.0000	1.0000	0.9375
1	2	1	2	0.9792	1.0000	0.8750	0.9792	1.0000	0.9583
1	2	2	1	1.0000	1.0000	0.9375	1.0000	1.0000	0.9792
1	2	2	2	0.9583	0.9583	0.9167	1.0000	1.0000	0.9583
1	2	3	1	0.9583	0.9583	0.9792	1.0000	1.0000	1.0000
1	2	3	2	1.0000	0.9792	0.9167	1.0000	1.0000	0.9375
1	2	4	1	0.9792	0.9792	0.9792	0.9583	0.9583	0.9375
1	2	4	2	0.9583	0.9792	0.8750	0.8958	0.8750	0.8958
2	1	1	1	0.8750	0.9583	0.9583	0.8333	0.8333	0.9583
2	1	1	2	1.0000	0.9167	0.8333	0.7500	0.5833	0.9167
2	1	2	1	1.0000	0.9583	1.0000	0.7917	0.7917	1.0000
2	1	2	2	0.8750	1.0000	0.9583	0.5417	0.6667	0.9583
2	1	3	1	0.9583	0.9583	1.0000	0.7917	0.7917	1.0000
2	1	3	2	0.9583	1.0000	0.8750	0.6667	0.6250	0.9583
2	1	4	1	0.9167	0.8750	0.9167	0.7500	0.8333	0.9167
2	1	4	2	1.0000	0.9583	0.9167	0.6250	0.6250	0.9583
2	2	1	1	0.9792	0.9583	0.9792	0.8750	0.7500	0.9792
2	2	1	2	0.9375	1.0000	0.9167	0.6042	0.7500	0.9375
2	2	2	1	1.0000	0.9792	1.0000	0.8542	0.8125	1.0000
2	2	2	2	0.9375	1.0000	0.8750	0.6667	0.7083	0.9375

2	2	3	1	0.9583	0.9792	0.9583	0.8125	0.8333	0.9583
2	2	3	2	0.9375	0.9167	0.8750	0.6667	0.6250	0.9167
2	2	4	1	1.0000	0.9375	0.9375	0.8750	0.7708	0.9375
2	2	4	2	0.9792	0.9375	0.8750	0.7083	0.6667	0.8542
3	1	1	1	0.9583	1.0000	1.0000	1.0000	1.0000	1.0000
3	1	1	2	1.0000	1.0000	0.9167	1.0000	1.0000	1.0000
3	1	2	1	0.9583	1.0000	1.0000	1.0000	1.0000	1.0000
3	1	2	2	1.0000	1.0000	0.9583	0.9583	1.0000	1.0000
3	1	3	1	0.9583	1.0000	0.9583	0.9583	1.0000	0.9583
3	1	3	2	0.8750	1.0000	0.9583	0.9583	0.9583	1.0000
3	1	4	1	1.0000	1.0000	1.0000	0.9167	0.9583	0.9583
3	1	4	2	0.9583	1.0000	0.8333	0.9583	1.0000	0.9583
3	2	1	1	0.9792	1.0000	0.9792	0.9375	1.0000	1.0000
3	2	1	2	1.0000	1.0000	0.9167	0.9583	1.0000	0.9167
3	2	2	1	0.9583	1.0000	0.9167	0.9792	1.0000	0.9583
3	2	2	2	0.8958	1.0000	0.8958	0.9583	1.0000	0.9167
3	2	3	1	0.9583	1.0000	0.9375	0.9792	1.0000	0.9583
3	2	3	2	0.9167	1.0000	0.9375	0.9375	1.0000	0.9792
3	2	4	1	1.0000	1.0000	0.9375	0.8958	0.9792	0.9792
3	2	4	2	0.8750	1.0000	0.8958	0.8750	0.9583	0.9375
4	1	1	1	0.9583	1.0000	1.0000	0.6667	0.9583	1.0000
4	1	1	2	0.8333	1.0000	0.9583	0.4583	0.7083	1.0000
4	1	2	1	0.8750	1.0000	1.0000	0.7083	0.9167	1.0000
4	1	2	2	0.9167	1.0000	0.9167	0.5000	0.8333	0.9583
4	1	3	1	0.8333	1.0000	1.0000	0.7500	0.8750	1.0000
4	1	3	2	0.9583	1.0000	0.8333	0.5417	0.6667	0.8333
4	1	4	1	0.9583	1.0000	0.9583	0.7500	0.8333	1.0000
4	1	4	2	0.9167	1.0000	0.8750	0.3750	0.8333	0.9167
4	2	1	1	0.9792	1.0000	0.9375	0.7292	0.8542	0.9583
4	2	1	2	0.8958	1.0000	0.8958	0.3750	0.8542	0.9375
4	2	2	1	0.9375	1.0000	1.0000	0.7292	0.8958	1.0000
4	2	2	2	0.9375	1.0000	0.8958	0.3750	0.8333	0.9375
4	2	3	1	0.8750	1.0000	0.9583	0.6667	0.9167	1.0000
4	2	3	2	0.8750	1.0000	0.9583	0.3542	0.9167	0.9792
4	2	4	1	0.9375	1.0000	1.0000	0.6250	0.8958	1.0000
4	2	4	2	0.8333	0.9792	0.8750	0.3750	0.8542	0.9167

A list of true positive and true negative variable selection rate over 50 replications in all simulation settings in functional QQ modeling is provided in Table E3 and Table E4, respectively.

Table E3. A Summary of Average Simulation Variable Selection True Positive Rate over 50 Replications

Scenario	Number of Variables	Correlation Structure	Density	Proposed Linear $m = 1$	Proposed Linear $m = 0$	Proposed Logistic	Benchmark Linear $m = 1$	Benchmark Linear $m = 0$	Benchmark Logistic
1	1	1	1	1.0000	1.0000	0.8000	1.0000	1.0000	1.0000
1	1	1	2	1.0000	1.0000	1.0000	1.0000	1.0000	1.0000
1	1	2	1	1.0000	1.0000	1.0000	1.0000	1.0000	1.0000
1	1	2	2	1.0000	1.0000	0.8889	1.0000	1.0000	0.8889
1	1	3	1	1.0000	1.0000	1.0000	1.0000	1.0000	1.0000

1	1	3	2	1.0000	1.0000	0.8750	1.0000	1.0000	1.0000
1	1	4	1	1.0000	1.0000	1.0000	1.0000	1.0000	1.0000
1	1	4	2	1.0000	1.0000	1.0000	1.0000	1.0000	1.0000
1	2	1	1	1.0000	1.0000	0.6667	1.0000	1.0000	0.6667
1	2	1	2	0.9333	1.0000	0.6471	0.9333	1.0000	0.8824
1	2	2	1	1.0000	1.0000	0.6667	1.0000	1.0000	0.8889
1	2	2	2	0.8824	0.8824	0.7647	1.0000	1.0000	0.8824
1	2	3	1	0.7500	0.7500	0.8889	1.0000	1.0000	1.0000
1	2	3	2	1.0000	0.9286	0.7647	1.0000	1.0000	0.8235
1	2	4	1	0.8889	0.8889	0.9000	1.0000	1.0000	0.9000
1	2	4	2	0.8889	0.9412	0.6471	0.9444	0.9412	0.7647
2	1	1	1	0.8000	1.0000	0.8000	0.8000	1.0000	0.8000
2	1	1	2	1.0000	0.7500	0.6000	1.0000	0.7500	0.8000
2	1	2	1	1.0000	0.8000	1.0000	1.0000	1.0000	1.0000
2	1	2	2	0.7500	1.0000	0.9000	0.8750	1.0000	0.9000
2	1	3	1	1.0000	1.0000	1.0000	1.0000	1.0000	1.0000
2	1	3	2	1.0000	1.0000	0.6667	1.0000	1.0000	0.8889
2	1	4	1	0.6000	0.8000	0.3333	0.6000	0.8000	0.3333
2	1	4	2	1.0000	0.8571	0.7143	0.7778	0.8571	0.8571
2	2	1	1	0.8750	0.8000	0.8889	0.8750	0.5000	0.8889
2	2	1	2	0.8125	1.0000	0.7778	0.5000	0.7333	0.8333
2	2	2	1	1.0000	0.8750	1.0000	1.0000	0.8750	1.0000
2	2	2	2	0.7857	1.0000	0.6471	0.7857	0.8125	0.8235
2	2	3	1	0.7778	0.8750	0.8000	0.8889	1.0000	0.8000
2	2	3	2	0.8235	0.7647	0.6471	0.8235	0.7647	0.7647
2	2	4	1	1.0000	0.6667	0.6250	1.0000	0.6667	0.6250
2	2	4	2	0.9333	0.8000	0.6667	0.8667	0.8000	0.7222
3	1	1	1	0.8000	1.0000	1.0000	1.0000	1.0000	1.0000
3	1	1	2	1.0000	1.0000	0.7778	1.0000	1.0000	1.0000
3	1	2	1	0.8000	1.0000	1.0000	1.0000	1.0000	1.0000
3	1	2	2	1.0000	1.0000	0.8889	1.0000	1.0000	1.0000
3	1	3	1	0.7500	1.0000	0.8000	1.0000	1.0000	0.8000
3	1	3	2	0.7000	1.0000	0.8889	1.0000	1.0000	1.0000
3	1	4	1	1.0000	1.0000	1.0000	1.0000	1.0000	1.0000
3	1	4	2	0.8889	1.0000	0.5000	1.0000	1.0000	0.8750
3	2	1	1	0.8571	1.0000	0.8889	1.0000	1.0000	1.0000
3	2	1	2	1.0000	1.0000	0.7333	1.0000	1.0000	0.7333
3	2	2	1	0.7778	1.0000	0.6000	1.0000	1.0000	0.8000
3	2	2	2	0.7059	1.0000	0.6875	1.0000	1.0000	0.8125
3	2	3	1	0.7778	1.0000	0.7000	1.0000	1.0000	0.8000
3	2	3	2	0.7500	1.0000	0.8125	1.0000	1.0000	0.9375
3	2	4	1	1.0000	1.0000	0.6667	1.0000	1.0000	0.8889
3	2	4	2	0.6000	1.0000	0.7059	1.0000	1.0000	0.8824
4	1	1	1	1.0000	1.0000	1.0000	0.2500	1.0000	1.0000
4	1	1	2	0.7000	1.0000	0.8571	0.7000	1.0000	1.0000
4	1	2	1	0.5000	1.0000	1.0000	0.5000	1.0000	1.0000
4	1	2	2	0.6667	1.0000	0.7143	0.6667	1.0000	0.8571
4	1	3	1	0.7500	1.0000	1.0000	0.7500	1.0000	1.0000
4	1	3	2	1.0000	1.0000	0.5556	1.0000	1.0000	0.5556
4	1	4	1	1.0000	1.0000	0.8000	0.8000	1.0000	1.0000
4	1	4	2	0.7778	1.0000	0.6667	0.4444	1.0000	0.8889
4	2	1	1	0.9000	1.0000	0.5714	0.7000	1.0000	0.7143
4	2	1	2	0.7222	1.0000	0.6875	0.3889	1.0000	0.8125
4	2	2	1	0.6250	1.0000	1.0000	0.6250	1.0000	1.0000
4	2	2	2	0.8421	1.0000	0.7059	0.3684	0.9474	0.8235
4	2	3	1	0.5000	1.0000	0.7778	0.4000	1.0000	1.0000
4	2	3	2	0.6250	1.0000	0.8462	0.2500	1.0000	0.9231
4	2	4	1	0.6667	1.0000	1.0000	0.3333	1.0000	1.0000
4	2	4	2	0.5000	1.0000	0.6471	0.3750	1.0000	0.8824

Table E4. A Summary of Average Simulation Variable Selection True Negative Rate over 50 Replications

Scenario	Number of Variables	Correlation Structure	Density	Proposed Linear $m = 1$	Proposed Linear $m = 0$	Proposed Logistic	Benchmark Linear $m = 1$	Benchmark Linear $m = 0$	Benchmark Logistic
1	1	1	1	1.0000	1.0000	1.0000	1.0000	1.0000	1.0000
1	1	1	2	1.0000	1.0000	1.0000	1.0000	1.0000	1.0000
1	1	2	1	1.0000	1.0000	1.0000	1.0000	1.0000	1.0000
1	1	2	2	1.0000	1.0000	1.0000	1.0000	1.0000	1.0000
1	1	3	1	1.0000	1.0000	1.0000	1.0000	1.0000	1.0000
1	1	3	2	1.0000	1.0000	1.0000	1.0000	1.0000	1.0000
1	1	4	1	1.0000	1.0000	1.0000	0.9500	0.9500	1.0000
1	1	4	2	1.0000	1.0000	1.0000	0.8571	0.8571	1.0000
1	2	1	1	1.0000	1.0000	1.0000	1.0000	1.0000	1.0000
1	2	1	2	1.0000	1.0000	1.0000	1.0000	1.0000	1.0000
1	2	2	1	1.0000	1.0000	1.0000	1.0000	1.0000	1.0000
1	2	2	2	1.0000	1.0000	1.0000	1.0000	1.0000	1.0000
1	2	3	1	1.0000	1.0000	1.0000	1.0000	1.0000	1.0000
1	2	3	2	1.0000	1.0000	1.0000	1.0000	1.0000	1.0000
1	2	4	1	1.0000	1.0000	1.0000	0.9487	0.9487	0.9474
1	2	4	2	1.0000	1.0000	1.0000	0.8667	0.8387	0.9677
2	1	1	1	0.8947	0.9524	1.0000	0.8421	0.8095	1.0000
2	1	1	2	1.0000	1.0000	1.0000	0.6250	0.5000	1.0000
2	1	2	1	1.0000	1.0000	1.0000	0.7368	0.7368	1.0000
2	1	2	2	0.9375	1.0000	1.0000	0.3750	0.4667	1.0000
2	1	3	1	0.9474	0.9474	1.0000	0.7368	0.7368	1.0000
2	1	3	2	0.9333	1.0000	1.0000	0.4667	0.4375	1.0000
2	1	4	1	1.0000	0.8947	1.0000	0.7895	0.8421	1.0000
2	1	4	2	1.0000	1.0000	1.0000	0.5333	0.5294	1.0000
2	2	1	1	1.0000	1.0000	1.0000	0.8750	0.8158	1.0000
2	2	1	2	1.0000	1.0000	1.0000	0.6563	0.7576	1.0000
2	2	2	1	1.0000	1.0000	1.0000	0.8250	0.8000	1.0000
2	2	2	2	1.0000	1.0000	1.0000	0.6176	0.6563	1.0000
2	2	3	1	1.0000	1.0000	1.0000	0.7949	0.8000	1.0000
2	2	3	2	1.0000	1.0000	1.0000	0.5806	0.5484	1.0000
2	2	4	1	1.0000	1.0000	1.0000	0.8500	0.7949	1.0000
2	2	4	2	1.0000	1.0000	1.0000	0.6364	0.6061	0.9333
3	1	1	1	1.0000	1.0000	1.0000	1.0000	1.0000	1.0000
3	1	1	2	1.0000	1.0000	1.0000	1.0000	1.0000	1.0000
3	1	2	1	1.0000	1.0000	1.0000	1.0000	1.0000	1.0000
3	1	2	2	1.0000	1.0000	1.0000	0.9333	1.0000	1.0000
3	1	3	1	1.0000	1.0000	1.0000	0.9500	1.0000	1.0000
3	1	3	2	1.0000	1.0000	1.0000	0.9286	0.9286	1.0000
3	1	4	1	1.0000	1.0000	1.0000	0.9000	0.9474	0.9474
3	1	4	2	1.0000	1.0000	1.0000	0.9333	1.0000	1.0000
3	2	1	1	1.0000	1.0000	1.0000	0.9268	1.0000	1.0000
3	2	1	2	1.0000	1.0000	1.0000	0.9355	1.0000	1.0000
3	2	2	1	1.0000	1.0000	1.0000	0.9744	1.0000	1.0000
3	2	2	2	1.0000	1.0000	1.0000	0.9355	1.0000	0.9688
3	2	3	1	1.0000	1.0000	1.0000	0.9744	1.0000	1.0000
3	2	3	2	1.0000	1.0000	1.0000	0.9063	1.0000	1.0000
3	2	4	1	1.0000	1.0000	1.0000	0.8810	0.9737	1.0000

3	2	4	2	1.0000	1.0000	1.0000	0.8182	0.9310	0.9677
4	1	1	1	0.9500	1.0000	1.0000	0.7500	0.9474	1.0000
4	1	1	2	0.9286	1.0000	1.0000	0.2857	0.5000	1.0000
4	1	2	1	0.9500	1.0000	1.0000	0.7500	0.8947	1.0000
4	1	2	2	1.0000	1.0000	1.0000	0.4444	0.7143	1.0000
4	1	3	1	0.8500	1.0000	1.0000	0.7500	0.8421	1.0000
4	1	3	2	0.9412	1.0000	1.0000	0.3529	0.4286	1.0000
4	1	4	1	0.9474	1.0000	1.0000	0.7368	0.7895	1.0000
4	1	4	2	1.0000	1.0000	1.0000	0.3333	0.7143	0.9333
4	2	1	1	1.0000	1.0000	1.0000	0.7368	0.8158	1.0000
4	2	1	2	1.0000	1.0000	1.0000	0.3667	0.7586	1.0000
4	2	2	1	1.0000	1.0000	1.0000	0.7500	0.8684	1.0000
4	2	2	2	1.0000	1.0000	1.0000	0.3793	0.7586	1.0000
4	2	3	1	0.9737	1.0000	1.0000	0.7368	0.8947	1.0000
4	2	3	2	1.0000	1.0000	1.0000	0.4063	0.8621	1.0000
4	2	4	1	1.0000	1.0000	1.0000	0.6923	0.8684	1.0000
4	2	4	2	1.0000	0.9655	1.0000	0.3750	0.7586	0.9355